The role of cortico-basal ganglia systems in the construction of movement: Action selection and sequencing

Sjöbom, Joel

2021

Document Version:
Publisher's PDF, also known as Version of record

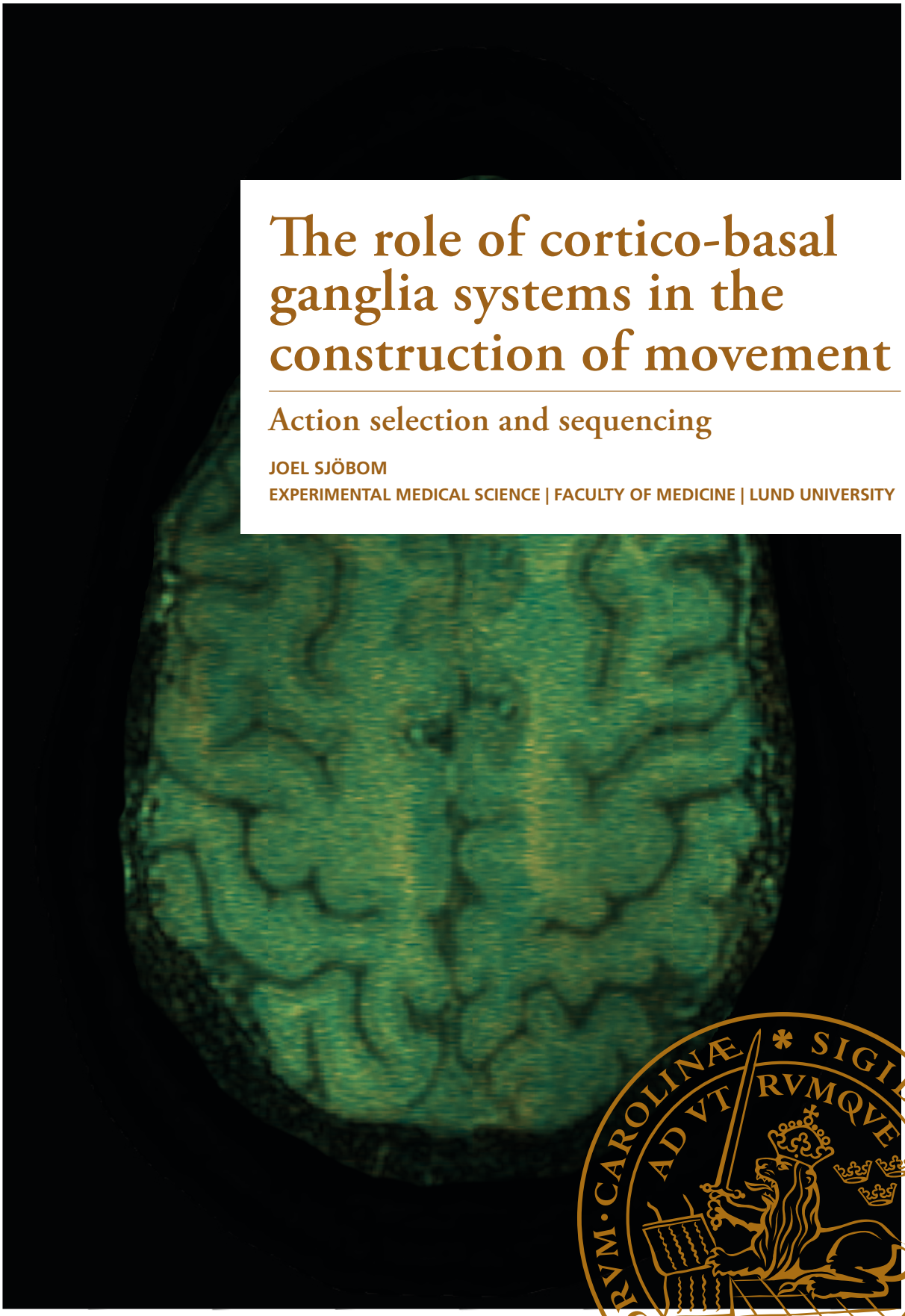

The role of cortico-basal ganglia systems in the construction of movement

Action selection and sequencing

JOEL SJÖBOM
EXPERIMENTAL MEDICAL SCIENCE | FACULTY OF MEDICINE | LUND UNIVERSITY

The role of cortico-basal ganglia systems in the construction of movement

The role of cortico-basal ganglia systems in the construction of movement

Action selection and sequencing

by Joel Sjöbom

LUND
UNIVERSITY

Thesis for the degree of Doctor of Philosophy
Thesis advisors: Ass. Prof. Per Petersson, Prof. Martin Garwicz, Pär Halje, Ulrike Richter
Faculty opponent: Prof. Hagai Bergman

To be presented, with the permission of the Faculty of Medicine of Lund University, for public criticism in the Segerfalk lecture hall at the Department of Experimental Medical Science on Friday, the 29th of January 2021 at 09:00.

Organization	Document name
LUND UNIVERSITY Department of Experimental Medical Science Integrative Neurophysiology, Lund University Scheelevägen 2 223 63, Lund, Sweden	**DOCTORAL DISSERTATION** Date of disputation 2021-01-29 Sponsoring organization
Author(s) Joel Sjöbom	

Title and subtitle

The role of cortico-basal ganglia systems in the construction of movement: Action selection and sequencing

Abstract

The cortico-basal ganglia system is instrumental in the construction of movement, through its involvement in aspects such as action selection, initiation/termination and sequencing, though the precise role of the different structures and how they collaborate on a network level to allow us to fluidly change from one behavior to another has long proven to be elusive.

We have here recorded neuronal activity throughout the cortico-basal ganglia circuit in rats, in a series of projects in order to understand more about how some of these functions are controlled.

We first set out to study the sequencing of actions through the rat grooming behavior, whose phases were shown to be concatenated in a stepwise manner where the selection of an upcoming phase depended primarily on the current one. Our data also suggested an involvement of both cortex and striatum in the initiation and termination of the behavior as a whole, while mainly primary motor cortex was modulated during the transitions between phases. In the primary motor cortex activity we also found correlation to the transition probability in the moment of transition, as well as the momentaneous probability of transitioning away from the current phase throughout its execution.

Next, we showed that out of the neuronal changes in activity that occur after administration of D1 or D2 type receptor antagonists, the only one that reliably precede the onset of catalepsy in any of the structures throughout the loop is a balanced change in firing rate.

Finally, we show that tactile input to the cortico-basal ganglia system in rats changes as an effect of acquiring a novel reaching skill, indicating that reshaping the representation of tactile input to motor circuits could be an important part of the learning process in skill acquisition in reaching and grasping.

Key words

Neurophysiology, Electrophysiology, Voluntary movement, In-vivo, Motor cortex, Corticostriatal, Basal ganglia

Classification system and/or index terms (if any)

Supplementary bibliographical information	Language
	English
ISSN and key title 1652-8220 Doctoral dissertation series (Lund University, Faculty of Medicine)	ISBN 978-91-8021-015-7
Recipient's notes	Number of pages 194 / Price
	Security classification

The role of cortico-basal ganglia systems in the construction of movement

Action selection and sequencing

by Joel Sjöbom

LUND
UNIVERSITY

A doctoral thesis at a university in Sweden takes either the form of a single, cohesive research study (monograph) or a summary of research papers (compilation thesis), which the doctoral student has written alone or together with one or several other author(s).

In the latter case the thesis consists of two parts. An introductory text puts the research work into context and summarizes the main points of the papers. Then, the research publications themselves are reproduced, together with a description of the individual contributions of the authors. The research papers may either have been already published or are manuscripts at various stages (in press, submitted, or in draft).

Cover illustration front: The real brain behind this thesis: An MRI scan of my own brain overlaid on a raster of neural data from Paper I.

Cover illustration back: Don't worry, it's the good kind of mad.

Funding information: The thesis work was financially supported by grants from the Magnus Bergvall Foundation, Crafoord Foundation, Kempe Foundation, Insamlingsstiftelserna, Umeå University, Kockska Foundation, Olle Engkvist Foundation, Parkinson Foundation, The Swedish Brain Foundation, Segerfalk Foundation, Åke Wiberg Foundation, Åhlén Foundations, MultiPark, Kungliga fysiografiska sällskapet, Sven-Olof Jansons livsverk, Sigurd och Elsa Goljes minne, Svenska Sällskapet för Medicinsk Forskning (SSMF), BABEL (Erasmus Mundus), The e-Science Collaboration, and Vetenskapsrådet (VR) grant 325-2011-6441 and grant 2018-02717. The computations were enabled by resources provided by the Swedish National Infrastructure for Computing (SNIC) at LUNARC, partially funded by the Swedish Research Council through grant agreement no. 2016-07213..

Faculty of Medicine, Department of Experimental Medical Science

ISBN: 978-91-8021-015-7
ISSN: 1652-8220 Doctoral dissertation series (Lund University, Faculty of Medicine)

Printed in Sweden by E-Husets Tryckeri, Lund University, Lund 2020

"Sometimes, the best answer is a more interesting question."

Terry Pratchett

Contents

Acronyms

BG basal ganglia

DLS dorsolateral striatum

DMS dorsomedial striatum

FSI Fast Spiking Interneuron

GLME generalized mixed-effects model

GP globus pallidus

GPe external globus pallidus

GPi internal globus pallidus

IN interneuron

KDE kernel density estimate

LFP local field potential

MI primary motor cortex

MSN medium spiny neuron

OU Ornstein-Uhlenbeck

PC principal cell

PCA principal component analysis

PETH perievent time histogram

PSTH peristimulus time histogram

RFA rostral forelimb area

SI primary somatosensory cortex

SNc substantia nigra pars compacta

SNr substantia nigra pars reticulata

STN subthalamic nucleus

TAN tonically active neuron

VA/VL ventral anterior/lateral nucleus of thalamus

List of publications

This thesis is based on the following publications, referred to by their Roman numerals:

I **Cortical and striatal circuits together encode transitions in natural behavior**

Joel Sjöbom, Martin Tamtè, Pär Halje, Ivani Brys, Per Petersson.
Science Advances, 2020, DOI: 10.1126/sciadv.abc1173

II **Neuronal correlates of probabilistic models describing the duration of actions in sequential behavior**

Joel Sjöbom, Kalle Åström, Per Petersson and Pär Halje.
Manuscript (Unpublished)

III **Changes in neuronal activity of cortico - basal ganglia – thalamic networks induced by acute dopaminergic manipulations in rats**

Nedjeljka Ivica, Ulrike Richter, **Joel Sjöbom**, Ivani Brys, Martin Tamtè and Per Petersson.
European Journal of Neuroscience, 2018, DOI: 10.1111/ejn.13805

IV **The organization of somatosensory input to cortico-striatal circuits is functionally adapted following practice of skilled reaching**

Nedjeljka Ivica, **Joel Sjöbom**, Luciano Censoni, Ulrike Richter and Per Petersson.
Manuscript (Unpublished)

Acknowledgements

Thank You

Per Petersson for your everlasting patience, for always showing interest in my projects, for your enthusiasm about my findings (be they significant or not), for having a near eidetic memory, and always, always being happy when I find a bug in my code for the hundredth time and just commenting "good thing you found it before we published".

Pär Halje for always being an inspiration with your contagious curiosity, and generally for being such an amazing person.

Sebastian Barrientos for your ever positive outlook on life, to be happy even after a day when everything goes wrong in the lab.

Luciano Censoni for being a great work partner, we made a fearsome coding duo!

Martin Tamtè for believing in my from day one, and for graciously letting me continue your work.

Nela Ivica for being nice to me even when times were hard.

Ulrike Richter for your eye for detail and never settling before things are done properly.

Katrine Skovgård for your amazing work morale and for sharing you expertise of all things danish.

Tiberiu Loredan Stan for your great work in the lab.

Ivani Brys for your positive vibes.

Martin Garwicz for seeing things from a fresh perspective and for your on-point and friendly questions.

Kalle Åström for your great enthusiasm, you have been an inspiration since day one and have stayed so through both a master and a PhD.

Christian Balkenius & Trond Arild Tjøsheim for a very interesting collaboration, I only wish we could have seen it come to fruition.

Mikael Novén & Daniella Grassi & Esbjörn Melin & Jenny Wickham & Anders Wahlbom for being true neurobuddies!

Anders Wahlbom & Matilde Forni for keeping the endless lab tutor hours fun, with in-depth discussion both on- and off-topic, warm tea, and warmer company.

Agneta Sanmartin & Linda Eliasson & Andrea Nord for tirelessly keeping everyone on top of things, and for always helping me in my administrative tasks.

Mengliang Zhang & Hiroyuki Watanabe & Marlene Storm Arnesen for making the lunchtime so much better.

Matilde Forni & Mohsin Mohammed & Lina Pettersson & Palmi Thor Thorbergsson & Alexander Holmkvist & Johan Agorelius & Jonas Thelin & Lucas Kumosa & Lina Gällentoft & Cecilia Eriksson & Niclas Lindqvist & Petter Pettersson & Bengt Ljungquist & Alle Retelund & Peter Paulander & Jens Schouenborg for creating a truly friendly work environment

Moa Svensson For telling me about the notice for two students to do a master thesis project in a cool brain lab, and asking me if I wanted to partner up for it. If it weren't for that, I might not have found my way into neuroscience.

Tobias Sjöbom for your brotherly support and all the great links to interesting brainy stuff.

Mats Sjöbom & Gunilla Rohlin for your pride and encouragement.

Gunilla Sjöbom for always showing a genuine interest in, and having patience with, my ramblings about the brain.

Johanna Mader Olsson For holding me together.

Popular summary in English

The basal ganglia are a collection of areas situated deep within the brain that has a wide array of responsibilities. It forms a loop with the cortex, the surface of the brain, where information is received from the cortex, processed sequentially and in parallel throughout the basal ganglia before being sent back to the cortex in a refined state. In this thesis we study the part of the loop that is involved in processing motor information, that is, decisions about how to move. More specifically, this part of the loop deals with things such as selecting specific movements, learning new tasks, and building sequences of movements. An example of such a sequence could be: Reaching for a glass of water, grasping it, bringing it to the mouth, drinking, and then placing the glass back at the table. Each of these require a different set of movements, and they need to be performed with great timing and in the right order for us to successfully quench our thirst.

Dopamine is a substance that is vital for the basal ganglia to perform its normal roles. A burst of dopamine is released when we receive an unexpected reward which tweaks our decision making in a way that encourages us to perform the actions that led to the reward again. Additionally, a certain amount of dopamine is needed to function normally, to grease the wheels in a way. When the supply of dopamine dwindles, as happens in people with Parkinson's disease, our posture becomes rigid, the joints stop moving smoothly, and we have trouble initiating or stopping movements. Although we know the connection between the lack of dopamine and these symptoms, it is not known exactly what the lack of dopamine changes so that the symptoms occur.

In the projects in this thesis we have investigated some of the ways of how the basal ganglia in healthy rats are involved in the construction of action sequences, how the areas change their connection to sensory input when learning a new task, and observed how a sudden change in the brains ability to bind dopamine changes the communication in these areas. Together this gives us important knowledge of how the brain works in a healthy animal. In addition to what this tells us about our human brains, it can also allow us to understand what has changed in the brain when something is wrong, leading to better understanding and treatments for diseases of the brain.

Populärvetenskaplig sammanfattning på svenska

De basala ganglierna är en grupp områden djupt ner, nära mitten av hjärnan som har många ansvarsområden. Tillsammans med hjärnbarken bildar den en cirkulär slinga där information ifrån hjärnbarken bearbetas både seriellt och parallellt genom de basala ganglierna innan den destillerade informationen skickas tillbaka till hjärnbarken. I den här avhandlingen studerar vi den del av slingan som behandlar motorinformation, det vill säga den delen som är inblandad med beslut hur vi ska röra oss. För att utveckla, den här delen av loopen väljer specifika rörelser, hjälper med att lära oss nya beteenden, och bygger sekvenser av rörelser. Ett exempel på en sådan sekvens är när vi ska dricka; vi sträcker oss efter glaset, greppar det, för det till munnen, dricker, och ställer tillbaka glaset på bordet. Var och en av dessa komponenter kräver timing och måste utföras i rätt ordning för att vi ska kunna släcka vår törst.

Dopamin är ett ämne som behövs för att de basala ganglierna ska kunna fungera normalt. När vi får en oväntad belöning släpper hjärnan ut extra dopamin vilket ändrar kopplingarna i hjärnan på ett sätt som uppmuntrar oss att upprepa det som ledde till belöningen. Utöver den mekanismen behövs också en viss mängd dopamin för att vi ska fungera normalt, för att smörja kuggarna så att säja. När dopaminnivån går ner för långt, som till exempel hos personer med Parkinsons sjukdom, blir vår hållning stel, lederna slutar vara medgörliga och känns som att de går på kugghjul, och vi får svårt att initiera och stoppa rörelser. Även om vi vet att en brist på dopamin leder till de här symptomen är det fortfarande inte känt exakt vad som i hjärnan som leder från dopaminbrist till symptomen.

I arbetena som ingår i den här avhandlingen har vi undersökt några av sätten som basala ganglierna kretsen i friska råttor är involverad i konstruktionen av rörelsesekvenser, hur områdena ändrar sina kopplingar till känselinput när råttorna lär sig en ny uppgift, och har observerat hur hjärnaktiviteten förändras när hjärnans förmåga att binda dopamin plötsligt förändras. Tillsammans har detta gett oss viktig kunskap om hur hjärnan fungerar i ett friskt djur. Förutom parallellerna som kan dras till hur människans hjärna fungerar så är den här kunskapen viktig för att förstå vad som förändras när något inte fungerar som det ska, vilket leder till bättre förståelse för hjärnsjukdomar och hur vi kan behandla dem.

Preface

Movement, it is so easy to take for granted. Taking a shower, drinking a glass of water, or just going for a walk. These simple tasks require a precision and versatility that no machine can yet reproduce. So how is it done? How can the brain piece together simple muscle movements to create a meaningful and complex motor behavior? What is more it needs to decide when to choose one behavior over another. Every species with a nervous system has the ability to move, making the choice of when and how to move one of life's most fundamental challenges.

As we strive to understand more about how this challenge is so competently met by our central nervous system, it quickly becomes apparent that the answer is far from simple, as the brain consist of billions of interconnected neurons whose signalling all depend on each other. Through years of hard work, scientists have found many answers but there is still much that remains unknown.

Today it is clear that in order to find answers to many of the more elusive aspects of the workings of the brain, a truly interdisciplinary effort is required, where medical experts team up with engineers and computer scientists. Each of whom bring their own unique knowledge and expertise, and together can reach that which none could achieve by themselves. This is the future of neuroscience.

The role of cortico-basal ganglia systems in the construction of movement: Action selection and sequencing

Background

Background

Signalling within the brain

The central nervous system is our only way of perceiving the world, and by signalling our muscles to move, also the only way we can interact with the world. All this communication and processing is done by the neurons in the central nervous system. There are a veritable host of varieties and types of neurons, whose cell bodies can vary almost two orders of magnitude in size, from the smallest granular cells in the cerebellum at around 4 μm to the comparatively huge Betz cells in the cerebral cortex at up to 100 μm. There are neurons that connect to only a handful of other neurons, and there are those that are connected to tens of thousands.

The neuron have three main components; the dendrite that receives input from other neurons, the soma which is the cell body of the neuron and from where the action potential originates (the output signal of the neuron), and the axon that propagates the output to other neurons. The connections between neurons are made by synapses, and generally send information in a single direction. While the signalling within a neuron is mostly electrical, the signalling in the synaptic cleft between neurons are mainly chemical. When an action potential reaches the synapse that connects to the next neuron, called the presynaptic terminal, a neurotransmitter is released that receptors in the postsynaptic terminal in the receiving neuron will react to. There are many different types of neurotransmitters and this together with the type of postsynaptic receptor defines the type of connection. The most common neurotransmitter is glutamate that, when bound to an AMPA receptor in the post synapse, leads to a depolarization of the membrane potential, and thus an increased probability that the postsynaptic neuron will fire an action potential. Connections like this are known as an excitatory connections. Another common neurotransmitter is gamma-Aminobutyric acid, more commonly known as GABA, which instead usually decreases the probab-

ility that the next neuron will fire an action potential, known as an inhibitory connection. For completeness it should be mentioned that, as so often is the case in the brain, this refers to the general case, and there are exceptions where the glutamate receptor in the post-synapse leads to an inhibition of the neuron, and likewise there are also excitatory GABAergic synapses.

When a neuron receives excitatory input, the electric potential inside the cell increases from its negative resting potential. When the membrane potential reaches a certain threshold, the neuron will fire an action potential (also known as a spike). Generally, it takes a simultaneous input from many connecting neurons for this threshold to be reached. Through a clever automated and timed combination of ion channels opening and closing as a reaction to the change in potential, this spike in the action potential is actively transported through the axon to the synapses bridging to the dendrites of neurons downstream. This propagation can be likened with how a wave propagates along a rope when flicked.

Measuring neuronal activity

When attempting to understand how the brain functions, one of the biggest challenges is measuring the activity within the brain. The most obvious problems are, of course, that the activity occur within the brain, that the amplitude of each action potential is relatively small, and that there are many, many neurons that are active at the same time.

One of the approaches is to implant electrodes into the areas one want to study. In the projects included in this thesis we use an array of 64 or 128 microwire electrodes, each of which are as wide as a hair. The changes in potential around the electrodes can then be measured, and spiking, as well as local field potential (LFP) activity can be extracted. Spiking activity is identified based on the action potentials' waveform shape, and attributed to individual neurons. The LFP activity is the average oscillatory activity of many nearby neurons, band pass filtered at much lower frequencies than the spiking, and as such it is mainly the dendritic currents that contributes.

There are many alternatives to implanting electrodes, each of which have different tradeoffs. The non-invasive electroencephalography (EEG) measures activity through the skull, it has poor resolution and can only report the average activity of many neurons, and only in the surface areas of the brain. Electrocorticography (ECoG) is a slightly more invasive alternatives that instead places

the electrode directly on the surface of the brain, this gives better resolution but still largely suffers from the same drawbacks of EEG, and neither can measure activity in deep brain structures. Functional magnetic resonance imaging (fMRI) measures brain activity indirectly through changes in blood-flow in active areas. Although this allows to see activity in deeper structures and in the whole brain at once, it has very poor spatial resolution and can only detect large-scale changes in activity. Another promising method that has emerged in recent years is calcium imaging of neurons, and improvements in voltage sensitive dyes, that has the potential to detect activity in hundreds of single neurons simultaneously, and shows great potential for the future.

The Cortico - Basal Ganglia - Thalamic Loop

The cortico-basal ganglia-thalamic loop, (also referred to as the cortico-basal ganglia loop, or simply the BG loop) in the brain is a group of areas that have long been implicated in the selection (Mink, 1996), initiation/termination (Jin and Costa, 2010) and sequencing of motor actions (Graybiel, 1998; Jin and Costa, 2010; Jin et al., 2014). These areas are interconnected in a circular fashion, where the classic description of the loop describes two main pathways in the basal ganglia for information flow named the direct and indirect pathways, where the direct pathway has been believed to promote desired motor outcomes, while the indirect pathway inhibit undesired motor actions (Albin et al. (1989); DeLong (1990); see Figure 1). All areas within the basal ganglia, with the exception of subthalamic nucleus (STN), have inhibitory output, and the explanation for the contribution from each pathway is the sign of the signal when it reaches the output areas of the BG, that is, the number of times a signal will be inverted along each pathway. The main output from the basal ganglia is the internal globus pallidus (GPi) and the functionally similar substantia nigra pars reticulata (SNr), that chronically supress activity in the ventral anterior/lateral nucleus of thalamus (VA/VL), and action is initiated when this inhibition is lifted. The logic, that can be followed in Figure 1, is that if the direct pathway is activated it inhibits GPi that in turn disinhibits VA/VL in thalamus, and if the indirect pathway is activated it inhibits external globus pallidus (GPe) which disinhibits STN, which activates GPi/SNr, which then strengthens the inhibition on VA/VL. This hypothesis on the effect of the direct and indirect pathways has had a large impact on research in the field, and has been of much help, perhaps most notably to the development of deep stimulation electrodes for the alleviation of motor symptoms in Parkinson's disease, which has proven extremely effective for some, although the underlying mechanism is not well

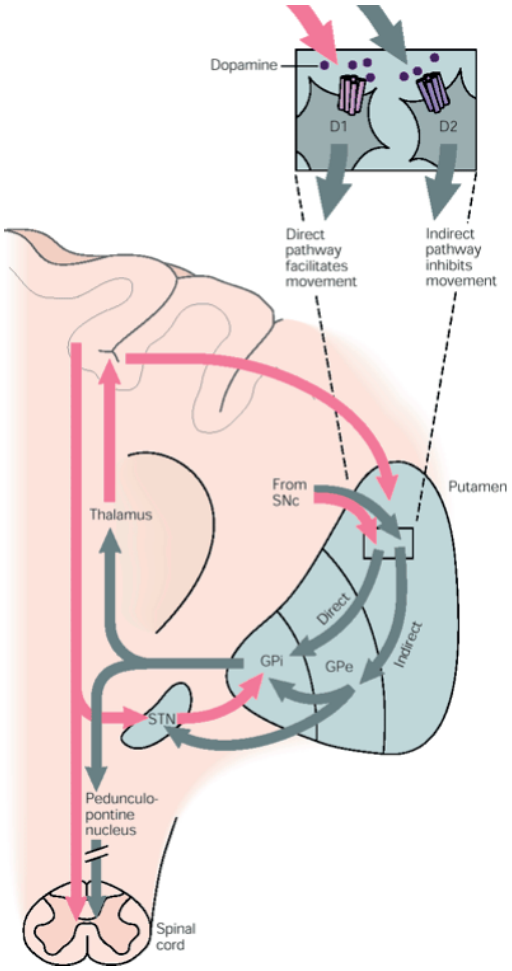

Figure 1: The basal ganglia consist of a series of connected areas. These are the striatum (here shown as the most lateral segment of putamen), the globus pallidus (GP) (further split into internal and external segments; GPi and GPe respectively), the substantia nigra pars compacta (SNc), and the subthalamic nucleus (STN). Red arrows denote excitatory connections while gray arrows denote inhibitory connections.

understood.

More recently there has also been a number of works that in general confirms the hypothesis, but in some aspects also contradicts this rather simplistic explanation for how the two pathways process information (Calabresi et al., 2014), indicating that a more in depth explanation is likely required. This might not be surprising, as each of the structures in the pathway probably processes the input more than just inverting the sign of the input. The full picture for how

the cortico-basal ganglia-thalamic loop process information is not yet known.

Apart from the direct and indirect pathways there is also a hyperdirect pathway, which has a similar effect on GPi as the indirect pathway, via excitatory projections from the STN, which in turn gets its input directly from the cortex (see Figure 1). This pathway has been shown to play a part in cancelling an action that is being prepared to be executed (Schmidt et al., 2013).

The BG loop also extends to receive input from different parts of the cortex, where primary motor cortex (MI) primarily projects onto putamen, and the supplemental motor areas (such as the rostral forelimb area (RFA) in rats) primarily projects to caudate nucleus. More anterior areas in the cortex also forms similar loops for cognitive functions (Graybiel, 2000).

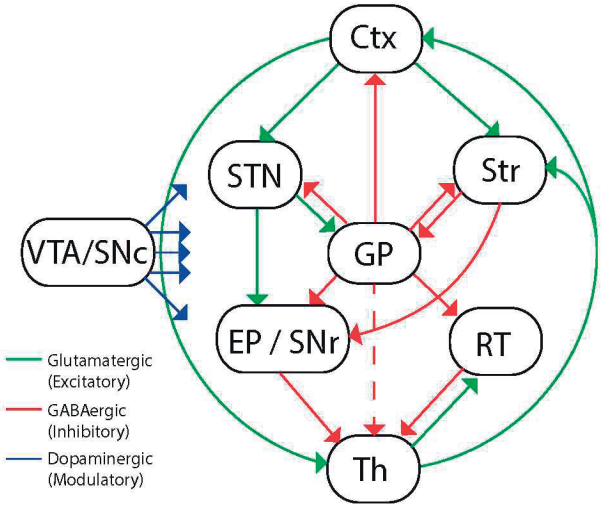

Figure 2: A more complete view of the connections between areas in the basal ganglia loop in rats. Ctx - Cortex, Str - Striatum, GP - Globus Pallidus, STN - Subthalamic nucleus, VTA - Ventral tegmental area, SNc - Substantia nigra pars compacta, EP - Entopeduncular nucleus, RT - reticular thalamus, Th - Thalamus

In recent years additional connections have been found within the basal ganglia, providing feedback between areas in the pathways (see Figure 2, and Cenci et al. (2018)). Additionally it should be cautioned that in rodents, at least, no neurons project solely along the direct pathway, as all striatofugal neurons also send collaterals to areas along the indirect pathway (Wu et al., 2000).

The Cortex

Korbinian Brodmann was one of the first scientists that endeavored to map the different areas of the surface of the brain, known as the cerebral cortex. He

identified 52 different areas based on the cytoarchitecture (cell size, spacing, and lamination) that have come to be known simply as Brodmann's areas (Brodmann, 1909). Today, the areas of the brain is mostly defined by its respective functions, but many of the boundaries of Brodmann's areas also turned out to define functional borders.

Some of these functionally defined areas of the cortex process sensory information, often of a particular modality, such as the posteriorly situated visually cortex, the laterally situated auditory cortex, or the primary somatosensory cortex (SI) located in a band close to the anteroposterior midline. Other areas process motor information, foremost among these is the primary motor cortex (MI), that lies parallel and immediately anterior to the primary sensory cortex. The name primary motor cortex stems from its neurons that project directly onto the spinal cord to activate downstream motor neurons. These projections are organized so that specific parts of MI controls certain parts of the body, where areas with a complex motor repertoire, such as the hands, takes up a much larger area of the cortex than areas with a relatively simple repertoire, such as the chest. This organization is usually referred to as the motor homunculus. The somatosensory homunculus is a similar representation of the areas of SI that receive input from different parts of the body (Penfield and Rasmussen, 1950).

Anterior of MI lies the premotor cortex, these areas deal with motor preparation and planning, and receives input mainly from VA/VL in thalamus which is the largest target for the output of the BG. In this thesis one of the areas we focus on is the rostral forelimb area (RFA), a premotor area in rats involved in the movements of the forelimbs.

Most areas of the cortex is organized into six distinctive cell layers, numbered I through VI, where layer I is the most superficial, and is defined mainly based on the distinct types of cells and connections in the layer. In addition to the layered organization, there is also a columnar organization. Each of these columns are a fraction of a millimeter wide, wherein neurons tend to process very similar information, and are believed to be the fundamental computational module of the cortex (Kandel et al., 2000). Generally speaking, information within the cortex is passes serially from one processing center to another, primarily via units in superficial layers II and III, that receives input from their dendrites in layer IV, and that projects to layer IV in other parts of the cortex. Meanwhile, units in layer V and VI, also receives input from their dendrites in layer IV, and mainly project to deeper structures, but also send some corticocortical collaterals to layer I and VI. These principal neurons in the cortex have a triangular shape and is known as pyramidal neurons, the largest of which are known as Betz cells

and are located within layer V. Throughout all layers there are also interneurons that connect to other units closeby. The cells in layer V of the motor cortex contains neurons projecting to the striatum, and it is these that we target when measuring from the cortex.

In spite of over a century of research, the functional organization of the motor areas is still not fully understood. While Penfield and Rasmussen showed that stimulations in MI gave rise to activation of specific muscles, it has more recently been shown that applying a longer stimulation pulse instead give rise of a movement toward a specific point regardless of the current position of the arm (Graziano et al. (2005); study done in macaque monkeys). Challenging the role of the motor cortex even further, it turns out that rats can perform skilled movements even after large lesions to the motor cortex. Meaning that the execution of motor behaviors can be done by deeper structures such as the basal ganglia, even without the help of the primary motor cortex (Grillner (2015); Kawai et al. (2015))).

It should be noted that although existing motor skills could still be activated, the learning of new behaviors was severely impacted. This is in line with the discovery of mirror neurons in premotor cortex. These units are proposed to be involved in imitation learning, that is, learning from watching someone else perform a goal directed movement (Rizzolatti and Craighero, 2004).

The Striatum

The striatum, named after its striped appearance, is the main input to the basal ganglia and is largely divided into a ventral, and a dorsal section. The ventral striatum consist of nucleus accumbens and the olfactory tubercle, and primarily mediates reward-related behavior (Schultz, 2016), while the dorsal striatum consist of the putamen and the caudate nucleus (dorsolateral striatum (DLS) and dorsomedial striatum (DMS) respectively in rats), and is involved in action selection and stimulus-response behavior such as habit formation (Groenewegen, 2003). In this work, the focus is on the dorsal section of striatum, which is further differentiated into DMS that mainly receives input from supplementary motor areas such as the RFA, and DLS that receives most of its input from MI.

The most numerous cell group in the striatum is the medium spiny neurons (MSNs), which makes up 95% of the neuronal population. They are inhibitory GABAergic cells and project into the deeper nuclei of the BG, are known for their sparse firing, and have their name from their many dendritic spines with a multitude of synapses that integrates input from many neurons. In addition to

the connections from outside of the striatum, this input also comes from Fast Spiking Interneurons (FSIs), and collaterals from other MSNs. The striatum is further modulated by dopaminergic input from the substantia nigra pars compacta (SNc), and also receive feedback from the thalamus. The MSNs can be divided into two groups based on their dopaminergic receptors and projections, where the first group have D1 type dopamine receptors that facilitate movement and project along the direct pathway, and the second have D2 type dopamine receptors impede signalling and mainly project along the indirect pathway.

The FSIs are a group of cells known for their high baseline activity. They receive cortical input, and have GABAergic connections to nearby MSNs close to their soma, giving them a large inhibitory influence over MSN spiking. The FSIs are also tightly coupled to each other with gap junctions which, unlike the previously described chemical synapses, allows the membrane potential to travel directly from one neuron to another in either direction.

As hinted previously, dopamine is a neuromodulator that is vital to the normal functioning of the basal ganglia, and the striatum in particular. Dopamine is supplied by dopaminergic neurons from the SNc, and phasic changes in dopamine innervation is used to facilitate learning and signal things of behavioral significance such as the reward prediction error (Schultz, 2016). A base level of dopamine is needed, where reduced dopamine innervation results in hypokinesia and difficulty in initiating different motor patterns, and addictive drugs induce exaggerated, uncontrolled dopamine effects.

Cholinergic interneurons in the striatum known as tonically active neurons (TANs), is a less studied class of neurons that are also modulated by reward, and have widespread connections to striatal MSNs, and that can also directly innervate the axon terminals of the nigrostriatal dopamine neurons. It has been shown that reward related information signalled by the dopaminergic neurons coincide with a pause in TAN activity, suggesting an important complementary role to the dopaminergic signalling (Morris et al., 2004).

Globus Pallidus

The globus pallidus (GP) is located medially of the striatum and is divided into two segments; the internal segment (GPi), and external segment (GPe), that both have inhibitory GABAergic projections. GPi, together with the functionally related SNr, acts as the output of the basal ganglia by selectively disinhibiting the VA/VL nuclei of the thalamus (in rodents also VM). GPe is part of the indirect pathway that is believed to work to suppress undesirable actions. This

is achieved by indirectly activating GPi/SNr by disinhibiting STN, although all GPe neurons that project to STN also send collaterals directly to GPi and/or SNr (Sato et al., 2000).

Apart from the classical pathways, there are also a number of other connections, in GPe there are projections back into the dorsal striatum, the cortex, and thalamus, as well as excitatory input from the STN, cortex and thalamus (Hegeman et al., 2016). Much is still unknown about these connections, but there seems to be a connection between the feedback loop with the STN and oscillations in Parkinson's disease (Hegeman et al., 2016), and the feedback to the dorsal striatum could play a role in timing or coordination of action execution through coordinated disinhibition of striatal FSIs (Berke, 2011).

In rats, the GP is not divided in the same way as in primates and takes on the role of GPe, while the role of GPi is taken over by SNr together with the entopeduncular nucleus (EN) (cf. Figure 1 and Figure 2).

Subthalamic Nucleus

The subthalamic nucleus (STN) is located immediately below the thalamus and is the only structure withing the BG with excitatory projections. The STN receives excitatory input from the thalamus and the cortex, and also inhibitory input from the GPe as part of the indirect pathway. The STN sends excitatory glutamatergic projections mainly to the GPi, but also feedback to the GPe.

The excitatory input from the cortex to STN and onto GPi forms the hyperdirect pathway, which has been suggested is involved in suppressing motor output. One way this can be done is by conveying a wide inhibition of the thalamus in preparation of movement, where the movement chosen through the direct pathway then selectively disinhibits parts of the thalamus (Nambu et al., 2002), while another study shows that the STN is modulated to stop cues where an intended action needs to be cancelled (Schmidt et al., 2013).

The STN has also been one of the most successful targets for deep brain stimulation for alleviating the motor symptoms of Parkinson's disease.

Substantia Nigra

Substantia nigra has its name from its distinctive black coloration due to a high concentration of neuromelanin, a dark pigment derived from oxidized and

polymerized dopamine. It is another structure that is divided into two parts; substantia nigra pars reticulata (SNr), one of the output nuclei of the BG and functionally similar to GPi, and substantia nigra pars compacta (SNc) that is the main supplier of dopamine to the brain, which plays an especially important role in the basal ganglia.

The SNr provides tonic inhibition to the thalamus VA/VL, and also to brainstem nuclei, through GABAergic projection, and is thought to selectively disinhibit part of the thalamus and thus "releasing" specific motor programs. The SNr receives inhibitory GABAergic projections from the striatum and GPi and excitatory glutamatergic projections from the STN.

SNc provides dopaminergic projections to large parts of the brain. It is modulated by reward, particularly by the difference between expected and received reward. So that if an unexpected reward is received there is a burst of activity, and if an expected reward is not forthcoming there is a lowering of the baseline firing.

Thalamus

The thalamus is a central hub in the brain. All sensory input except for olfaction passes through the thalamus, it was previously believed that it was simply a relay for information but now it is clear that it also gates and modulates the sensory information. Apart from this the ventral anterior/lateral nucleus of thalamus (VA/VL) nuclei also integrates information from the GPi and SNr output nuclei of the basal ganglia and cerebellum on its way to the cortex. This loop is not, however, only feed forward as the VA/VL also receives major input from neurons in layer VI in the cortex. The input is organized so that any given neuron in the thalamus either receives input from the BG or from the cerebellum, and additionally there are both reciprocal and non-reciprocal connections, meaning that there are both feed forward and feedback loops to the cortex.

Applicability of animal studies

All results discussed in this thesis are based on data from behavioral and electrophysiological recordings in rats. As such it is important to reflect on the applicability of this knowledge on the human brain.

In a comprehensive review, Grillner and Robertson (2016) concludes that the

basal ganglia is an evolutionarily old group of areas and it's function is thus likely to have a preserved functional role between rats, that we study here, and humans .

Statistics

According to the Cambridge dictionary, statistics is "the science of using information discovered from collecting, organizing, and studying numbers". In practise, statistical tests are applied when one wants to know if there is a significant relationship between two or more variables, for example if they have different means or are correlated. Within the field of statistics, the word "significance" has a very special meaning and is further discussed in the Significance section below.

The following sections have been allowed to take up a significant amount of space in this thesis as this has been where I have contributed most to the projects; the intricacies of analysis.

Data

There are a number of different types of data, and most statistical tests assumes that the input data is of a particular type. There can be some confusion about the specific difference between the words variable, observation, data point, data, and dataset.

A variable is a property that can take on different values. The age of a person could be such a variable. An observation is the value of a variable at a specific point, and a data point refers to the simultaneous observation across one or multiple variables (for example the x, and y coordinates at a specific time). Data refers to a group of such data points, and a dataset, here, usually refers to the entire set of data used in a project.

A variable can be represented by one of many different types. Time, for example can take on any real number, while the number of plates in a cupboard might be best represented by an integer. There are also grouping variables, such as person 1, person 2, etc, that might be best represented by a categorical variable.

Normalization

It is often prudent to normalize data prior to analyzing it. Normalization can refer to a number of different procedures aimed at making the data more interpretable, or comparable. In this project the most common normalization, or more accurately standardization, is Z-scoring of the neurons' firing rates. The Z-scoring is defined as

$$Z = \frac{X - \mu}{\sigma},$$

where X is the input, μ is the mean, and σ is the standard deviation of the data, and is employed so that the spiking of neurons with different baseline firing rates can be meaningfully compared. Additionally, if the mean and standard deviation is drawn from a baseline, and the firing rate of the neuron follows a normal distribution (as is, at least roughly, often the case), after Z-scoring it will have mean 0 and standard deviation 1, which allows for an easy estimation for if the firing rate has change since the baseline. More specifically, the probability that the firing rate of a neuron has changed more than two standard deviations is approximately 0.05, which is a common threshold for significance.

Another important normalization used is to normalize the LFPs to the pink background noise in the brain. This makes it easier to detect frequency changes that would otherwise be missed. Another powerful, but computationally heavy, tool to the same end is fractal normalization, or irregular-resampling auto-spectral analysis (IRASA) that allows for even cleaner LFPs.

Statistical hypothesis tests

While getting a feel for the data through visualization is very important, a statistical hypothesis test is needed to claim that the observed differences are significant. A statistical hypothesis test usually works from the hypothesis that there is no change in the data; that two groups have the same mean, or that there is no connection between two variables. This hypothesis is called the null hypothesis. The output of the test is a p-value that tells the probability that the null hypothesis is true. If the p-value is low enough it is possible to reject the null hypothesis, meaning that it is highly probable that there is, for example, a difference between the groups.

There are a host of different tests to choose from, each with its own requirements and assumptions about the data. One of the main divisions within the available statistical tests are parametric and non-parametric tests. Parametric

tests makes assumption about the distribution from which the observations are drawn, most commonly that they are drawn from a normal distribution. The most common way to ensure this is by visualizing the collected data with a histogram plot. Non-parametric tests, on the other hand, does not assume anything about the distribution of the data.The trade-off is that it is somewhat harder to detect true differences among the groups in the data, but a big advantage is that it is very robust to outliers (abnormally large values) in the data.

All tests that are not specifically designed to handle it assumes that the data is drawn from independent observations, meaning that the value of one observation should not effect the value of another, such as can happen, for example, when sampling observations very closely in time.

t-test

Student's t-test is probably one of the most well known statistical tests in the world. This test is a parametric test that assumes the data is drawn from a normal distribution with unknown variance. It tests for a difference in the mean of two distributions with the null hypothesis that they are the same. It comes in two main variations: One- or two-sample, also called paired or unpaired.

In a two-sample t-test, each observation is drawn independently from each other. A relevant example here could be how whether animals are more active after receiving one drug than after another drug, where each animal is only given one of the drugs.

In the one-sample t-test the observations from the two groups are drawn in pairs, and the test works directly with the difference between each pair. If the mean of the difference is significantly separate from zero it is possible to reject the null hypothesis. Each of these paired differences are usually observation from within one individual during two conditions. From the example above, such a pair could be the activity in one animal after receiving each of the two drugs (with sufficient time passed between them so that there is no lingering effects from the first drug). One even more common example would, of course, be activity before and after a drug was administered, and yet another one would be to compare the drug against a placebo drug.

With the paired test design the variations between individuals is greatly diminished and as such it is easier to find if there is a true difference between the groups.

Wilcoxon signed-rank and rank sum tests

The Wilcoxon signed-rank and rank sum tests are the non-parametric equivalent of the one- and two-sample t-tests, respectively, mentioned above. The rank-sum test also goes under the names Mann-Whitney U-test, and Mann-Whitney-Wilcoxon.

A rank test means that instead of using the measured values they are replaced with their rank, that is, the number of their sorted order, and estimate the median of the rank rather than the mean.

Binomial test

The binomial test is probably the most common exact test. An exact test is one where the probability can be calculated exactly. A binomial variable is a categorical variable with exactly two categories where the likelihood of observing each category constitutes the null hypothesis. A classical example is a simple coin toss situation, where, if there is a very improbable outcome it is reasonable to assume that the probability is not actually 50/50. One of the most common ways this test in used in these projects is to test if the number of modulated cells are above chance level.

Two-proportion Z-test

The two-proportion Z-test is used to determine if the probability of a variable with two categories are different in two different groups. It is similar to a binomial test between two groups where, where the probability of belonging to the two categories does not need to be known.

Fisher's exact test

Fisher's exact test is another very common test where the goal is to test if there are a connection between two two-categorical variables. It is said this test was invented by Fisher to test his friend Muriel Bristol's claim that she could taste whether milk or tea had been added to the cup first. The two variables were whether milk or tea had been added first, and which one she thought had been added first. The test answers what the probability is of getting the observed result and if it is sufficiently unlikely, significant that is, the null hypothesis can

be rejected. In this case the null hypothesis would be that there is no relationship between Bristol's answer and which of the milk or tea had been added first. As it happened, Bristol answered correctly eight times out of eight (where milk and tea were added first four times each), and thus convinced Fisher of her claim.

Chi-squared test

The Chi-squared test is a non-exact version of the Fisher's exact test, where the probability is estimated from a chi-squared distribution. The strength of this test is that it can handle more than two categories in each of the two variables.

ANOVA

The Analysis of Variance test, more commonly know as the ANOVA test, tests, as its name suggest, the variance in the data. More specifically whether a grouping variable can explain the variance in the data, meaning that if the variance is significantly lower within each group than in the total data, the groups have different means. The ANOVA allows to check for a difference in means among more than the two groups allowed in a t-test.

Two-way ANOVA, ANOVAN, MANOVA

The basic ANOVA described above is actually called a one-way ANOVA, referring to the one response variable. A two-way ANOVA is similar to the one-way, except there is two response variables. The ANOVAN extends it to any number of indipendent variables, and in the MANOVA the variables can be dependent on one another. There are a number of other variations on the ANOVA as well, and generally they answer if there is any difference in the means among the variables in any group. To further understand where the significance arises, visualization and post-tests are needed (See post-tests section below).

Kruskal-Wallis

Kruskal-Wallis test is a non-parametric one-way analysis of variance by ranks, that generalizes the one-way ANOVA to non-normally distributed data.

Linear Regression

Linear regression is way to find the relationship between two variables, it finds the line that best explain how the two variables vary with each other. The most common visualization is a scatter plot of simultaneously sampled observations of the two variables, with the fitted line plotted on top. The best line here means the line with the smallest sum of squared distances between all points and the fitted line (referred to as the least squares approach). If the coefficient for the slope is significantly different from zero, it means that the observed values of variables probably depend on each other.

Correlation

Correlation is closely related to a linear regression in that it is also used to find the relationship between two variables. The correlation is, however, invariant to scale and offset, and has a coefficient bounded between -1 and 1. An example of two variables with a correlation of 1, could be simultaneous samples from two sine waves with the same frequency, but not necessarily the same amplitude or offset. The counter-example of a correlation of -1 would be sampling from two sine waves where one was inverted. A significant correlation between two variables mean that the correlation coefficient has a sufficiently low probability of being zero.

Generalized Linear Mixed-Effects Model

With the help of computers it is possible to analyze datasets that would previously have taken years to calculate by hand. In the same spirit, it is now possible to calculate models with a much higher complexity than previously. The generalized mixed-effects model (GLME), sometimes also called a generalized linear mixed models (GLMM) is a very powerful tool when analyzing the relationship between a response variable in data with multiple fixed and random effects, interactions, and repetitions, for data that is not necessarily normally distributed.

A GLME consists of fixed-effects terms and random-effects terms. Fixed-effects terms represent the main part of the model, and usually make up the conventional regression part of the model. In a GLME, however, they can be a combination of any of the data types mentioned above, with the caveat that the input data must be of full column rank, meaning that all combinations of effects

must exist. A practical example of this is that to test if there is a difference in firing rates of neurons in a rat before and after training in each of its paws, we would need to have data from units in each of those four combinations. Random effects on the other hand represent a grouping variable. Here the grouping is usually done on the neuron-id, so that if there are multiple observations (usually z-scored firing rates) from the same unit those are grouped as repeated measures, and assumed to be drawn from it's own distribution of firing rates.

The GLME was here implemented using the fitglme function in MATLAB. In order to make the model perform as expected, the input data must first be organized in a table where each observation is on a separate line, with columns for the response variable, as well as each of the terms used. Then a formula that describes the relationship of the terms. This formula follows a format called Wilkinson notation. This formula takes the following form:

$$y \sim a * b + c + (1|g)$$

Where y is the response variable, a, b, and c are the fixed effects terms, and g is the random effects (grouping) term. The multiplication signals that the model should check for an interaction between the terms in addition to their main effects.

When interpreting a GLME model, an ANOVA is usually done, which gives an indication to which factors and terms are of interest. After which, a series of post-tests can be performed to determine more precisely between which groups the significance stems from.

The GLME is a powerful tool, but one of the drawbacks is that is can be hard to visualize the results, because of the complexity of the model.

post-tests

When doing tests such as the ANOVA, the reported significance shows if there is a significant difference between some of the groups in the data, but in order to know between which specific groups there is a difference, post-tests are needed. A series of post-tests is generally a batch of tests for differences between each pair of groups. For example, if the ANOVA showed a significant difference among the groups A, B, and C, the post-tests would be done to detect differences between A-B, B-C, and A-C respectively.

Significance

Within all of science, and statistics in particular, the word significance has a special meaning. When referring to something as being significant there should always be a statistical hypothesis test to back up the claim. Generally it means that the p-value should be below some pre-defined threshold, most commonly 0.05, meaning that the estimated probability of observing the given results is less than 5%, and as such the null hypothesis can be safely rejected. It should be noted, however, that the opposite is not true; a large p-value does not mean that the null hypothesis is true, only that there is no grounds to reject it based on the given data.

Correction for multiple comparisons

The observant reader will have realised that if a large number of statistical tests are performed there will inevitably come a point where a null hypothesis was rejected, even though it was in fact true, and the differences in the data were observed purely by chance. This is called a type I error, also known as a false positive, and poses a grave pitfall when interpreting and analyzing data. The more tests that are performed, the greater the risk that some of them are false positives, and with modern techniques such as fMRI it is not uncommon to do tens of thousands of tests. The winner of the 2012 IgNobel prize in neuroscience (a prize for achievements that first make people laugh, and then think) did a fMRI study on a dead salmon, where the salmon was shown images of people in social settings and asked to determine their emotions. The study showed areas in the brain of the dead salmon that was significantly more active during the task, and was performed without properly controlling for multiple comparisons, which was quite common within the field at that time (Bennett et al., 2009).

There are many ways to correct for multiple comparisons, some of the most common methods are outlined below. They all work by the principle of adjusting the required significance threshold based on the group size.

The opposite, where a true difference is dismissed can also happen, is called a type II error or a false negative. This is generally not as dire, but could lead the research away from avenues research that could potentially wield interesting results. The main reason for type II errors are generally too small sample sizes, small differences between groups, and overly strict thresholds for significance.

Bonferroni

Bonferroni correction is probably the most well known correction for multiple comparisons. It aims to reduce the familywise error rate, that is, the risk of making one or more type I errors. It adjusts the significance threshold by a factor of n, where n is the number of comparisons. For example, if the pre-defined threshold is $p < 0.01$ and there is 10 comparisons, the Bonferroni corrected threshold is $0.01/10 = 0.001$. Sometimes it is instead implemented by multiplying the p-values by n, instead of adjusting the threshold, which leads to the same results. It is exceedingly simple to implement, but very strict, which means it reduces the risk of type I errors, but also increases the risk of type II errors.

Holm-Bonferroni

The Holm-Bonferroni method is an alternative to Bonferroni correction that also aims to reduce the familywise error rate. It works by reducing adjusting the threshold by the sorted rank of the p-values instead of the total n. That is, it divides the threshold by by n for the smallest p-value, by $n-1$ for the second smallest and so forth. Each p-value that is smaller than its adjusted threshold, and is preceeded by p-values that all passed their respective threshold is seen as significant. The Holm-Bonferroni method is uniformly more powerful than the Bonferroni correction, meaning that is is always more likely to determine the true significance.

Benjamini-Hochberg

In contrast to the two methods mentioned above, the Benjamini-Hochberg procedure instead aims to limit the number of type I errors to an acceptable fraction, called the false discovery rate. It is best used when each significant result in and by itself is not important, but rather the total fraction of significant results, as is the case for example, when counting the number of significant responders in a group.

Aims

Aims

In this thesis my aim is:

- To determine the nature of cortical and striatal involvement in the sequencing of natural behavior
- To evaluate to what degree probabalistic models can describe aspects of behavior and how it is reflected in the neuronal activity in the corticostriatal circuit
- To characterize the physiological effects of reduced dopamine signaling in cortico-basal ganglia-thalamic networks
- To characterize the changes in the encoding of somatosensory input to cortico-basal ganglia motor circuits as an effect of learning

Introduction

Introduction

The four projects covered in this thesis all touch on different aspects of how the motor cortex work with the basal ganglia to construct different aspects of motor control. Because many aspects of the questions of issue within this area of research are largely unexplored, much of the work has been descriptive, although a number of hypotheses revolving around the involvement of these circuits have also been posed and tested.

The findings relate to the fundamental role of the cortico-basal ganglia-thalamic loop on the control of movement, and should therefore be of interest for a wide audience within the research community of motor control regarding both the healthy and diseased brain.

Paper I

Many aspects of movement generation is already known, but how different behaviors is concatenated into a functioning whole is still poorly understood. The BG-loop is implicated in, among other functions, action selection and sequencing. Here we show some of the ways the loop is involved in action switching and sequencing during self-grooming in rats.

There are no previous studies on behavioral sequencing of natural behavior on a circuit level, although the involvement of specific cell groups have been studied using calcium imaging, more specifically MSNs in dorsal striatum by Markowitz et al. (2018), where all behavior was automatically divided into groups, most of which could be seen as groupings in a continuum of behavior, and as such often does not have very stereotypical kinematics. Earlier, there have also been impactful studies on action sequencing involving e.g. repeated lever pressing in rodents (Jin and Costa, 2010; Jin et al., 2014), and as such is hard to generalize to more complex action sequences of natural behavior.

The grooming behavior studied here is a spontaneous behavior that has a number of highly stereotypical phases that can be concatenated in any number of combinations and is as such a very good candidate for studying complex sequentially patterned behaviors (Kalueff et al., 2015). In this study we investigate how the involvement of neurons in the cortex and striatum during the sequencing of natural behavior, through the natural grooming behavior in rats.

Paper II

One of the questions that remained unsolved in paper I was how the duration of each grooming phase was controlled. From the behavior it was clear that the duration of the different phases followed distinct and different distributions. However, no evidence for the direct encoding of the duration could be found in the spiking of the units. If the duration is not coded directly, an alternative explanation for the distributions emerging from the durations for the phases could be that is is stochastically encoded, rather than deterministically. That would mean that there would be no strong correlation between the average neuron firing rate and the duration spent in a phase, but rather between spiking and the probability of transitioning away from the current phase at each point in time. To clarify, if a neuron is active every time a transition occurs, it would be indicative of deterministic coding, but if instead a neuron is active when there is a high probability for a transition to occur, whether or not the transition actually happen, it would be a stochastic coding.

In this paper we have tested this hypothesis by fitting a number of distributions to the observed behavior and tested whether their hazard functions correlate to the observed neuronal activity of the units. For the Ornstein-Uhlenbeck (OU) drift diffusion distribution, where the model parameters have a clear functional implication, we also tested if the average firing rate during the different phases correlate to those parameters.

Paper III

Parkinson's disease is a serious and widespread illness that causes the loss of the dopamine-producing cells in the midbrain. Dopamine has an important role in the normal functioning of the cortico-basal ganglia-thalamic circuit and is thought to be involved in facilitating movement, marking unexpected rewards, and as a signal for learning by inducing plasticity (Mink, 1996; Graybiel, 1998;

Jin and Costa, 2010; Jin et al., 2014). The loss of the dopamine producing cells leads to the characteristic rigidness and difficulty of initiating movement that is associated with Parkinson's disease. Although the symptoms of the loss of dopamine input are well described, the mechanism that leads from a lack of dopamine to the symptoms is not, and neither is its normal physiological effect.

In this paper we study how the neural signalling in the the cortico-basal ganglia-thalamic circuit is affected by acute, but transient, manipulations to the dopamine signalling. More specifically, we study the effect of dopaminergic receptor type 1 and/or 2 (D1R, D2R respectively) antagonists on the spiking and LFP in eight simultaneously recorded structures. These manipulations affected dopamine input, either by antagonizing D1R, D2R, or D1R+D2R, or by blocking endogenous dopamine production. These acute changes were also compared to a chronic dopamine depletion using 6-hydroxydopamine (6-OHDA) lesions.

The observations in this paper points to some likely neurophysiological causes to the akinesia seen after dopamine depletion.

Paper IV

In a number of influential studies in cats and monkeys, it was found that neurons in the motor cortex receive sensory input from the same areas that they were involved in activating (Asanuma et al., 1968; Asanuma and Rosén, 1972; Rosén and Asanuma, 1972). That is for example, if a neuron in the motor cortex is responsible for flexing a finger, it most likely is modulated by (i.e. receives input from) touch to the skin in that finger and passive bending of the finger joint.

The same type of organization is true for the climbing fibers in the cerebellum (Apps and Garwicz, 2005), and also for the nociceptive reflex circuits in the spinal cord (Ekerot et al., 1991; Schouenborg and Weng, 1994). Interestingly, the organization of this circuit has been shown to arise thanks to spontaneous muscle twitches during sleep that appear to guide the network plasticity in a functional self-organization (Petersson et al., 2003).

In the motor cortex, it is reasonable that this organization is to provide information that is relevant to the function of the neurons, and if this is the case a pertinent follow up question would be whether this functional input changes to reflect important information when new a new motor skill is learned.

In this project we hypothesize that the organization of somatosensory input to cortico-basal ganglia circuits change as a consequence of intense motor practice.

We record the neural response in lightly anesthetized rats during tactile stimulation to their forepaws before and after being trained in a new motor skill involving reaching for food with one of its paws.

Methods

Methods

Outlined here are the central methods used in the studies included in this thesis. For further details about each project, see attached articles and manuscripts in the the appendix.

Animals

Adult female Sprague-Dawley rats were used, who were kept on a 12h day-night cycle and had access to food and water ad libitum. The exception to this was during the training of the rats in paper IV, who had food restricted for 22h before training.

Ethical Permits

The Malmö/Lund ethical committee of animal experiments approved all experiments in advance.

Electrodes and Implantation

A multi-array of 64 or 128 33 μm insulated tungsten wire electrodes were chronically implanted. The electrodes were spread bilaterally among the areas of interest in the cortico-basal ganglia-thalamic loop. The z-coordinate was controlled using a 3D-printed scaffold with varying depth, while using two spaced and matching plastic sheets, with matching holes at the desired coordinates to control x- and y-coordinates, as specified in each study. Each wire was attached to electrical connector with conducting epoxy and fixed in place with UV-resin.

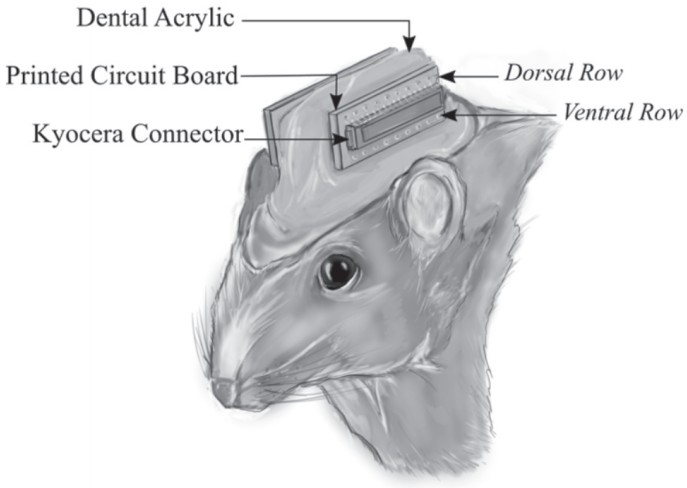

Figure 3: An example of the implanted electrode. *Credit:Pomesh Kumar*

The electrode array was implanted while the rat was deeply anesthetized using Fentanyl/Medetomidine, while secured in a stereotax for a stable cranium position. The electrode was positioned above the correct area using bregma as reference, implanted using a hydraulic micromanipulator (Kopf Instruments, USA) and secured to the skull with dental cement and stainless steel screws that could also serve as a reference for the recording. See Figure 3 for an overview of the implanted electrode, and (Ivica et al., 2014) for a detailed description of the electrode design.

Signal and video acquisition

The neural activity was acquired using a Neuralynx multichannel recording system together with the Cheetah software. Each channel (recording electrode) was sampled at 32 kHz, from which the spiking and LFP activity were recorded in parallel. Spikes were extracted as 32 samples (1 ms) band pass filtered at 600-9000 Hz, while LFPs were band pass filtered at 0.1-300 Hz and subsampled to 1 kHz.

Videos were recorded using a Dalsa Genie camera at 25 Hz in Paper I, II, and III.

The neurophysiological data and videos were synchronized using a Master-8 pulse generator.

Spike sorting and neuron classification

In Paper I and II spike sorting was done manually using the Offline Sorter software and classified into putative cell groups (principal cells (PCs)/interneurons (INs)/unknown) using fuzzy k-means clustering based on the spike waveform features peak width, valley width and peak to valley time, while Paper III and IV used manual validation of automatically clustered spikes using slightly modified code from the Chronux toolbox (see (Fee et al., 1996), (Halje et al., 2012), (Tamtè et al., 2016)) and in Paper III neurons were divided into putative cell groups based on peak-to-valley time (although both peak- and valley width were also reviewed and deemed not to improve the clustering).

Experimental setup

In Paper I and II the rat was placed in a long and narrow area inside a transparent acrylic glass container (45 cm long, 15 cm wide, and 35 cm high) and allowed to move about freely. The narrow width encourages the rat to orient itself sideways which makes scoring of the grooming behavior easier. The recordings generally lasted around 2-3 hours, depending in part on how much time the animal spent grooming.

In Paper III the rat was allowed to move freely within a circular open field, roughly 70 cm in diameter, where movement was tracked automatically and verified manually. When testing for catalepsy, the rat's forepaws were placed on a bar, and was deemed cataleptic if it did not move away for 30 s. The recordings consisted of 40-50 minutes baseline recording followed by drug injection. Depending on the drug used in the recording onset of catalepsy varied and for AMPT a second injection was also given. Around the time of onset of catalepsy subsequent tests were done at 30 minute intervals.

In Paper IV, the animal was kept lightly anesthetized using isoflurane while receiving cutaneous stimulation to its paws. The stimulation was tactile and performed with a hand-held stimulator, tapping the skin in bouts of 10 pulses, spaced 500 ms apart. Each paw had 16 sites that were stimulated in a pseudorandom order, using a known seed for the random generator so for later reconstruction, and repeated 15 times for a total of 150 stimulation on each of 32 sites.

Multiple recordings, before and after training was performed. The training consisted of a task where the rat learned to reach for food pellets through a slit

in the long and narrow box described for Paper I and II above.

Classification of behavior

Grooming phases in Paper I and II were manually scored from the videos offline, based of previous descriptions from Berridge and coworkers (Berridge et al., 1987), with the exception of phase 1 that was split into two separate phases; P1A and P1B. If a non-grooming behavior, such as a shake, was observed close to the grooming behavior, any phase close in time was excluded from analysis.

Construction of peri-stimulus/event time histograms

Peristimulus time histograms (PSTHs) and perievent time histograms (PETHs) for neurons around stimulations/events were constructed using an in-lab toolbox in MATLAB. Exact settings varied depending on project and the question posed, but the main parameters that was changed was if they were constructed using histograms or kernel density estimate (KDE), as well as bin size. For the histogram approach, the average firing rate within each time bin over the different events was calculated as the average number of spikes divided by bin size. For the KDE approach, each spike added a fraction to the time bins around it, using a gaussian distribution with standard deviation sigma, and where the sigma used was generally the same as the bin width. Meaning that instead of each spike adding a 1 to one bin, it adds a fraction to multiple bins, but still summing to 1.

Main Results

Main Results

Paper I

The grooming behavior in rats is classically described as having four phases, but from our observations we noted that the first phase looks very different when part of the prototypical grooming chain. This prompted us to classify it as two separate phases, for a total of five phases for all analysis in this project: P1A, P1B, P2, P3 and P4. In this paper we identified a total of 3697 grooming phases in seven rats where single unit activity was simultaneously recorded from 64 electrodes distributed between RFA, MI, DMS and DLS. The observed frequency of the phases varied a lot, where the most common ones were P1A and P2 which made up 80% of all phases (approximately 40% each). The least common was P1B which only constituted 3.5% of the phases. Additionally, the probability of switching to any given phase was clearly dependent on the current phase, and could be well described by a Markov chain. In order to find out whether it also depended on additional previous phases, two different analyses were employed. Firstly we noted that the transition probabilities between two phases could predict the longer phase combinations quite well (tested for combinations of 3, 4 and 5 phases), and secondly we noted that the uncertainty about the upcoming phase, in the sense of Shannon information, plateaued at a second order model, indicating that adding more information than the pairwise probabilities is largely unnecessary.

Except for RFA, all structures had a large excitatory response around start and end of the grooming behavior as a whole, that is, the beginning and end of grooming sequences. Notably the activity before onset reached peak activity shortly before the onset of behavior followed by a rapid decrease, and in striatum, even an inhibition immediately following onset, while activity around the offset was centered immediately on the behavioral transition. When further analysing the activity of units around both on- and offset we discovered

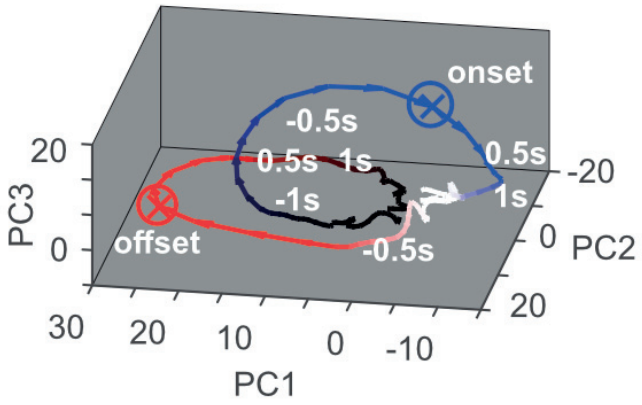

Figure 4: The first three principal components (PC1-3) from Paper I, Figure 2D, where the colored line traverses the components across time. Prior to grooming the line is black, and changes to blue as it draws closer to the onset of grooming (marked with a blue circled cross), and fades to white during grooming, which changes to red as it draws close to the offset of grooming (red circled cross) and fades back into black again after grooming. Note both the relative similarity of the in grooming and out of grooming states, and the conspicuous symmetry around on-/offset.

three different modulation types that are here named starters, stoppers and bracketers. As their names suggest, starters were modulated around the onset, while stoppers were modulated around the offset of grooming. Bracketers, on the other hand, were modulated before onset of behavior and after the offset. RFA differed from the other structures in that it had a peak in activity around two seconds before the start of the spontaneous grooming behavior. These cell groups were also reflected in the first principal components of the PETHs. When plotted together in one graph, the components also reveal some interesting symmetries, see Figure 4, which had to be left out of the published paper due to size constraints.

When it comes to the transition between phases, only MI had a significant fraction of modulated units around the time of transition. These cells had an even distribution of excitatory and inhibitory responders. The information present in the recorded structures about the upcoming phase transition also started to increase close to the transition. When dividing this last analysis by structure it was clear that the neurons in MI contributed most to this information (see Figure 5, which was not included in the published paper), although this could be because of the larger number of neurons recorded there than in the other structures ($N = 57/191/74/63$ for RFA/MI/DMS/DLS respectively).

Lastly we searched for an explanation for the observed transition probabilities in the neuronal code. From the firing rate of some neurons around different

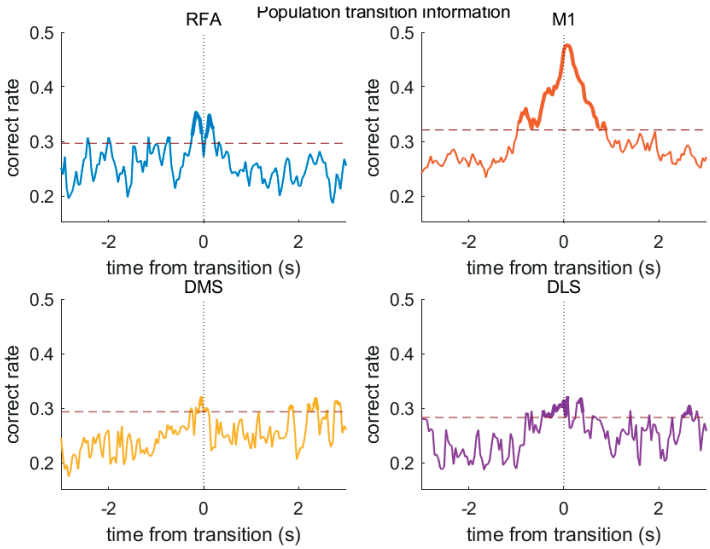

Figure 5: This is the same as figure 3C in Paper I, but including only cells from one area at a time. It shows that while all structures pass the chance threshold, at least briefly, MI has a much higher correct rate than the others. Note however that the total number of recorded neurons also was higher in MI.

transitions it was clear that this code could be quite complex, but we hoped that a simple measurement of average firing rates could capture some meaningful differences between the transitions. Indeed, by building a number of models that correlated Z-scored firing rates of units at a number of times around each transition event (using a pseudolinear discriminant analysis model for each time step), we found a significant correlation for neurons in MI and for MSNs in DMS.

Paper II

In order to elucidate if there is a correlation between neuronal firing rates and probability of transitioning out of the current phase at any given time, it was first necessary to determine the underlying distribution function that gives rise to the data. To that effect we first fitted a number of likely distribution functions to the observed data, each of which could explain the observed distributions with varying success.

Each model was fitted to the five phases using a sweep over the model parameters, where the parameters resulting in the lowest squared difference from the observed distributions were selected.

Firstly a regular homogenous Poisson model was fitted. As expected this yielded poor results as the distributions clearly do not follow an exponential decay. Next, two non-homogenous models were fitted. Here, the model parameter lambda were substituted for a time-dependent function, the first was one where lambda increased linearly, and the other exponentially over time. Both of these had decent fits, but the linear model failed to capture the very short peak of phase 1B and also had some trouble with the long tail of phase 4. On the other hand, while the exponential model had a much better fit for phase 1B, the distribution functions that captured the long tail of the observed distributions invariably did not decrease around t=0. However the two models that could capture the distributions the best were an Ornstein-Uhlenbeck drift-diffusion model, and a Weibull process.

From the fitted distribution functions, the corresponding hazard functions were extracted. The hazard function is the probability of transitioning from the current behavior at each time. For some of the distribution functions, the hazard function was already known or could be easily calculated analytically, but for the OU drift diffusion model, it was estimated directly from the fitted probability density function ($PDF(t)$) using the formula

$$\lambda = \frac{PDF(t)}{S(t)}$$

$$S(t) = Pr(T > t) = 1 - \int_0^t PDF(t)\, dt,$$

where $S(t)$ is the survival function of the $PDF(t)$, and is defined as the probability of surviving until at least time t, or in other words, one minus the area under the $PDF(t)$ from 0 until t. The hazard functions of the distribution functions were compared to the Z-scored firing rates of the units throughout the grooming phases, and revealed a significant correlation for units in MI for the two non-homogenous poisson processes, as well as for the OU drift diffusion distribution. It should be noted that while the hazard rates for both of the significant poisson processes were both strictly increasing, and were therefore somewhat similar, the OU hazard rate was more complex.

As a last step we looked for a direct correlation to the fitted input parameters of the different phases in the OU model, where we found a significant correlation in the DMS MSNs to both the drift parameter, diffusion parameter and the interaction between them.

Paper III

In this paper the dataset consist of 38 recordings from a total of 10 animals, and recordings from individual animals were spaced at least two days apart to make sure the previous drug was washed out from the system. All dopaminergic manipulations induced severe hypokinesia, making the animal virtually immobile. LFPs and unit activity was simultaneously recorded from a 128 channel electrode array with wires distributed between RFA, MI, DMS, DLS, GP, STN, SNr, and VA/VL in thalamus.

The time from drug injection to the onset of catalepsy varied depending on drug, where D1R antagonist (and D1R+D2R) was fastest at 20-30 minutes, followed by D2R at 90-120 minutes, and lastly AMPT at 200-300 minutes.

In the LFP the most noticeable effect from any of the drugs was a significant increase in the beta band (12-20 Hz) in cortex and striatum after injection with D2R antagonist, although there were also an increase in the same band in DLS for D1R+D2R, and in DMS for AMPT.

For the neuronal firing rates, for all drugs there were large population of cells that changed their firing rate, but the number of neurons with increased firing were roughly the same as the number that decreased their firing. The only combinations of drug, structure and cell type that showed a significantly shift in the number of units in either direction was MI PCs after D2R antagonist that had more up- than down regulated units, VA/VL after D1R+D2R antagonist that had more down- than up regulated units, and PCs in RFA and MI that also had more down- than up regulated units.

Another aspect that has been suggested could be even more important than the changes in average firing rate is the synchronization of single unit activity to slow wave oscillations that are known to have a relative increase following dopamine antagonist administration. Meaning that units are more likely to fire a spike at a specific phase in the LFP oscillation, for example at the peak of each oscillation. Upon inspection we found that a relatively large fraction of cells became significantly entrained to beta and/or theta (8-12 Hz) oscillations after drug injection. The results for specific sites and drugs were varied, but with exceptions, a higher fraction of cells were entrained to beta in cortex and striatum, and also to theta in cortex, than in the deeper structures.

Lastly we looked into the relationship between the observed neurophysiological changes over time and the onset of catalepsy with the goal to find possible links between the two. After D2R agonist injection, the increase in LFP beta power

was very rapid in cortex, striatum and VA/VL, and very late in GP, STN and SNr. After injection with D1R agonist, however, the onset of catalepsy occurred before any significant changes in the LFP beta power in any of the recorded structures. The firing rates of single units changed very rapidly after injection of either D1R or D2R making that a more likely cause for catalepsy.

Paper IV

In this paper we study the somatosensory input to the motor circuits. To this end we collected 21 recordings in a total of eight rats, where 16 sites on each paw were stimulated tactilely a total of 150 times per site. Most recording electrodes were placed in MI and DLS, but in a subset of the animals a smaller number were also implanted in each of RFA, DMS, GP, VA/VL,STN, and SNr.

Initially only pre-training recordings were studied. Here, most structures had a strong response in the hemisphere contralateral to the stimulation around 10-35 ms, but in the ipsilateral hemisphere the response was much weaker or even absent. This held true for both local field potential and neural firing rates, where over 30% of the neurons in MI and DLS were significantly modulated to the stimulation.

When we next moved to study the changes occurring due to the acquisition of the new reaching skill, we chose to study only MI and DLS due to the small dataset in the other structures. For these comparisons there were many levels upon which to reflect. The units were located contra- or ipsilateral to the stimulated paw, they were recorded from MI or DLS, there was a trained and an untrained paw, and the recordings were done before or after training.

One of the most eye-catching differences post-training could be seen in MI units, contralateral to stimulations of the trained paw, where a large late component could be seen in the PSTH response that wasn't there pre-training. The same late component could also be seen in MI units ipsilateral to the trained paw, and somewhat surprisingly also in units contralateral to the untrained paw.

Lastly we characterized the spatial distribution across the stimulated sites of the PSTHs. Here we found that the somatotopic arrangement of the input also changed as an effect of training, but only to a significant degree in the primary motor cortex and the nature of the change varied between animals.

Taken together these results suggests that a functional adaptation is taking place in these circuits.

Discussion

Discussion

This chapter contains reflections on the interesting findings in the four papers, as well as some broader observations and contemplation that go beyond the scope of any single study.

As mentioned earlier in this thesis, much of the details regarding the function of the BG loop remains unknown. Without this knowledge about the normal functioning of the brain it is not possible to understand how the changes caused by diseases of the brain, such as the loss of dopamine producing cells in Parkinson's disease, lead to the observed symptoms.

Paper I

This study provides knowledge about the involvement of corticostriatal circuits in the encoding of action sequencing. Some earlier studies have focused on reward driven, trained behaviors during a sequence where the same action is repeated a fixed number of times (Fujii and Graybiel, 2003; Jin and Costa, 2010; Jin et al., 2014), and while these have led to some very interesting results, it is unclear if it also applies to spontaneous natural behaviors. From the current study we now know that modulations similar to the Start/Stop signals that emerged in (Jin and Costa, 2010) also exist for the grooming behavior in largely non-overlapping cell groups in each of DMS, DLS, and MI, suggesting that these structures are important when moving from one behavior to another. Additionally, it shows that this type of coding is not necessarily acquired but does also exists for natural behaviors that are neither of fixed length or in a specific order. The last group of bracketers, though, were not present in their study. While the start and stop groups had a respective firing rate modulation before start and stop of grooming and could likely be more directly involved motor control, the bracketers were modulated before the onset of grooming and after the off-

set, which would make them more suited for a role like action evaluation (as proposed by, for example Smith and Graybiel (2013); Stephenson-Jones et al. (2013)). But in the current study, as mentioned, for a behavior with highly varying length and composition.

Whereas both MI and the striatum both were heavily involved in the on- and offset of the grooming behavior, only MI was modulated during the transitions between the phases. Also the information about the upcoming phase in the structures over time (Figure 5) would seemingly support this, although it cannot be discounted that was because of the larger number of neurons recorded in MI. Some effort was spent trying to discern if this was the case, using a bootstrapped confidence interval from models that used only a subset of the neurons in MI, but no clear conclusions could be drawn in either direction. This being said, there was a significant correlation between the transition probability and firing rates in DMS PCs, and also both cell groups of MI. Most of the individual neurons that were modulated to the transition probability had a negative correlation, meaning they have a higher firing rate around less likely transitions. Together with the late peak in significance in DMS, it might indicate an involvement in action evaluation.

It is noteworthy at this point that it has been shown that rats can perform movement such as lever pressing even after MI has been lesioned (Grillner, 2015; Kawai et al., 2015), so how come this is the only area where we have found modulations around transitions? It could be that the role of these neurons are not to control the behavior, but rather to monitor in order to facilitate general learning. This could also be the case for the encoded transition probability, where less usual transitions gave rise to higher firing rates. It should also be cautioned that this might hint at an important difference between rodents and humans as the effects of damage to the primary motor cortex in humans, from for example a stroke, can be severely debilitating.

Taken together these results are in line with the notion of stepwise control of the grooming behavior where each new phase (or termination of the sequence) is selected stochastically to some degree, as modeled by a simple Markov chain.

This study corroborates many of the findings of the recent work by Markowitz et al. (Markowitz et al., 2018), where they show the involvement of DLS MSNs the construction of behavioral sequences in mice, and show that their conclusions are also representative for other cell groups and structures in a more cohesive behavior.

While some of the analyses in this study that relied on the transitions with low probability could have benefited from a larger data set, it should be noted

that the current data set had four times as many recorded cells and three times as many scored grooming phases as any previous study (Aldridge et al., 1993; Aldridge and Berridge, 1998; Meyer-Luehmann et al., 2002).

Lastly, although many aspects in the encoding of action sequencing have been found in the investigated structures, other areas and mechanisms are likely also involved (Kalueff et al., 2015), possibly in concert with basal ganglia circuits.

The data presented here provides a first description of how neuronal ensembles in cortical and striatal circuits together encode the flexible sequencing of actions in a continuous, spontaneous, and natural motor behavior involving the combination of several distinct motor programs. An improved understanding of the mammalian cortico-basal ganglia system is, doubtless, also an important step toward improved therapies for motor disorders such as Parkinson's disease and for the development of more advanced prosthetic devices.

Paper II

In Paper I, no direct connection could be found between the firing rates of units and the duration spent in each phase. It is possible this could be because the corticostriatal circuits do not explicitly control the duration of behavior, but rather by influencing the probability of transitioning into another behavior.

With this hypothesis in mind we have here tested a number of models in an attempt to identify possible underlying probabilistic models that account for the observed distributions of phase durations.

The simplest model tested was a homogenous Poisson process, where the probability of transitioning, ie. the hazard function, is constant over time. This model was, however, quickly dismissed due to its poor fit. Next we tested an inhomogenous Poisson process with a linearly increasing hazard function. This could be explained by cumulative feedback to the neuronal circuit responsible for driving a transition. A similar mechanism has, for example, been observed in cell-groups with a pacemaking activity (Butera et al., 1999). Following this we also tested an inhomogenous Poisson process with an exponential hazard function, where a similar model has been used to describe transitions in C. elegans (Roberts et al., 2016). Next an Ornstein-Uhlenbeck drift diffusion model was tested, where the transition is modeled to occur when a threshold is reached through a random walk with an underlying drift component. Here the random walk would be represented by random firing of excitatory and inhibitory neurons in the network, and the long tails in the behavior arise when this firing, by

chance, moves away from the threshold in the beginning of a trial. Meanwhile, the drift component is a constant excitatory influence that drives the system towards the threshold, and can be thought of as an exogenous motor command signal (Uhlenbeck and Ornstein, 1930; Gerstein and Mandelbrot, 1964). Lastly a Weibul distribution was tested, which can be used to model a wide range of distributions with both increasing and decreasing hazard function over time (Weibul, 1951).

Most of these models could follow the distribution with relatively good success, but out of them the OU and Weibul models produced the best overall fits to the distributions. Out of these two, however, only the OU had a clear correlation between its hazard function and the neuronal firing rates, where the firing rate of MI PCs were significantly correlated to the momentaneous hazard rate. Notably, there was also a significant correlation to the OU model parameters of the different phases, but for the MSNs in DMS rather than the MI PCs.

These analyses suggest that the corticostriatal circuits regulate the duration of the individual phases of a grooming sequence by setting the probability of transitioning over time rather than sending explicit commands.

Paper III

One of the most commonly reported markers in patients with Parkinson's disease, and dopamine depletion in general, is an increase in beta power oscillations in the cortex and striatum (Sebban et al., 1999; Brown et al., 2001; Cassidy et al., 2002; Priori et al., 2004; Costa et al., 2006; Mallet et al., 2008; Dejean et al., 2009, 2011). The results shown here are in line with most of these studies, including the findings of Degos et al. (Degos et al., 2009), who found an increase in beta power synchronization only in chronic dopamine depletion and not during acute dopamine interruption (using the same D1R and D2R antagonsists as in this paper). At a glance their result seem to differ from our, but in fact corresponds with ours as they only report that the the beta power does not increase in motor and sensory cortex after D1R+D2R antagonist, which matches the D1R+D2R sessions in this paper, where we only saw a significant beta power increase in DLS. In our findings we do, however, see an increase in beta power in MI and RFA (and additionally in DLS and DMS) following only D2R antagonist, possibly hinting at an important difference between the two BG pathways.

The causal link between the beta power oscillations and the motor symptoms of

Parkinson's disease has been under debate, in part because they are suppressed by motor activity (Brittain and Brown, 2014), and also because these oscillations often appear after the emergence of akinesia following 6-OHDA lesions (Mallet et al., 2008; Degos et al., 2009). In this study, we observed a rapid increase in beta power following D2R antagonist injection that appeared well before the onset of catalepsy, for D1R antagonist however, it was not reliably observed before the onset of catalepsy in any of the structures. This would seem to disprove a causal link of an increase in beta power oscillation leading to akinesia in most of the cortico-basal ganglia-thalamic network.

As for the change in the spiking frequency of the recorded neurons, although a large fraction of the cells had a significant change in firing rate as an effect of each drug, these changes were largely balanced, where few cell groups had predominant change in either direction. It is also worth noting that these changes did not follow what would be expected from a change in dopamine in the striatal input of the direct- and indirect pathway (Albin et al., 1989), that would predict a decreased activity in GP of the indirect pathway following D2R antagonist and an increased activity the BG output nucleus SNr following both D1R and D2R antagonism, which we did not observe. We did however see a significant number of neurons with decreased firing in VA/VL following D1R+D2R antagonist, which could be due to an increased inhibition from SNr. It could also be important to note that in rats there are no neurons that project purely along the direct pathway as all neurons projecting from striatum to SNr also send collaterals to GP (Wu et al., 2000).

It is also important to remember that this acute scenario might differ from a chronic depletion of dopamine, as there might be long term changes that does not have time to manifest over the course of a recording. The type of acute manipulations done in this study do, however, have the strength of allowing us to follow the change in the neuronal circuit, capturing both baseline and the gradual transition into the drug affected state within the same recording.

The diverse firing rate changes observed here is hard to capture within a unified framework without further study, but the fact that rate changes were consistently observed prior to any motor symptoms could hint at an important underlying mechanism, and doubtlessly deserves to be investigated further.

Paper IV

In this paper we ask how somatosensory information is represented in the motor circuit of the cortico-basal ganglia loop and whether it changes as new motor skills are acquired. To do this we have recorded spiking as well as LFP activity in structures throughout the loop during tactile stimulation of the rat forepaw before and after intensive training to acquire a new motor skill.

In the initial analyses we found that sensory input provoked a strong response contralaterally to the stimulation site in all recorded structures, while the ipsilateral side exhibited a much weaker, sometimes even negligible response. The peak response latency on the contralateral side differed between structures and for the EPs neatly followed the expected order, for the PSTHs though, some of the deeper structures had a surprisingly fast response, although it should be cautioned that the PSTHs had a comparatively poor time resolution at 5 ms between timepoints, considering the average latency of 20 ms.

After the acquisition of a, for the rat, novel motor skill through intensive training where it learned to utilize its paw in a new way, a conspicuous late component in the PSTHs emerged. This second peak was most clearly seen in MI, in neurons contralaterally to stimulations of the trained paw, although it could also be seen ipsilaterally to the trained paw as well as contralaterally to the untrained paw, the last of which might indicate a cross education effect of training (Ruddy and Carson, 2013).

When comparing receptive fields in neurons for the 16 sites in each paw, it was clear that the biggest and most cohesive change was in MI neurons contralateral to the stimulated sites of the trained paw. For the receptive fields we focused on the early component of the PSTHs as there was no large variation in the response between sites in the late component, and it is also hard to reason around a change for receptive fields that were mostly not present before training. In the early component we found that the receptive fields were generally more similar between recordings after training than before training. Although the average change of the receptive fields varied from animal to animal, the largest effect of training was seen in radial, rather than ulnar sites, which could likely be of functional importance to the reaching task (Palmér et al., 2012).

These results support the notion that somatosensory input to, at least, the primary motor cortex is reorganized by the aquisition of a new motor skill. This can be taken to indicate that the functionally relevant input to the corticostriatal circuits (Asanuma et al., 1968; Asanuma and Rosén, 1972; Rosén and Asanuma, 1972), continuously change to reflect newly acquired functions and skills.

Overarching Observations

A common theme throughout these studies is the heavy involvement of MI in most of the tests relating to motor generation. It is perhaps not surprising to find correlations of movement in the primary primary motor cortex, but it is striking that so many different aspects of movement can be found reflected in MI neurons. Where the involvement of single units is studied, we commonly found a fraction of 15-30% of the cells in MI to be modulated to the current test, which can lead one to wonder just how many different aspects of movement each neuron is involved in. It is easy to envision a neuron as having one particular task; when this neuron fires a spike it is time to do this specific thing, but if a large fraction of the neurons is involved in each of so many different aspects of movement then naturally each neuron must be involved in several aspects. This is, of course, also much more resource efficient. As an example, imagine an array of N zeroes or ones, where each binary number represents one neuron and the state represents whether the neuron is currently active or not. Now, if each one is responsible for one specific thing, the array could encode N such things. If the array instead held a bitcode, where each unique combination represented a specific thing, the array could instead represent N^2 things, which, with the vast number of neurons in the brain, could represent an unimaginably large number of states. The drawback, however, of encoding something as a bitcode rather than having each neuron/number representing only one thing, is that it is impossible to represent more than one thing simultaneously. Seeing how hard it is to actively focus on more than one thing at a time, but also that we can multitask fairly well at least for moderately automated tasks, the truth is likely somewhere between the two.

This type of encoding, where a state or decision is represented across many neurons, and no single one holds the key to an outcome by itself, is called ensemble coding. This concept is definitely not new, as it stems back to the 1950s where Donald Hebb wrote about cell assemblies as "a diffuse structure comprising cells in the cortex and diencephalon, capable of acting briefly as a closed system, delivering facilitation to other such systems". More recently Andrew Schwartz's lab and others have successfully controlled prosthetic devises and robot arms using the assumption that the desired motor outcome can be decoded from a linear combination of the activity of neurons (Velliste et al., 2008) This approach is very similar to what was done in Paper I for the information content of the recorded neurons about an upcoming change in grooming. This type of measurement is interesting in that it requires that the modulation in relation to the trained classes, such as the different upcoming phases in this case, can actually differentiate between the classes, and as such is a stricter requirement

than just a change in average firing rate across trials. When this analysis was done for units split by recording area, it was clear that the models trained on units recorded in MI had a much higher chance to predict the upcoming phase than the other areas. This was not included in that paper, however as we could not discount the possibility that the higher predictive rate was due to the higher number of units recorded this structure.

This line of reasoning extends further to the concept of neural manifolds, where the neuronal activity can be modeled well by a lower dimensional space of so called latent variables (Gallego et al., 2017; Yu et al., 2009). In its simplest, linear, form this can be the principal components from a principal component analysis (PCA), that can reveal the underlying dynamics of the data. In Paper I and IV, this approach was used to find the most common types of modulation in the data and was very helpful in revealing some of the ways single units as well as the network as a whole respond to a situation (transitioning into/out of grooming for Paper I, and the average response profiles to stimulations of the paw for Paper IV). In Paper I an additional approach that was done but left out of the paper due to size constraints, and that much resembles what is presented in (Gallego et al., 2017) is to plot the first three principal components (Figure 4, constructed from the same data presented in Figure 2D of Paper I). From this combined view it is possible to do some observations that would be hard to see in the separated components. Firstly, the white and black parts of the lines are much closer than the colored parts of the lines, indicating that the states within and out of grooming are much more similar than the dynamics around transition into and out of grooming. Secondly, there is a clear symmetry between onset and offset, which hints that the onset and offset of grooming are represented as polar opposites in some group of units. Thirdly, while some opposites exist, there is clearly some parts of the modulation that is in the same direction (PC1) and some that are orthogonal (PC2 and PC3, individually).

In recent years the huge leaps in the field of AI and deep learning has led to some remarkable advances, from which I believe we will see many benefits in the field of neuroscience. One such benefit that has already revealed itself is the automatic tracking of animals in videos through advanced image recognition with the help of deep neural networks (Mathis et al., 2018). This type of advance will both spare researchers countless hours of manual tracking such as, for example, was done in Paper I in this thesis, and allow for more complex and dynamic behaviors to be tracked with a level of detail we could previously only dream of.

Reversely, the field of AI probably has a lot to gain from advances in neuroscience as well, seeing how many deep neural networks are modeled after the brain. I

also believe many advances can be made from modelling networks based on the dynamics of the BG loop. One example of such a success story is the DeepMind reinforcement learning research group that, with David Silver in the lead, developed the AlfaGo network that managed to beat the sitting world champion at the game of go a few years back (Silver et al., 2016). This group also recently published a paper about dopamine-based reinforcement learning, where they propose that the expectation for a future reward in the brain is represented as a distribution rather than a scalar value. They developed the theory based on advances in artificial intelligence, and found supporting evidence in mice, further highlighting the mutual benefits these fields have to gain from each other (Dabney et al., 2020).

Another advance that has opened the path for much more detailed questions to be asked is optogenetics. Through specific targeting using cleverly engineered viruses, specific cell groups can be made to express light sensitive receptors. With this method it is possible to mark cells that, to mention just a few examples, project to a specific area, receives input from a specific area, expresses some specific genes, or even cells that have been recently active. These cells can be made to express fluorescent proteins for visual identification, but it is also possible to excite or inhibit them when exposed to light of specific wavelengths. With the help of optogenetics, our view of the brain might be, quite literally, elucidated.

References

References

1

Albin, R. L., Young, A. B., and Penney, J. B. (1989). The functional anatomy of basal ganglia disorders. *Trends in neurosciences*, 12(10):366–375.

Aldridge, J. W. and Berridge, K. C. (1998). Coding of serial order by neostriatal neurons: a "natural action" approach to movement sequence. *The Journal of neuroscience : the official journal of the Society for Neuroscience*, 18(7):2777–87.

Aldridge, J. W., Berridge, K. C., Herman, M., and Zimmer, L. (1993). Neuronal Coding of Serial Order: Syntax of Grooming in the Neostriatum. *Psychological Science*, 4(6):391–395.

Apps, R. and Garwicz, M. (2005). Anatomical and physiological foundations of cerebellar information processing. *Nature Reviews Neuroscience*, 6(4):297–311.

Asanuma, H. and Rosén, I. (1972). Functional role of afferent inputs to the monkey motor cortex. *Brain research*, 40(1):3–5.

Asanuma, H., Stoney, S. D., and Abzug, C. (1968). Relationship between afferent input and motor outflow in cat motorsensory cortex. *Journal of Neurophysiology*, 31(5).

Bennett, C., Miller, M., and Wolford, G. (2009). Neural correlates of interspecies perspective taking in the post-mortem Atlantic Salmon: an argument for multiple comparisons correction. Technical report.

Berke, J. D. (2011). Functional properties of striatal fast-spiking interneurons. *Frontiers in Systems Neuroscience*, 5(JUNE 2011).

Berridge, K. C., Fentress, J. C., and Parr, H. (1987). Natural syntax rules control action sequence of rats. *Behavioural brain research*, 23(1):59–68.

Brittain, J. S. and Brown, P. (2014). Oscillations and the basal ganglia: Motor control and beyond.

Brodmann, K. (1909). *Vergleichende Lokalisationslehre der Grosshirnrinde*.

Brown, P., Oliviero, A., Mazzone, P., Insola, A., Tonali, P., and Di Lazzaro, V. (2001). Dopamine dependency of oscillations between subthalamic nucleus and pallidum in Parkinson's disease. Technical Report 3.

Butera, R. J., Rinzel, J., and Smith, J. C. (1999). Models of respiratory rhythm generation in the pre-Botzinger complex. I. Bursting pacemaker neurons. *Journal of Neurophysiology*, 82(1):382–397.

Calabresi, P., Picconi, B., Tozzi, A., Ghiglieri, V., and Di Filippo, M. (2014). Direct and indirect pathways of basal ganglia: A critical reappraisal.

Cassidy, M., Mazzone, P., Oliviero, A., Insola, A., Tonali, P., Di Lazzaro, V., and Brown, P. (2002). Movement-related changes in synchronization in the human basal ganglia. *Brain : a journal of neurology*, 125(Pt 6):1235–1246.

Cenci, M. A., Jörntell, H., and Petersson, P. (2018). On the neuronal circuitry mediating L-DOPA-induced dyskinesia. *Journal of neural transmission (Vienna, Austria : 1996)*, 125(8):1157–1169.

Costa, R. M., Lin, S. C., Sotnikova, T. D., Cyr, M., Gainetdinov, R. R., Caron, M. G., and Nicolelis, M. A. L. (2006). Rapid Alterations in Corticostriatal Ensemble Coordination during Acute Dopamine-Dependent Motor Dysfunction. *Neuron*, 52(2):359–369.

Dabney, W., Kurth-Nelson, Z., Uchida, N., Starkweather, C. K., Hassabis, D., Munos, R., and Botvinick, M. (2020). A distributional code for value in dopamine-based reinforcement learning. *Nature*, 577(7792):671–675.

Degos, B., Deniau, J. M., Chavez, M., and Maurice, N. (2009). Chronic but not acute dopaminergic transmission interruption promotes a progressive increase in cortical beta frequency synchronization: Relationships to vigilance state and akinesia. *Cerebral Cortex*, 19(7):1616–1630.

Dejean, C., Arbuthnott, G., Wickens, J. R., le Moine, C., Boraud, T., and Hyland, B. I. (2011). Power fluctuations in beta and gamma frequencies in rat globus pallidus: Association with specific phases of slow oscillations and differential modulation by dopamine D1 and D2 receptors. *Journal of Neuroscience*, 31(16):6098–6107.

Dejean, C., Hyland, B., and Arbuthnott, G. (2009). Cortical effects of subthalamic stimulation correlate with behavioral recovery from dopamine antagonist induced akinesia. *Cerebral Cortex*, 19(5):1055–1063.

DeLong, M. R. (1990). Primate models of movement disorders of basal ganglia origin.

Ekerot, C. F., Garwicz, M., and Schouenborg, J. (1991). Topography and nociceptive receptive fields of climbing fibres projecting to the cerebellar anterior lobe in the cat. *The Journal of Physiology*, 441(1):257–274.

Fee, M. S., Mitra, P. P., and Kleinfeld, D. (1996). Automatic sorting of multiple unit neuronal signals in the presence of anisotropic and non-Gaussian variability. *Journal of Neuroscience Methods*, 69(2):175–188.

Fujii, N. and Graybiel, A. M. (2003). Representation of action sequence boundaries by macaque prefrontal cortical neurons. *Science (New York, N.Y.)*, 301(5637):1246–9.

Gallego, J. A., Perich, M. G., Miller, L. E., and Solla, S. A. (2017). Neural Manifolds for the Control of Movement. 94(5):978–984.

Gerstein, G. L. and Mandelbrot, B. (1964). Random walk models for the spike activity of a single neuron. *Biophysical journal*, 4:41–68.

Graybiel, A. (1998). The basal ganglia and chunking of action repertoires. *Neurobiology of learning and memory*, 70(1-2):119–36.

Graybiel, A. M. (2000). The Basal ganglia.

Graziano, M. S. A., Aflalo, T. N. S., and Cooke, D. F. (2005). Arm Movements Evoked by Electrical Stimulation in the Motor Cortex of Monkeys. *J Neurophysiol*, 94:4209–4223.

Grillner, S. (2015). Action: The Role of Motor Cortex Challenged.

Grillner, S. and Robertson, B. (2016). The Basal Ganglia Over 500 Million Years.

Groenewegen, H. J. (2003). The basal ganglia and motor control.

Halje, P., Tamtè, M., Richter, U., Mohammed, M., Cenci, M. A., and Petersson, P. (2012). Levodopa-induced dyskinesia is strongly associated with resonant cortical oscillations. *The Journal of neuroscience : the official journal of the Society for Neuroscience*, 32(47):16541–51.

Hegeman, D. J., Hong, E. S., Hernández, V. M., and Chan, C. S. (2016). The external globus pallidus: Progress and perspectives.

Ivica, N., Tamtè, M., Ahmed, M., Richter, U., and Petersson, P. (2014). Design of a high-density multi-channel electrode for multi-structure parallel recordings in rodents. In *36th Annual International IEEE EMBS Conference of the IEEE Engineering in Medicine and Biology Society*, pages 393–396.

Jin, X. and Costa, R. M. (2010). Start/stop signals emerge in nigrostriatal circuits during sequence learning. *Nature*, 466(7305):457–62.

Jin, X., Tecuapetla, F., and Costa, R. M. (2014). Basal ganglia subcircuits distinctively encode the parsing and concatenation of action sequences. *Nature neuroscience*, 17(3):423–30.

Kalueff, A. V., Stewart, A. M., Song, C., Berridge, K. C., Graybiel, A. M., and Fentress, J. C. (2015). Neurobiology of rodent self-grooming and its value for translational neuroscience. *Nature Reviews Neuroscience*, 17(1):45–59.

Kandel, E. R., Schwartz, J. H., and Jessell, M. T. (2000). *Principles of neural science*. McGraw-Hill Health Professions Division, New York, 4th ed. edition.

Kawai, R., Markman, T., Poddar, R., Ko, R., Fantana, A. L., Dhawale, A. K., Kampff, A. R., and Ölveczky, B. P. (2015). Motor cortex is required for learning but not for executing a motor skill. *Neuron*, 86(3):800–12.

Mallet, N., Pogosyan, A., Sharott, A., Csicsvari, J., Bolam, J. P., Brown, P., and Magill, P. J. (2008). Disrupted dopamine transmission and the emergence of exaggerated beta oscillations in subthalamic nucleus and cerebral cortex. *Journal of Neuroscience*, 28(18):4795–4806.

Markowitz, J. E., Gillis, W. F., Beron, C. C., Neufeld, S. Q., Robertson, K., Bhagat, N. D., Peterson, R. E., Peterson, E., Hyun, M., Linderman, S. W., Sabatini, B. L., and Datta, S. R. (2018). The Striatum Organizes 3D Behavior via Moment-to-Moment Action Selection. *Cell*, 174(1):44–58.e17.

Mathis, A., Mamidanna, P., Cury, K. M., Abe, T., Murthy, V. N., Mathis, M. W., and Bethge, M. (2018). DeepLabCut: markerless pose estimation of user-defined body parts with deep learning. *Nature Neuroscience*, 21(9):1281–1289.

Meyer-Luehmann, M., Thompson, J. F., Berridge, K. C., and Aldridge, J. W. (2002). Substantia nigra pars reticulata neurons code initiation of a serial pattern: implications for natural action sequences and sequential disorders. *European Journal of Neuroscience*, 16(8):1599–1608.

Mink, J. W. (1996). The basal ganglia: focused selection and inhibition of competing motor programs. *Progress in neurobiology*, 50(4):381–425.

Morris, G., Arkadir, D., Nevet, A., Vaadia, E., and Bergman, H. (2004). Coincident but distinct messages of midbrain dopamine and striatal tonically active neurons. *Neuron*, 43(1):133 – 143.

Nambu, A., Tokuno, H., and Takada, M. (2002). Functional significance of the cortico-subthalamo-pallidal 'hyperdirect' pathway.

Palmér, T., Tamtè, M., Halje, P., Enqvist, O., and Petersson, P. (2012). A system for automated tracking of motor components in neurophysiological research. *Journal of neuroscience methods*, 205(2):334–44.

Penfield and Rasmussen (1950). *The Cerebral Cortex of Man*, volume 1.

Petersson, P., Waldenström, A., Fåhraeus, C., and Schouenborg, J. (2003). Spontaneous muscle twitches during sleep guide spinal self-organization. *Nature*, 424(6944):72–5.

Priori, A., Foffani, G., Pesenti, A., Tamma, F., Bianchi, A. M., Pellegrini, M., Locatelli, M., Moxon, K. A., and Villani, R. M. (2004). Rhythm-specific pharmacological modulation of subthalamic activity in Parkinson's disease. *Experimental Neurology*, 189(2):369–379.

Rizzolatti, G. and Craighero, L. (2004). THE MIRROR-NEURON SYSTEM. *Annual Review of Neuroscience*, 27(1):169–192.

Roberts, W. M., Augustine, S. B., Lawton, K. J., Lindsay, T. H., Thiele, T. R., Izquierdo, E. J., Faumont, S., Lindsay, R. A., Britton, M. C., Pokala, N., Bargmann, C. I., and Lockery, S. R. (2016). A stochastic neuronal model predicts random search behaviors at multiple spatial scales in C. elegans. *eLife*, 5:1–41.

Rosén, I. and Asanuma, H. (1972). Peripheral afferent inputs to the forelimb area of the monkey motor cortex: input-output relations. *Experimental brain research. Experimentelle Hirnforschung. Expérimentation cérébrale*, 14(3):257–73.

Ruddy, K. L. and Carson, R. G. (2013). Neural pathways mediating cross education of motor function. *Frontiers in Human Neuroscience*, 7(JUL):397.

Sato, F., Lavallée, P., Lévesque, M., and Parent, A. (2000). Single-axon tracing study of neurons of the external segment of the globus pallidus in primate. *Journal of Comparative Neurology*, 417(1):17–31.

Schmidt, R., Leventhal, D. K., Mallet, N., Chen, F., and Berke, J. D. (2013). Canceling actions involves a race between basal ganglia pathways. *Nature Neuroscience*, 16(8):1118–1124.

Schouenborg, J. and Weng, H.-R. (1994). Sensorimotor transformation in a spinal motor system. *Experimental Brain Research*, 100(1):170–174.

Schultz, W. (2016). Reward functions of the basal ganglia. *Journal of Neural Transmission*, 123(7):679–693.

Sebban, C., Zhang, X. Q., Tesolin-Decros, B., Millan, M. J., and Spedding, M. (1999). Changes in EEG spectral power in the prefrontal cortex of conscious rats elicited by drugs interacting with dopaminergic and noradrenergic transmission. *British Journal of Pharmacology*, 128(5):1045–1054.

Silver, D., Huang, A., Maddison, C. J., Guez, A., Sifre, L., Van Den Driessche, G., Schrittwieser, J., Antonoglou, I., Panneershelvam, V., Lanctot, M., Dieleman, S., Grewe, D., Nham, J., Kalchbrenner, N., Sutskever, I., Lillicrap, T., Leach, M., Kavukcuoglu, K., Graepel, T., and Hassabis, D. (2016). Mastering the game of Go with deep neural networks and tree search. *Nature*, 529(7587):484–489.

Smith, K. and Graybiel, A. (2013). A Dual Operator View of Habitual Behavior Reflecting Cortical and Striatal Dynamics. *Neuron*, 79(2):361–374.

Stephenson-Jones, M., Kardamakis, A. A., Robertson, B., and Grillner, S. (2013). Independent circuits in the basal ganglia for the evaluation and selection of actions. *Proceedings of the National Academy of Sciences*, 110(38):E3670–E3679.

Tamtè, M., Brys, I., Richter, U., Ivica, N., Halje, P., and Petersson, P. (2016). Systems-level neurophysiological state characteristics for drug evaluation in an animal model of levodopa-induced dyskinesia. *Journal of neurophysiology*, 115(3):1713–29.

Uhlenbeck, G. E. and Ornstein, L. S. (1930). On the Theory of the Brownian Motion. *Physical Review*, 36(5):823–841.

Velliste, M., Perel, S., Spalding, M. C., Whitford, A. S., and Schwartz, A. B. (2008). Cortical control of a prosthetic arm for self-feeding. *Nature*, 453(7198):1098–1101.

Weibul, W. (1951). A Statistical Distribution Function of Wide Applicability. *J. Appl. Mech.*

Wu, Y., Richard, S., and Parent, A. (2000). The organization of the striatal output system: A single-cell juxtacellular labeling study in the rat. *Neuroscience Research*, 38(1):49–62.

Yu, B. M., Cunningham, J. P., Santhanam, G., Ryu, S. I., Shenoy, K. V., and Sahani, M. (2009). Gaussian-Process Factor Analysis for Low-Dimensional Single-Trial Analysis of Neural Population Activity. *Journal of Neurophysiology*, pages 614–635.

Appendix

Scientific publications

Author contributions

Co-authors are abbreviated as follows:
Joel Sjöbom (**JS**), Martin Tamtè (MT), Nedjeljka Ivica (NI), Pär Halje (PH), Luciano Censoni (LC), Ulrike Richte (UR), Ivani Brys (IB), Kalle Åström (KÅ), Per Petersson (PP).

Paper I: Cortical and striatal circuits together encode transitions in natural behavior

JS did all visualisation, statistics, and analysis, except the ones surrounding Figure 1A, B and E, and 2A. **JS** also interpreted the results, did some of the data sorting, helped write parts of the manuscript and reviewed the manuscript. MT did the study design and the majority of data collection and data sorting, and helped interpret the results. PH did the visualisation, analysis and statistics surrounding the figures mentioned above, and helped interpret the results. IB collected data for the EMG control experiments. PP did the study design, interpreted results, and wrote and reviewed the manuscript.

Paper II: Neuronal correlates of probabilistic models describing the duration of actions in sequential behavior

JS and PH did study design. **JS** did all statistics and visualisation, and the majority of the analysis. PH calculated the hazard functions, and KÅ defined a mathematical OU model. **JS**, PH and PP interpreted the results, and PP wrote the manuscript with help from PH and **JS**.

Paper III: Changes in neuronal activity of cortico - basal ganglia – thalamic networks induced by acute dopaminergic manipulations in rats

NI performed the naive drug-treated animal experiments and sorted the unit data; UR and **JS** developed analytical approaches and analyzed the data; IB and MT performed experiments in 6-OHDA lesioned animals; PP and NI designed the experiments, contributed in analyses and wrote the manuscript.

Paper IV: The organization of somatosensory input to cortico-striatal circuits is functionally adapted following practice of skilled reaching

NI collected all the data, NI and PP did the study design, and **JS**, LC and UR did the analysis, figures and statistics. **JS**, LS and PP wrote the manuscript, and NI and UR commented.

Paper I

NEUROPHYSIOLOGY

Cortical and striatal circuits together encode transitions in natural behavior

Joel Sjöbom[1], Martin Tamtè[1], Pär Halje[1], Ivani Brys[1]*, Per Petersson[1,2†]

In natural behavior, we fluidly change from one type of activity to another in a sequence of motor actions. Corticostriatal circuits are thought to have a particularly important role in the construction of action sequences, but neuronal coding of a sequential behavior consisting of different motor programs has not been investigated at the circuit level in corticostriatal networks, making the exact nature of this involvement elusive. Here, we show, by analyzing spontaneous self-grooming in rats, that neuronal modulation in motor cortex and dorsal striatum is strongly related to transitions between behaviors. Our data suggest that longer action sequences in rodent grooming behavior emerge from stepwise control of individual behavioral transitions, where future actions are encoded differently depending on current motor state. This state-dependent motor coding was found to differentiate between rare behavioral transitions and as opposed to more habitual sequencing of actions.

INTRODUCTION

Natural behaviors generally consist of distinct action phases that are sequentially implemented and that can be flexibly combined depending on the behavioral context and goals. Corticostriatal circuits are considered to play a central role in the organization of this behavior (*1*). However, rather than analyzing complex action sequences, consisting of several discrete motor programs, previous neurophysiological studies of this circuitry have mainly focused on simple movements that animals are trained to repeatedly perform in expectation of a reward, e.g., saccades or movement of a manipulandum (*2*–*4*). While this experimental design has led to several important insights, e.g., relating to the gradual automatization of learned behaviors involving bouts of repetitive stereotypic movements (*3*, *5*, *6*), it tells little about the neuronal control of natural behaviors involving complex action sequences. More recently, imaging of calcium dynamics of medium spiny neurons (MSNs) in the dorsal part of the striatum has been used to assess activity changes in this cell group in mice during spontaneous behavior in an open field (*7*–*9*). These experiments have the advantage of encompassing natural behaviors, which are, however, nonstereotypical and are displayed as a continuum of behaviors with different kinematics, including, e.g., different locomotion speeds and turning behaviors. Other studies have experimentally interfered with the corticostriatal processing by local stimulation of neuronal populations in the striatum and cortex. The outcome of these experiments have, however, been quite diverse and difficult to incorporate into a single conceptual framework, reporting changes in action selection and movement reaction time (*10*, *11*), movement velocity (*12*), contraversive turning behavior (*13*), probability of maintaining an ongoing behavior (*14*), etc. A probable limitation to this experimental approach is the patchy organization of the striatum, where cells located close to each other are considered functionally dissimilar, leading to mixed effects (*15*). Here, we instead used chronic multielectrode neuronal recordings combined with detailed analyses of complex motor behavior that allowed us to obtain information from neuronal circuits that can also belong to different, but spatially overlapping, subsystems. We analyzed the spontaneous grooming behavior displayed by rodents, which represents a natural complex behavior that includes sequential execution of discrete action phases consisting of a limited number of highly stereotypic motor programs, each with well-characterized kinematic features, which are governed by brainstem circuits (*16*). These motor programs are often implemented in specific sequences (*17*, *18*) but can also be flexibly concatenated such that the involved action phases are expressed in various combinations (see Supplementary Movies). Convincing evidence that striatal circuits are involved in the control of this behavior has been presented, e.g., by Cromwell and Berridge (*19*) who showed that lesions as small as 1 mm^3 in the dorsolateral striatum disrupts grooming sequencing while animals are still able to execute the individual grooming phases. Using rodent grooming as a model behavior (*20*), we have, here, performed a comprehensive study of how corticostriatal networks encode the organization of actions in complex action sequencing.

RESULTS

Action sequencing in grooming

Spontaneous grooming was studied in seven rats and analyzed offline on the basis of video recordings. The grooming events displayed [$n = 67 \pm 32$ per rat (means ± SD)] were composed of a number of discrete phases ($n = 3697$ in total), defined according to previously described criteria. These phases have been reported to often occur in a rapid succession (P1, rapid elliptical strokes; P2, asymmetrical strokes; P3, bilateral strokes; and P4, body licking], sometimes referred to as a grooming "chain" (*21*). However, in the current dataset, sequences containing several other phase combinations were much more commonly observed (see Supplementary Movies). Notably, in such "non-chain" grooming patterns (encompassing >93% of the phases), the rapid elliptical stroke phase was replaced by another motor pattern involving licking and stroking of the forepaws. This prompted us to divide the P1 phase into two different phases, where every P1B event signaled the start of an in-chain grooming event, whereas P1A was selective for non-chain events. When analyzing the total lengths of all observed sequences, we found that sequences were actually not biased toward a specific number of phases. Instead,

[1]Integrative Neurophysiology and Neurotechnology, Department of Experimental Medical Sciences, Lund University, Sweden. [2]Department of Integrative Medical Biology, Umeå University, Sweden.
*Present address: Universidade Federal do Vale do São Francisco, José de Maniçoba, s/n Centro, Petrolina, PE, Brazil.
†Corresponding author. Email: per.petersson@umu.se

sequence lengths followed a roughly exponential distribution, indicating that the overall probability of terminating a sequence is relatively constant and independent of the number of phases performed so far (Fig. 1A). We therefore analyzed the transition probabilities between all types of phases in further detail, including the probability of terminating a grooming sequence. The five phases differed substantially in their relative frequency of occurrence, and some phase transitions were clearly more common than others (Fig. 1B, top; while this distribution was very similar across animals and sequence length; fig. S1). Yet, transition probabilities between pairs of phases were not trivially determined by the overall frequency of occurrence of the individual phases [e.g., phase transitions that were also part of the prototypical grooming chain (1B - 2 - 3 - 4) (*18*) were found to be overrepresented; Fig. 1B, middle/bottom]. These probabilities were remarkably stable across animals with a correlation coefficient of 0.90 ± 0.063 (means ± SD; fig. S1). Similarly, the probability of exiting the grooming behavior was not the same from all phases [$P < 0.001$; chi-squared test, $\chi^2(4, n = 3634) = 752$]. We also found that the observed pairwise transition probabilities can be used to successfully model both the observed frequency of specific grooming phase permutations (Fig. 1C) and the full length of the entire grooming sequences (Fig. 1A, black line) as a series of stepwise transition probabilities (creating a mathematical Markov chain). This implies that the future state depends primarily on the current state and not on the events that occurred before it. A notion that was further strengthened by an analysis of the decrease in uncertainty about the upcoming phase as a function of model order (Fig. 1D) (*22*). Last, we found that the durations of grooming phases differed considerably both within and between different types of phases (Fig. 1E) but not between animals [two-way analysis of variance (ANOVA); $P < 0.001$ for phase type and not significant for animal]. Notably, in contrast to the other phases, 1B showed a comparatively small variance in duration and generally contained the same number of movements, i.e., six to eight rapid repetitive elliptical strokes [compare (*3*, *6*)].

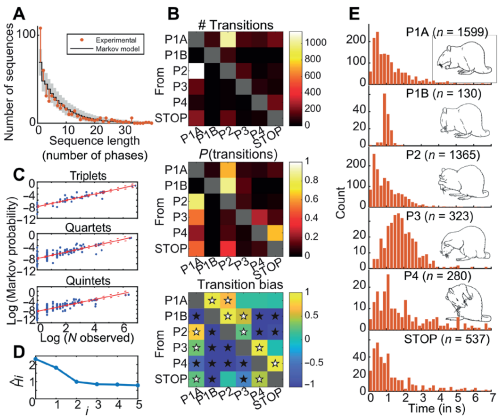

Fig. 1. The organization of the grooming behavior. (**A**) Histogram of the number of phases making up all the observed grooming sequences (shown for sequences that have less than 40 phases, only 1.3% were longer). Markov model of predicted sequence length distribution overlaid with 95% confidence interval (CI). (**B**) Phase transitions. (Top) Total number observed of each type; range, [0 to 1144]. (Middle) Conditioned transition probability [0 to 1] (probability of going to a given column given the current state, indicated by row). (Bottom) Transition bias (transition pairs where the conditioned probability significantly deviates from the expected number on the basis of the observed frequency of the constituent parts; white/black stars denote statistical over-/underrepresentation, outside a bootstrapped 95% CI). (**C**) Calculated Markov probabilities for higher-order transition sequences containing specific combinations of phases (containing 3, 4, and 5 phases, respectively) plotted against the corresponding observed numbers within all the grooming sequences (correlation is highly significant in all cases; $P < 0.0001$; Spearman rank correlation, with $rho = 0.92$, 0.80, and 0.77, respectively). (**D**) Average conditional uncertainty in terms of Shannon information as a function of model order. Note the drop in conditional uncertainty when the previous state is known compared to when it is not ($i = 2$; first order Markov), whereas the uncertainty drops only moderately when the state two steps back is included in the model ($i = 3$). (**E**) Histograms of phase durations for the five phases and the duration of pauses between grooming bouts {STOP; behavior illustrated by inserted schematics [adapted from Aldridge and Berridge, 1998 (*21*)]}. Two-sample Kolmogorov-Smirnov test showed a statistical difference between all pairs of distributions ($P < 0.001$ after Bonferroni correction). Total number of each phase indicated by "*n*," corresponding to (means ± SD) across recordings P1A, 42.7 ± 3.4%; P1B, 3.8 ± 1.3%; P2, 36.3 ± 4.6%; P3, 9.1 ± 2.6%; and P4, 8.1 ± 5.6%.

Hypothetical mechanisms underlying the sequential organization of grooming

While a probabilistic model was shown to closely reproduce the observed distributions of sequence lengths and phase sequences, it is not clear which neuronal processes could give rise to the observed transition patterns and how this activity is linked to motor commands that will ultimately give rise to the expression of the individual motor behaviors. In any case, the findings emerging from the behavioral characterizations may be taken to indicate that the neuronal control of behavioral transitions is a particularly important control mechanism for the sequential organization of grooming behavior. On the basis of this assumption, we formulated a couple of testable hypotheses concerning the neuronal motor commands that underlie the observed behavior, which extend beyond the classical view that neuronal activity in corticostriatal motor systems principally reflects the present behavior or the motor acts carried out in the very near future [see, e.g., (*23*)]. First, on the most basic level, we hypothesized that the corticostriatal system explicitly encodes the start and the end of a grooming sequence, as these events delineate transitions between distinct behavioral states. Second, we hypothesized that the involvement of the corticostriatal system in the sequential organization of grooming entails that neurons in cortical and striatal circuits specifically encode both the timing and nature of different phase transitions and that certain features of the neuronal code can account for the highly variable transition probabilities observed.

To test our hypotheses, we analyzed modulations of neuronal firing rates related to transitions into and out of the entire grooming sequences, as well as during the grooming behavior and in transitions between individual phases. Using chronically implanted electrode arrays, action potentials in individual neurons were recorded bilaterally in the following: primary motor cortex (MI, centered on forelimb representation), the rostral forelimb area (RFA; a supplementary motor area in rodents), and in the two striatal compartments, dorsolateral and dorsomedial striatum (DLS/DMS), which receive dense corticostriatal projections from MI and RFA, respectively (Fig. 2A) (*24*). Single-cell recordings in the cortex and striatum were attributed

to originate from either externally projecting principal cells [PCs; i.e., pyramidal cells (n = 158) and MSNs (n = 80)] or from interneurons [INs; (n = 58/22 for cortex/striatum); fig. S2 and table S1; (*25*)].

Encoding of grooming start and end points

When analyzing the overall changes in firing rate in the corticostriatal circuits associated with the execution of the grooming behavior, modulations of the neuronal activity was not primarily found during the expression of the active behavior. Instead, it was evident from the recordings that most of the rate modulations occurred close to the transitions into and out of the grooming behavior [as an example, the changes in average firing rate (including all recorded cells to rule out any potential effects of selection bias) associated with one of the most commonly observed grooming sequences are shown in Fig. 2B]. Overall, the firing rate of a substantial fraction of all cells (30.8%) recorded in the four structures, in both hemispheres, were found to be significantly modulated ($|Z| > 2$, with predominant rate increase) around the time a grooming sequence started and/or ended (Fig. 2C; electromyographic recordings of the forelimb muscle activity was used to confirm the time points of behavioral transitions extracted from video recordings; fig. S3). Increased activity was observed not only in MI, DLS, and DMS over about a 1-s epoch immediately before the start of the grooming (i.e., before the onset of the motor behavior) but also during a similar epoch around the time of grooming completion. These three structures all contained comparable fractions of cells showing significant modulations at onset and end of grooming sequences, although with slightly different proportions showing excitation versus inhibition (compare Fig. 2C versus fig. S4A) and were largely unaffected by the length of the pauses between successive grooming events and other sequence specific features (fig. S5). For the RFA, we observed a small average firing rate increase associated with grooming start that tended to precede the rate changes in the other three structures (peaking of ~2 s before the start). It is possible that this modulation reflects an early involvement of this premotor area in the action preparation (Fig. 2C), since no other motor behavior was consistently observed at this point

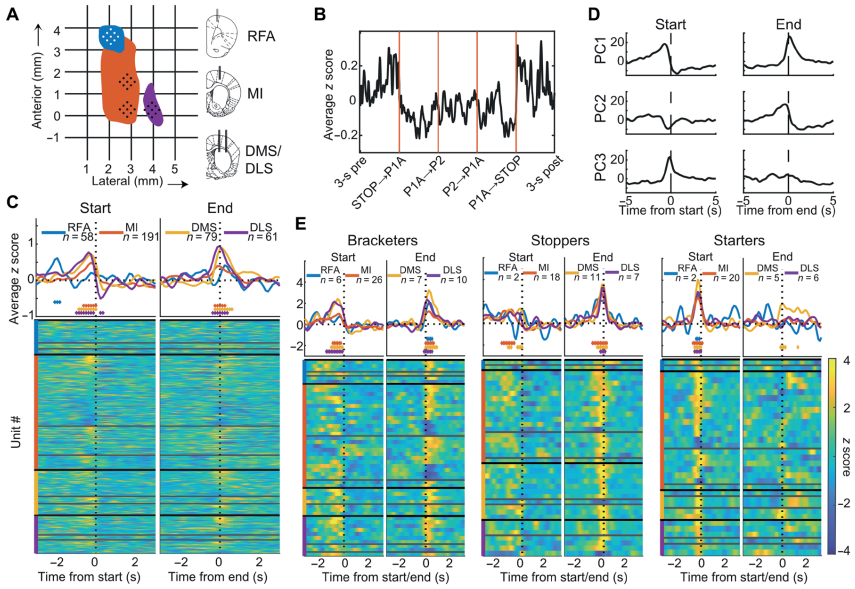

Fig. 2. Modulation of neuronal activity in relation to the onset and end of a grooming sequence. (**A**) Recording sites are shown for the right hemisphere. Colored areas in horizontal plane indicate the forelimb representation in primary motor cortex (MI, orange), RFAs (blue), sensorimotor striatum (DLS, purple), and associative striatum (DMS) corresponds to the posterior medial group of electrodes (where DMS is located ventral to the posterior part of MI). (**B**) Average of *z*-scored firing rates of recorded units during a specific grooming sequence. The *x* axis is time warped to align transitions. (**C**) Top: Average changes in firing rate show a net increase at behavioral transitions into and out of grooming. Bottom: Perievent time histograms (PETHs) for all recorded cells, showing the average standardized rate for each cell, sorted by structure (colored vertical lines), putative cell type (PCs, INs, and unclassified, from top to bottom within each structure), and average *z* score during significant time bins. The range of *Z* is indicated by the color bar in (E). (**D**) Cell firing dynamics represented in the subspace spanned by the first three principal components [of the PETHs shown in (C)], demonstrating symmetry between transitions into and out of grooming. (**E**) Left: Cells that display significant post-end modulation (bracketers) also show pre-onset modulation. Middle: Cells that show significant pre-end modulation (Stoppers) show minimal bracketing modulation. Right: Cells that show significant pre-onset modulation without significant end modulation (Starters). Note the close resemblance in firing rate modulations between (D) and (E) and that striatum displays a predominant excitation, whereas MI modulation is more balanced, resulting in lower average firing rates. Start, first contact between forepaw and snout; end, first instance of inactivity. Diamonds in (C) and (E) denote individual time bins (125 ms) where the distribution of *z*-scored firing rates differs significantly from a standard normal distribution ($P < 0.001$; *z* test).

in time. Thus, judging from our single-cell recordings, cortical and striatal firing rate modulations appear to be strongly associated with the state transitions into and out of the grooming behavior, rather than with the execution of the grooming behavior.

However, the neuronal control of behavior is thought to involve coordinated activity patterns in large cell populations, which may not be evident when analyzing rate changes one cell at a time. We therefore applied principal components analysis (PCA) to represent rate changes in all recorded neurons at the onset and end of grooming in a lower dimensional space. When plotting state transitions in a subspace spanned by the first three principal components, smooth trajectories with a certain symmetry between the start and end of grooming emerged, whereas the network states before and after the transitions were found to be essentially stationary (Fig. 2D). In other words, neuronal modulations are primarily associated with the switching of state per se (*26*). Moreover, the variance in standardized firing rates across neurons represented in these three dimensions implies that certain cell groups are involved in both of the transitions (as captured by PC1) and other cell groups, preferentially in one or the other, leading us to examine whether individual cells showed firing rate modulations that could be linked to these population measures.

Because modulation ($|Z| > 2$) associated with the end of the grooming sequence, in contrast to its onset, occurred both before and after the behavioral transition (compare Fig. 2, C to E, and fig. S4), the "end neurons" were split into two groups, cells that were only modulated after the end of the sequence versus others. These groups proved to be distinct in two ways. First, cells with pre-end modulation had almost no post-end modulation. Second, practically all cells that were selected for post-end modulation showed modulation also before grooming onset (Fig. 2E, left; compare Fig. 2D). These two cell groups, with cells showing either combined pre-onset and post-end modulation ("bracketers") (*27*) on the one hand and cells showing pre-end modulation on the other ("stoppers"; Fig. 2E, middle), thus appear to serve different functions.

Similarly, by excluding all bracketers (displaying $|Z| > 2$ after the end of grooming) from the cells with a significant modulation at onset, a separate group of "starters" could also be distinguished (Fig. 2E, right; notably, the starter and stopper groups were found to be mutually exclusive). Last, in this encoding of the onset and end of grooming, INs appear to have a more prominent role than PCs in the cortex because the fraction of the cortical INs that showed significant modulations was significantly higher than that for the PCs (25/58 and 42/158, respectively; $P = 0.020$; two-proportion z test; see also fig. S4). Hence, this would be in line with the notion that a fluctuating release of tonic inhibition from INs is a key mediator of state transitions of this type in cortical networks (*28*).

Encoding of phase transition events within a grooming sequence

We next investigated whether phase transitions within a grooming sequence are also associated with specific neuronal modulation patterns. All phase transitions analyzed were continuous (i.e., there were no pauses in motor behavior between the consecutive phases; see also Supplementary Movies), and the time between two consecutive transitions was often brief (48.9% of all grooming phases lasted for less than 1 s; fig. S6). Neuronal activity specifically related to phase transitions as opposed to more general in-phase behavior should, therefore, be expected to be relatively brief in time.

When aligning the neuronal activity around the time of phase transitions, the average firing rate changes were quite modest. However, we observed a small but significant reduction in cell firing rates in DMS [fig. S7; see also (*29*)]. More notably, however, a comparatively large fraction of cells in MI (15.2%) showed significant modulation ($|Z| > 2$ compared to the baseline activity), with a maximum modulation depth at the time of phase switching (Fig. 3A). Because this modulation was characterized by a reduced firing rate in some cells and an increased rate in others, the resulting net change in the firing rate at the population level was negligible. This distinct encoding of phase transition events, in general, was significantly higher in MI than in the other recorded structures ($P = 0.018$; two-proportion z test; 29/191 in MI versus 15/198 in the rest).

Encoding of the nature of grooming phases in phase transitions

Averaging the over all types of phase transitions (as in Fig. 3A) could potentially mask neural events linked to one or a few specific phase transitions. We considered this issue by analyzing the modulation depth for data categorized by type of phase. First, and perhaps somewhat trivially, since it is well known that sensory feedback is an important component in corticostriatal activity (*30*), when analyzing cell activity during the execution of the five different types of grooming phases, information about the ongoing motor behavior, in terms of current phase type, was found to be encoded in the recorded

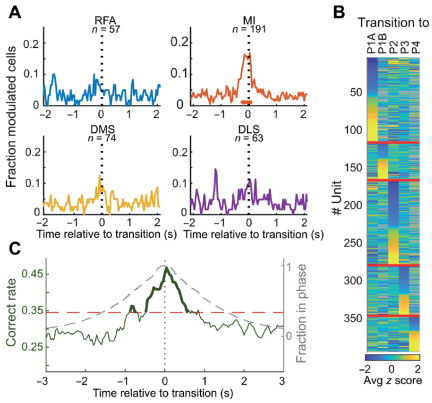

Fig. 3. Modulation of neuronal activity in transitions between grooming phases. (**A**) Only MI showed significant modulation in association with transition events, in general (n = same number of PETHs, as in Fig. 2C). (**B**) Standardized firing rate modulations of all cells grouped according to preference for a specific upcoming grooming phase (transitions too rarely observed to be included are denoted in gray; means from 200 ms immediately before transition). Note that a single phase is generally preferred. (**C**) Fraction correct phase predictions for the coming phase obtained from cortical and striatal ensemble activity plotted as a function of time (dark green). Note that most information about which phase is being executed after the transition point ($t = 0$) is available in a relatively narrow time window around $t = 0$ (the much broader time interval enclosed by the gray dashed line indicates the fraction of events where no additional phase switches were observed before/after phase transition, i.e., the animal remains in the same phase pair that make up the transition at $t = 0$). Horizontal red dashed line marks chance level + 2.3 SD, corresponding to $P = 0.01$.

structures, except for RFA ($P \leq 0.001$, ANOVA; measured during a 200-ms window in the middle of phase execution; see also fig. S8). This activity, which probably reflects a mix of motor signal and sensory feedback, is in line with previous reports (*4*, *21*). Second, a much larger fraction of cells proved to show modulation patterns more in line with a pure motor command, i.e., specific encoding of the upcoming phase before transitioning into the new behavior, thus ruling out any role of sensory feedback [Fig. 3B; significant modulation with preference for a specific upcoming grooming phase with $|Z| > 2$ measured −200 to 0 ms before transition (i.e., a time window large enough to also precede delay time for signal transduction to spinal motor circuits and biomechanical muscle activation)], reaching a significance compared to chance level ($P < 0.001$ for MI and DLS, binomial test; table S2 and fig. S7D). To complement these single-cell analyses, we also analyzed the temporal evolution of the prediction accuracy of the upcoming phase, evaluated on the neuronal ensemble level (i.e., for a constellation of neurons recorded in parallel, using linear discriminant analysis with leave-one-out cross validation; see Materials and Methods). This analysis showed that the ensemble information builds up from about −1 s and peaks at the point of transition. After phase transition, information contents (for the ongoing phase) then relatively rapidly drops back (Fig. 3C). These results indicate that both present and future motor states are encoded in the recorded circuits (however, neuron inclusion analyses of the ensemble decoding accuracy indicated that MI might be particularly important for the encoding of the upcoming phase; see fig. S9).

A closer inspection of firing rate modulations in individual cells, which were recorded across a large number of phase transitions, hinted at an even more complex type of motor encoding, relating to the specific combination of phase pairs making up each phase transition (Fig. 4A illustrates an example cell). Specifically, rather than showing the same type of modulation patterns immediately before the transition into a specific phase, as would be expected for a generic motor command, these cells instead displayed modulation patterns that were determined by both the current and the upcoming motor state. Intuitively, this type of motor state–dependent motor commands would be well suited to create functional links between consecutive actions within longer motor sequences, similar to what has been observed in the primate supplementary motor areas (*4*) but which has not, to our knowledge, been systematically investigated in corticostriatal circuits.

While several cells appeared to display this type of differential modulation in association with different transitions, a complete examination of the encoding of all possible phase transitions was not possible, as neuronal data in this case had to be broken down on a large number of transition types, leaving relatively few events of each type during a single recording, and some phase combinations were simply too rare to be analyzed at all (as shown in Fig. 1B). Nevertheless, a more restricted analysis, searching for cells preferring a single phase transition type, was carried out (preferred phase transition versus median response for all phase transition types). This revealed a significant fraction of cells displaying a single transition type preference but only in MI (fig. S10).

Encoding of phase transition probabilities

The role of state-dependent motor commands in action sequencing is not entirely clear, but, hypothetically, particular features of the neuronal code that differentiates between different action transitions could, e.g., explain the highly diverse transition probabilities observed for different upcoming phases within a grooming sequence, depending on the current motor state (Fig. 1B, middle). To investigate this possibility, we examined the available phase transition data (in total, 63,298 data points spread across 318 cells, distributed in the four structures and divided into putative cell types). To this end, we fitted a linear model-relating standardized firing rate, *Z*, to transition probability, *P*(*trans*), for each structure and cell type and point in time (see Materials and Methods). The model revealed a significant linear relationship for several of the analyzed groups (Fig. 4B). The observed relation between *Z* and *P*(trans) was found to display a strong temporal dependence, where the cortex showed significant correlations already before phase transition, whereas the striatum showed correlations predominantly afterward (Fig. 4B), suggesting different roles of the cortex and striatum in the control of phase transitions of different likelihood indicated by a tendency to temporally link actions pairs either forward or backward in time. In any case, this finding shows that the corticostriatal circuits encode unusual action transitions differently to more habitual transitions. We therefore next analyzed, at the single-cell level, to what extent cells belonging to the different putative groups in the different structures tended to be more active in association with low or high *P*(*trans*) events [Fig. 4, C and D; using a similar linear model, relating *Z* to *P*(*trans*), for each single cell]. As expected, single cells displayed different preferences. Nevertheless, it was evident that both MI and DMS had larger fractions of cells showing significant negative rather than positive correlation to *P*(*trans*) at time points close to the transition [(−1 s to +1 s), lighter versus darker shaded areas in Fig. 4D; MI (PCs/INs) and DMS (PCs); $P < 0.05$, Wilcoxon signed rank test with Bonferroni correction for multiple comparisons]. This implies that cells in these structures are relatively more active in association with unusual behavioral transitions rather than in the more habitual transitions.

DISCUSSION

The central advance of this study is that it provides a first account of how neurons in cortical and striatal circuits together are involved in the encoding of action sequencing, on the spatial and temporal scale of single-unit action potentials, in a spontaneous and natural behavior involving multiple distinct motor programs (grooming phases). This study of the corticostriatal system, therefore, offers an important complementary perspective to earlier studies that have largely focused on neuronal activity recorded in a single structure, during either highly practiced rewarded behaviors [(*2*–*6*); in contrast to rodent grooming, which is a naturally developing behavior with a well-studied ontogeny (*31*)] or spontaneous behaviors expressed on a continuum of variable kinematics and movement speeds [rather than distinct stereotypic action patterns such as the rodent grooming phases; (*7*–*9*)]. Our results suggest that, in spontaneous grooming, cortical and striatal circuits have an important role in the switching of motor behavior [pointing to a role of corticostriatal network dynamics as a requirement for the system to move from one attractor state to another (*26*)] and that the full action sequences emerge from a stepwise control of the individual behavioral transitions. On the most basic level, this is manifested by the explicit encoding of the start and the end of each grooming sequence in the cortical and striatal cell groups, where net increases were most evident in the striatum (*32*). These cells were, however, found to belong to separate

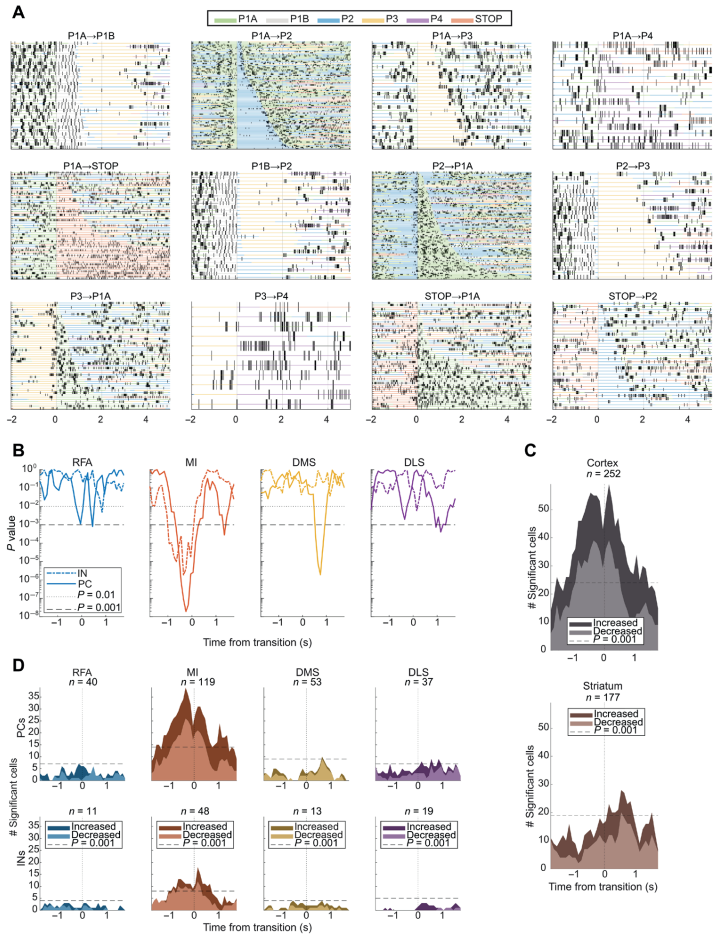

Fig. 4. State-dependent motor commands. (**A**) Rate changes observed in an example MI principal cell in conjunction with specific phase transitions ($t = 0$ in each panel). Vertical lines mark the time points of single spikes, and colors of horizontal lines within panels denote the duration of preceding and succeeding phases. The cell displays a complex modulation pattern, showing specific firing patterns associated with present, as well as upcoming phases. Note, however, that transitions into the same phase are, in some cases, associated with diverse transition activity before transition (e.g., P1A to P2 versus P1B to P2; indicative of state-dependent motor coding). (**B**) Transition probability coding at population level. Colored lines show the *P* value for a linear model between the *z* scored firing rates and probability of transition (fitlm in MATLAB) for the respective groups. One linear model was fitted for each time bin and each group (500-ms window and 100-ms steps; see Materials and Methods). The plotted *P* values are presented without correction for multiple comparisons. (**C**) Transition probability coding for single cells. The estimated slope for each cell was compared to a shuffled CI. Cells that had a slope outside the shuffled 95% CI were considered significant (1000 shuffles of transition types). (Top) Total number of significant cells in cortex (RFA and MI) and (bottom) striatum (DMS and DLS). Light shaded area: Decreased firing rate during relatively more common transitions. Dark shaded area (not including the light area): Increased firing rate during relatively more common transitions. Dashed horizontal lines denote the number of significant cells required for a binomial test with chance level at 5% to reach alpha of 0.001 for the corresponding total *n* (without correction for multiple comparisons; fitlm in MATLAB with 500-ms window and 100-ms steps). (**D**) Same as for (C) but grouped by cell type and recording location.

functional groups that we have here referred to as starters, stoppers, and bracketers, where it seems plausible that the former groups are more directly involved in direct motor control, whereas the last group (in which almost all cells with post-offset activity were found to also have pre-onset activity and consequently mark the outer boundaries of an entire action sequence) may have a role in action evaluation (*27*, *33*), as has been proposed for the matriosome/striasome cell populations (*33*, *34*). In any case, the robust encoding of behavioral

boundaries in this natural behavior goes beyond the notion that on–/offset coding emerges only as a consequence of extensive overtraining of a specific sequence, as previously reported [compare (*3*, *5*)]. It is also of potential importance that previous studies have used behavioral paradigms involving the learning of either a specific number (*3*, *6*) or a specific order of actions (*5*, *32*). In the current study, analyzing natural behavior, we however found a similar type of action boundary activity in association with sequences of highly varying length and phase content.

For the switching of phases within a grooming sequence, we found that both the timing and nature of the different transitions were encoded by certain cell groups in the recorded structures. Specifically, while only MI had a significant fraction of cells, marking the time point of phase transitions independent of transition type, selective encoding of the upcoming phase type was found in both MI and DLS. Moreover, although clearly more challenging to analyze, the recorded circuits as a whole showed evidence of selective encoding of transitions involving specific combinations of phases. For a substantial fraction of cells, this translated into a negative/positive linear relationship between firing rates and the overall probability of observing a given phase transition. Thus, our neuronal data support the concept of a stepwise control mechanism in action sequencing, where individual transition probabilities are encoded by corticostriatal circuits. Such a mechanism is in complete accordance with our behavioral analyses of grooming sequences (Fig. 1, A to C), where we found that the sequence composition and length of the entire grooming sequences were well modeled by a stepwise process assuming fixed transition probabilities (a Markov chain).

These findings were unexpected in several ways and have important implications for our understanding of how motor commands are encoded in these circuits. First, it is somewhat unexpected that grooming action sequences are well described by this relatively simplistic model and that the probabilities for the different specific phase transitions were found to be almost identical across all animals (fig. S1). Second, these state-dependent transition probabilities have a direct neuronal correlate, as reflected in state-dependent motor commands, where many cells, in particular, showed a strong association between firing rate and the observed transition probability of different phase pairs. The temporal separation between the cortex and the striatum hints at the possibility that these structures link action sequences in different directions in time, forward in cortex and backward in striatum [this latter property could also be of particular relevance for action value assignment, see, e.g., (*35*)]. Although all analyses were performed, taking putative cell type into consideration, a relatively stronger involvement of the cortical INs in transitions into and out of the entire grooming sequences was the only instance where coding properties could be shown to clearly differ between cell types. This may indicate that while network activity often engages different cell types in a similar way within action sequences, INs could have a particularly important role in larger behavioral state transitions. However, at present, this remains a speculation that will need further experimental corroboration.

Last, it deserves to be mentioned that, in contrast to the encoding of the nature of phase transitions, we were unable to establish any direct links between the neuronal firing patterns and the action duration of individual grooming phases (Fig. 1C). Instead, the distributions of the phase durations for the different phases could be well described by a probabilistic drift-diffusion model [akin to previous findings analyzing spontaneous locomotion bouts in zebrafish larvae (*36*)]. Hence, to the extent that cortical and striatal circuits do, indeed, influence action duration, this neuronal control mechanism appears to be fundamentally different from the control of action sequencing and deserves to be investigated in further detail in future studies.

In the perspective of a previous work, the study having greatest resemblance to our current work is probably the study conducted by Markowitz and colleagues (*8*). A direct comparison between results is, therefore, of interest. These authors characterized neuronal modulations of individual MSNs in DLS in association with behavioral transitions in spontaneous behavior using Ca^{2+} imaging techniques and automatized behavioral classifications. They could demonstrate strong MSN modulation occurring shortly after the transition into a new behavior. While the exact temporal activation pattern in relation to behavioral transitions is a bit difficult to compare between our two studies because of the relatively slower kinetics of Ca^{2+} dynamics, our present results, nevertheless, clearly seem to corroborate their finding (see PCs in DLS in Fig. 4B).

Markowitz and colleagues also demonstrated two other properties of MSN ensembles in DLS (which was the cell group investigated in their study) that match what was, here, observed at the level of corticostriatal circuits. First, different behaviors were found to be encoded differently on the cell ensemble level (compare Fig. 3C; although the diversity of the different behaviors analyzed in terms of kinematic differences was considerably larger in their study, leading to a slightly more distinct state separation for a similar number of action classes). Second, it was reported that, out of the cells that showed different modulation for behavioral transitions of high versus low probability, a slightly higher proportion showed a negative correlation with transition probability. This is also in line with our data (corresponding to Fig. 4D, top right), while this tended to be more pronounced in DMS. However, the distinction between the medial and lateral aspects of the dorsal striatum is complicated by the lack of anatomical landmarks and may in addition not be directly comparable between mice and rats. Together, although Markowitz *et al.* (*8*) restricted their recordings to DLS, our data show that their findings, nevertheless, are largely representative of the modulation patterns observed throughout motor cortical and striatal circuits. This is of potential relevance for a large number of recent studies using similar techniques to characterize the involvement of striatal projection neurons in motor control [see, e.g., (*7*, *9*, *11*–*14*, *37*, *38*)].

An inherent limitation to our study is the need for very large datasets to compare many different combinations of actions. At the same time, because detailed manual scoring procedures were found to be required to reliably identify behavioral transitions with high temporal resolution, this inevitably constraints sample sizes. To mitigate this limitation, the current investigation contained at least four times as many cells and three times as many grooming phases as any previously published study (*17*, *21*, *39*). Furthermore, while rodent self-grooming offers several unique opportunities to investigate how complex behaviors are regulated by the brain, this behavior may not be representative for all types of action sequencing. For example, action sequencing in sensorimotor tasks typically involve a desired goal state at the sequence end, which is often represented in sensorimotor circuits in terms of desired sensory consequences. It remains unclear to what extent self-grooming has a functional goal and whether its actions are adapted by sensory information (*20*). It should also be cautioned that because electromyographic recordings were not obtained in parallel with the neuronal recordings, a direct

assessment of possible links between neuronal modulations and muscle activity could not be carried out. Similarly, it is reasonable to assume that the coding principles revealed in this study are not the only control mechanism underlying action sequencing, and complementary control strategies might be involved in more complex behaviors that are not limited to stereotypic motor programs actuated by brainstem circuits (*16*). On the other hand, these situations are probably not completely distinct since more advanced goal-directed action choices are thought to act in conjunction with basal ganglia sensorimotor circuits in most everyday situations.

Together, the data presented herein provide the first description of how ensembles of neurons in cortical and striatal circuits encode the flexible sequencing of actions in a continuous, spontaneous, and natural motor behavior involving the combination of several distinct motor programs. Improving our functional understanding of the mammalian cortico-basal ganglia system is, no doubt, also an important first step toward improved therapies for motor disorders and for the development of more advanced prosthetic devices.

MATERIALS AND METHODS

Experimental model and subject details

Seven adult female Sprague-Dawley rats (230 to 250 g) were used in the study. The animals were kept on a natural light cycle (~12/12 hours) and received food and water ad libitum. The Malmö/Lund ethical committee of animal experiments approved all experiments in advance.

Joint behavioral and electrophysiological recordings

Spontaneous grooming behavior was recorded during daytime hours. Before the recording started, rats were placed and habituated to a transparent rectangular 450 × 70 × 300 mm (length/width/height) box, in which they could move around freely. The relatively narrow width of the transparent box caused the rat to preferentially orient sideways to the camera, which facilitated the offline classification of the types of grooming phases performed. The behavior was recorded with a digital video camera (Teledyne Dalsa Genie HM640) triggered from an external TTL pulse generator (Master 8, AMPI) at a rate of 25 fps (frames per second), which also sent pulses to the multichannel electrophysiological recording system for the offline alignment of the behavioral and neuronal datasets. Joint recordings of electrophysiological data and grooming behavior were obtained in 14 sessions that normally lasted about 2 to 3 hours, and each lasted until the animal had performed at least 10 grooming sequences (mean of 33 and interquartile range of [21 51]).

Classification of grooming phases

The grooming behavior was classified according to the guidelines published by Berridge and coworkers (*40*) with some minor modifications. In short, the grooming sequence was considered initiated when an animal, from a nonmoving state, first touched its snout to start grooming. For every grooming sequence, the observed action phases were categorized into one of the five previously described grooming phases, and the time of initiation and termination of each phase was identified. Videos were analyzed by two expert reviewers. The classified phase types and exact time points of transitions were cross validated between the two scorers for a large subset of the data to ensure full interscorer agreement before the full material was analyzed. Within a grooming sequence, the initiation time of a phase corresponded to the termination time of the preceding phase. A grooming sequence was considered terminated when an animal entered a period of complete immobility, for at least two video frames. The five individual phases are characterized by the following motor patterns:

1) P1A: Repetitive licking of forepaws and whiskers in vicinity to the mouth [~1 to 10 s; corresponding to the P1 out-of-chain grooming in the nomenclature of Aldridge and Berridge (*21*)].

2) P1B: Five to nine rapid and bilaterally synchronized elliptical strokes to the mystacial vibrissae [~1 s; corresponding to P1 in the nomenclature of Aldridge and Berridge (*21*)].

3) P2: Unilateral strokes over dorsal and lateral parts of the anterior half of the head (~0.5 to 2 s).

4) P3: Bilateral strokes over the posterior part of the head around the ears (~1 to 3 s).

5) P4: Postural change followed by licking of the body, generally progressing from midline outward (~1 to 30 s).

When a unilateral phase (P2 or P4) was immediately followed by the same phase on the other side, both phases were considered as one continuous phase. Moreover, because P2 was generally performed in a somewhat bimanual manner, using the contralateral paw to support the head, this behavior was not divided into left- and right-sided grooming. Last, note that the pattern of licking behavior in P4 displayed a higher degree of behavioral variability than the other highly stereotypic phases. Other types of stereotypic nongrooming motor behavior were not observed during the baseline, except for body shakes; hence, as a precaution, grooming events close to body shakes were manually excluded from the data analyzed. Note that as a result of the camera acquisition frame rate (25 fps), the temporal resolution in the time assignment of a phase transition was 40 ms (i.e., the transition was always assigned to a specific camera frame).

Markov model of behavior

The conditional probability $P(Y|X)$ of a transition to phase Y, given being in phase X, was estimated as $N(Y \leftarrow X) / N(X)$, where $N(Y \leftarrow X)$ is the observed number of transitions from X to Y and $N(X)$ is the observed number of phases X. The transition bias was calculated as

$$\beta = \log\left(\frac{P(Y \leftarrow X)}{P(X)\,P(Y)}\right)$$

where the numerator is the joint probability of observing a certain transition $P(Y \leftarrow X) = N(Y \leftarrow X)/\Sigma_{X,Y}N(Y \leftarrow X)$ and the denominator is the product of the probabilities of observing each of the phases independently, $P(X) = N(X)/\Sigma_X N(X)$. Ninety percent confidence intervals (CIs) for β were calculated from the distribution created by randomly generating new values, substituting for $N(Y \leftarrow X)$ and $N(X)$, from 1000 simulated experiments using the estimated values for $P(Y \leftarrow X)$ and $P(X)$ and the same number of samples as in the experimental data.

The estimated conditional probabilities $P(Y|X)$ were used to define a Markov model. A Markov chain with ~10 million transitions was generated with the MATLAB function hmmgenerate (with no hidden states). The set of grooming sequence lengths were split into ~2000 sets containing 470 sequence lengths each (equal to the number of observed lengths in the real dataset). The sets were used to calculate 95% CI. For the experimental data, 5 of 60 data points lay outside the CI. If we assume that this Markov model is the true generator of the observed sequences, then the probability of observing five or more data points outside the CI is 18% according to the binomial cumulative distribution.

Shannon information

The estimated Shannon information, $\hat{H}_i$, was calculated as follows:

i	$\hat{H}_i$
0	$\log_2(c)$
1	$\hat{H}$
2	$\hat{H}$(pairs) – $\hat{H}$
3	$\hat{H}$(triplets) – $\hat{H}$(pairs)
4	$\hat{H}$(quartets) – $\hat{H}$(triplets)
5	$\hat{H}$(quintets) – $\hat{H}$(quartets)

Where $c = 5$ for the five grooming phases and

$$\hat{H} = \log_2 N - N^{-1} \sum_{j=1}^{c} n_j \log_2 n_j$$

$$\hat{H}(\text{pairs}) = \log_2 N - N^{-1} \sum_{j,k=1}^{c} n_{j,k} \log_2 n_{j,k}$$

etc.

where n is the total number of each phase, pair, triplet, etc. observed, and N is the total sum of n. For $i = 2$ to 5, N and n for the lower order $\hat{H}$ were estimated from the higher order n [for details see (*22*)].

Surgical procedures

All surgical procedures were carried out under antiseptic conditions. Implantations of microwire recording electrodes were performed under fentanyl/medetomidine anesthesia [0.3/0.3 mg/kg, intraperitoneally (ip)]. Electrodes were implanted bilaterally in dorsomedial/-lateral striata and in the forelimb area of the rostral and caudal motor cortex in both hemispheres targeting striatally projecting sublayers (MI, center coordinates: anteriorposterior (AP), +1.5; mediolateral (ML), ±2.8; dorsoventral (DV), −1.0 from the bregma and cortical surface; RFA, center coordinates: AP, +3.75; ML, ±2.0; DV, −1.0; and in the dorsomedial and dorsolateral striatum, respectively: AP, −0.2; ML, ±2.8; DV, −4; AP, −0.2; ML, ±3.8; DV, −3.5) (*25*). Screws in the occipital bone of the skull and anterior of the brain cavity served as connection points for the electrode ground wire, and the implant was fixated with dental acrylic attached to the screws. Anesthesia was reversed by atipamezole hydrochloride (5 mg/kg, ip) after surgery, and postoperative analgesic was administered (buprenorphine, 0.5 mg/kg, subcutaneously). The animals were allowed to recover for 1 week after implantation before the testing commenced.

Histology

Tissue material was unfortunately not available for complete postmortem verification of electrode positions. While a more restricted analysis of the available tissue sections, in a subgroup of animals, indicated correct electrode placement, the tissue quality was regrettably of poor quality, precluding a complete three-dimensional reconstruction.

Recording electrodes

Formvar-insulated tungsten wires (Ø of 33 µm; California Fine Wire Co.) were arranged into four 3 × 3 arrays in each hemisphere with 250-µm spacing in each dimension and cut to the length corresponding to the implantation site for each group. Each array consisted of nine recording channels and two adjacent reference channels. Reference wires were cut shorter than the recording electrodes so that they were positioned in cell-sparse regions superficial to the recording sites (cortical surface and the corpus callosum for cortical and striatal electrodes, respectively). Reference wires were deinsulated ~200 µm at the tip to lower impedance. A Ø of 200-µm silver wire was used for ground connection to skull screws. The wires were attached to a printed circuit board, linking them to board-to-board connectors (Kyocera 5602) with conducting epoxy (EPO-TEK EE 129-4), which were, in turn, connected to the acquisition system via a custom-made Kyocera-to-Omnetics connector adapter. Flexible insulated copper wires threaded through bellies of the biceps/triceps muscles were used for electromyography (EMG) recordings. A small area of the part of the wire positioned in the middle of each muscle belly was deinsulated for about 1 mm. The wires were passed under the skin to the connectors attached to the cranium.

Signal acquisition

Local field potentials and single-unit activity data were collected and stored using a Neuralynx multichannel recording system together with the Cheetah software (v5.x). Action potentials were band-pass–filtered at 600 to 9000 Hz [low-cut 64-tap and high-cut 32-tap finite impulse response (FIR)] and digitized at 32,552 Hz. For each channel, the amplitude threshold criteria for discriminating action potentials corresponded to three SDs of the signal recorded during a 30-s period. EMG signals were band-pass–filtered at 60 to 500 Hz (64-tap FIR) and digitized at 2034.5 Hz.

Spike sorting and cell classification

Action potentials were sorted manually offline either into single units (SUs) or multiunits (MUs) on the basis of the spike waveform features using the Offline Sorter software (Plexon Inc.). Clusters with <0.1% interspike intervals below 1.6 ms together with a separation from noise in feature space were classified as SUs. Only SUs were used in the further analysis. On the basis of the valley width, peak width, and peak-to-valley time of the average waveform, SUs were then further classified into two putative cell types per structure. The peak and valley widths were defined as the full width at half maximum. Cell type classification was performed by fuzzy k-means clustering with a threshold for probability of membership set to 0.75 so that SUs with a probability of membership <0.75 were unclassified (see fig. S2).

Construction of perievent time histograms

Perievent time histograms (PETHs) of spikes from each cell were constructed by averaging over the total number of grooming events in each recording. Action potentials were divided into time bins that were adapted to fit the relative difference in transition times into and out of grooming sequences compared to between individual phases inside a sequence (125 ms for Fig. 2 and 40 ms for Fig. 3) following a temporal smoothing with a Gaussian kernel (with sigma of 167 ms for Fig. 2 and 40 ms for Fig. 3). The average firing rate of each bin was calculated and standardized using the mean firing rate and SD of all bins ±10 s around the time of the event for Fig. 2 and ±3 s for Fig. 3 (i.e., containing a mix of grooming/non-grooming behaviors in the case of Fig. 2 but only in grooming behavior for Fig. 3, after excluding periods containing the start or end of a grooming sequence).

For EMG recordings, the band-pass–filtered signals were standardized with respect to the baseline period [−4 to −1] s for each channel

(six channels in biceps and three in triceps). An additional temporal smoothing (square 24-ms window) was applied before averaging the overall trials ($n = 16$) for all channels in each muscle.

PCA of population rate changes

To represent population dynamics, PCA was applied to the full set of neurons, where each time bin in the PETH was treated as an observation and each neuron as a variable.

Phase predictions from neuronal ensemble analyses

To estimate the information contents in neuronal ensembles as a function of time in relation to phase transitions, linear discriminant analysis was applied (fitcdiscr in MATLAB). A classifier was fitted for each time bin [including firing rates from 11 adjacent bins (±220 ms) using a Gaussian window to give increased importance to spikes close to $t = 0$] and transition on the basis of all the other transitions in that experiment and was then validated against the current phase transition (i.e., leave-one-out cross validation). The model was fitted using a pseudolinear discrimination type and uniform prior probability.

For the construction of neuron inclusion curves, multiclassifiers (fitcdiscr in MATLAB) were constructed for each recording using normalized firing rates from n randomly selected units from each area analyzed in a 100-ms window immediately before the phase transition. One classifier was constructed for each transition analyzed by using the firing rates from all other transitions (leave one out). To get a good estimate for the average correct rate in a subset of n units, this was then repeated 100 times. Subsequently, the average and SEM of the average correct rate between recordings were calculated. To estimate the chance level, the process was repeated, but all normalized firing rates were replaced with random numbers drawn from z scored distribution (a normal distribution with a mean of 0 and an SD of 1; using MATLAB randn).

Similar analyses were also performed, investigating the information added from each of the structures to the information contained by the total ensemble of neurons, recorded in parallel, from the other structures. In this case, correct rates were calculated using the units from all other brain structures, recorded in parallel, when including n units from the area analyzed.

Quantification and statistical analysis

Statistical tests used to assess the significant group difference are specified in the main text and/or in the respective figure legends. For in-phase analysis, a 440-ms window (containing five 40-ms bins) around $t = 0$ of a PETH centered in the middle of each grooming phase was used for ANOVA. For the number of cells modulated to a single upcoming phase ($|Z| > 2$ for only one of the grooming phases), a 200-ms window right before transition was used. To test for significance, a binomial test was applied. For this, another 200-ms time window 1.5 s before the phase transition was used to calculate chance level (i.e., relatively close in time to ensure that the animal was in grooming behavior and, thus, displaying similar neuronal base-level activity). The baseline used when creating the z scores for the respective sample windows was a 5-s period, centered on each window (but excluding ±200 ms around the sampled window).

SUPPLEMENTARY MATERIALS

Supplementary material for this article is available at http://advances.sciencemag.org/cgi/content/full/6/41/eabc1173/DC1

View/request a protocol for this paper from *Bio-protocol*.

REFERENCES AND NOTES

1. J. W. Mink, The basal ganglia: Focused selection and inhibition of competing motor programs. *Prog. Neurobiol.* **50**, 381–425 (1996).
2. N. Fujii, A. M. Graybiel, Representation of action sequence boundaries by macaque prefrontal cortical neurons. *Science* **301**, 1246–1249 (2003).
3. X. Jin, R. M. Costa, Start/stop signals emerge in nigrostriatal circuits during sequence learning. *Nature* **466**, 457–462 (2010).
4. J. Tanji, K. Shima, Role for supplementary motor area cells in planning several movements ahead. *Nature* **371**, 413–416 (1994).
5. T. D. Barnes, Y. Kubota, D. Hu, D. Z. Jin, A. M. Graybiel, Activity of striatal neurons reflects dynamic encoding and recoding of procedural memories. *Nature* **437**, 1158–1161 (2005).
6. X. Jin, F. Tecuapetla, R. M. Costa, Basal ganglia subcircuits distinctively encode the parsing and concatenation of action sequences. *Nat. Neurosci.* **17**, 423–430 (2014).
7. G. Barbera, B. Liang, L. Zhang, C. R. Gerfen, E. Culurciello, R. Chen, Y. Li, D.-T. Lin, Spatially compact neural clusters in the dorsal striatum encode locomotion relevant information. *Neuron* **92**, 202–213 (2016).
8. J. E. Markowitz, W. F. Gillis, C. C. Beron, S. Q. Neufeld, K. Robertson, N. D. Bhagat, R. E. Peterson, E. Peterson, M. Hyun, S. W. Linderman, B. L. Sabatini, S. R. Datta, The striatum organizes 3D behavior via moment-to-moment action selection. *Cell* **174**, 44–58 (2018).
9. A. Klaus, G. J. Martins, V. B. Paixao, P. Zhou, L. Paninski, R. M. Costa, The spatiotemporal organization of the striatum encodes action space. *Neuron* **95**, 1171–1180.e7 (2017).
10. L. Ding, J. I. Gold, Separate, causal roles of the caudate in saccadic choice and execution in a perceptual decision task. *Neuron* **75**, 865–874 (2012).
11. L.-H. Tai, A. M. Lee, N. Benavidez, A. Bonci, L. Wilbrecht, Transient stimulation of distinct subpopulations of striatal neurons mimics changes in action value. *Nat. Neurosci.* **15**, 1281–1289 (2012).
12. E. A. Yttri, J. T. Dudman, Opponent and bidirectional control of movement velocity in the basal ganglia. *Nature* **533**, 402–406 (2016).
13. F. Tecuapetla, S. Matias, G. P. Dugue, Z. F. Mainen, R. M. Costa, Balanced activity in basal ganglia projection pathways is critical for contraversive movements. *Nat. Commun.* **5**, 4315 (2014).
14. F. Tecuapetla, X. Jin, S. Q. Lima, R. M. Costa, Complementary contributions of striatal projection pathways to action initiation and execution. *Cell* **166**, 703–715 (2016).
15. A. W. Flaherty, A. M. Graybiel, Two input systems for body representations in the primate striatal matrix: experimental evidence in the squirrel monkey. *J. Neurosci.* **13**, 1120–1137 (1993).
16. K. C. Berridge, Progressive degradation of serial grooming chains by descending decerebration. *Behav. Brain Res.* **33**, 241–253 (1989).
17. J. W. Aldridge, K. C. Berridge, M. Herman, L. Zimmer, Neuronal coding of serial order: Syntax of grooming in the neostriatum. 4, 391–395 (1993).
18. J. C. Fentress, F. P. Stilwell, Letter: Grammar of a movement sequence in inbred mice. *Nature* **244**, 52–53 (1973).
19. H. C. Cromwell, K. C. Berridge, Implementation of action sequences by a neostriatal site: A lesion mapping study of grooming syntax. *J. Neurosci.* **16**, 3444–3458 (1996).
20. A. V. Kalueff, A. M. Stewart, C. Song, K. C. Berridge, A. M. Graybiel, J. C. Fentress, Neurobiology of rodent self-grooming and its value for translational neuroscience. *Nat. Rev. Neurosci.* **17**, 45–59 (2016).
21. J. W. Aldridge, K. C. Berridge, Coding of serial order by neostriatal neurons: A "natural action" approach to movement sequence. *J. Neurosci.* **18**, 2777–2787 (1998).
22. C. Chatfield, Statistical inference regarding markov chain models. *Appl. Stat.* **22**, 7 (1973).
23. R. S. Turner, M. R. DeLong, Corticostriatal activity in primary motor cortex of the macaque. *J. Neurosci.* **20**, 7096–7108 (2000).
24. E. M. Rouiller, V. Moret, F. Liang, Comparison of the connectional properties of the two forelimb areas of the rat sensorimotor cortex: Support for the presence of a premotor or supplementary motor cortical area. *Somatosens. Mot. Res.* **10**, 269–289 (1993).
25. P. Halje, M. Tamtè, U. Richter, M. Mohammed, M. A. Cenci, P. Petersson, Levodopa-induced dyskinesia is strongly associated with resonant cortical oscillations. *J. Neurosci.* **32**, 16541–16551 (2012).
26. M. Djurfeldt, Ö. Ekeberg, A. M. Graybiel, Cortex–basal ganglia interaction and attractor states. *Neurocomputing.* **38–40**, 573–579 (2001).
27. K. S. Smith, A. M. Graybiel, A dual operator view of habitual behavior reflecting cortical and striatal dynamics. *Neuron* **79**, 361–374 (2013).
28. M. M. Karnani, M. Agetsuma, R. Yuste, A blanket of inhibition: Functional inferences from dense inhibitory connectivity. *Curr. Opin. Neurobiol.* **26**, 96–102 (2014).
29. N. Mallet, R. Schmidt, D. Leventhal, F. Chen, N. Amer, T. Boraud, J. D. Berke, Arkypallidal cells send a stop signal to striatum. *Neuron* **89**, 308–316 (2016).
30. R. Reig, G. Silberberg, Multisensory integration in the mouse striatum. *Neuron* **83**, 1200–1212 (2014).
31. M. T. Colonnese, E. L. Stallman, K. C. Berridge, Ontogeny of action syntax in altricial and precocial rodents: Grooming sequences of rat and guinea pig pups. *Behaviour* **133**, 1165–1195 (1996).

32. N. Martiros, A. A. Burgess, A. M. Graybiel, Inversely active striatal projection neurons and interneurons selectively delimit useful behavioral sequences. *Curr. Biol.* **28**, 560–573. e5 (2018).
33. M. Stephenson-Jones, A. A. Kardamakis, B. Robertson, S. Grillner, Independent circuits in the basal ganglia for the evaluation and selection of actions. *Proc. Natl. Acad. Sci. U.S.A.* **110**, E3670–E3679 (2013).
34. P. Berthet, M. Lindahl, P. J. Tully, J. Hellgren-Kotaleski, A. Lansner, Functional relevance of different basal ganglia pathways investigated in a spiking model with reward dependent plasticity. *Front. Neural Circuits* **10**, 53 (2016).
35. E. S. Her, N. Huh, J. Kim, M. W. Jung, Neuronal activity in dorsomedial and dorsolateral striatum under the requirement for temporal credit assignment. *Sci. Rep.* **6**, 27056 (2016).
36. T. Palmér, F. Ek, O. Enqvist, R. Olsson, K. Åström, P. Petersson, Action sequencing in the spontaneous swimming behavior of zebrafish larvae - implications for drug development. *Sci. Rep.* **7**, 3191 (2017).
37. S. Nonomura, K. Nishizawa, Y. Sakai, Y. Kawaguchi, S. Kato, M. Uchigashima, M. Watanabe, K. Yamanaka, K. Enomoto, S. Chiken, H. Sano, S. Soma, J. Yoshida, K. Samejima, M. Ogawa, K. Kobayashi, A. Nambu, Y. Isomura, M. Kimura, Monitoring and updating of action selection for goal-directed behavior through the striatal direct and indirect pathways. *Neuron* **99**, 1302–1314.e5 (2018).
38. J. K. O'Hare, H. Li, N. Kim, E. Gaidis, K. Ade, J. Beck, H. Yin, N. Calakos, Striatal fast-spiking interneurons selectively modulate circuit output and are required for habitual behavior. *eLife* **6**, e26231 (2017).
39. M. Meyer-Luehmann, J. F. Thompson, K. C. Berridge, J. W. Aldridge, Substantia nigra pars reticulata neurons code initiation of a serial pattern: Implications for natural action sequences and sequential disorders. *Eur. J. Neurosci.* **16**, 1599–1608 (2002).
40. K. C. Berridge, J. C. Fentress, H. Parr, Natural syntax rules control action sequence of rats. *Behav. Brain Res.* **23**, 59–68 (1987).

Acknowledgments: We would like to thank R. Johansson for insightful comments on the manuscript. **Funding:** The study was supported by grants from the Magnus Bergvall Foundation, Crafoord Foundation, Kempe Foundation, Insamlingsstiftelserna, Umeå University, Kockska Foundation, Olle Engkvist Foundation, Parkinson Foundation, The Swedish Brain Foundation, Segerfalk Foundation, Åke Wiberg Foundation, Åhlén Foundations, MultiPark, Kungliga fysiografiska sällskapet, Sven-Olof Jansons livsverk, Sigurd och Elsa Goljes minne, Svenska Sällskapet för Medicinsk Forskning (SSMF), BABEL (Erasmus Mundus), The e-Science Collaboration, and Vetenskapsrådet (VR) grant 325-2011-6441 and grant 2018-02717. The computations were enabled by resources provided by the Swedish National Infrastructure for Computing (SNIC) at LUNARC, partially funded by the Swedish Research Council through grant agreement no. 2016-07213. **Author contributions:** M.T. performed the main experiments and contributed in analyses and manuscript writing. J.S. developed analytical approaches and analyzed the data and contributed in manuscript writing. P.H. developed analytical approaches and probabilistic models and contributed in manuscript writing. I.B. performed EMG control experiments. P.P. designed the experiments, contributed in analyses, and wrote the manuscript. **Competing interests:** The authors declare that they have no competing interests. **Data and materials availability:** All data needed to evaluate the conclusions in the paper are present in the paper and/or the Supplementary Materials. Additional data related to this paper may be requested from the authors.

Submitted 8 April 2020
Accepted 19 August 2020
Published 9 October 2020
10.1126/sciadv.abc1173

Citation: J. Sjöbom, M. Tamtè, P. Halje, I. Brys, P. Petersson, Cortical and striatal circuits together encode transitions in natural behavior. *Sci. Adv.* **6**, eabc1173 (2020).

ScienceAdvances

Cortical and striatal circuits together encode transitions in natural behavior

Joel Sjöbom, Martin Tamtè, Pär Halje, Ivani Brys and Per Petersson

Sci Adv **6** (41), eabc1173.
DOI: 10.1126/sciadv.abc1173

Science Advances (ISSN 2375-2548) is published by the American Association for the Advancement of Science, 1200 New York Avenue NW, Washington, DC 20005. The title *Science Advances* is a registered trademark of AAAS.

Paper II

This unpublished manuscript has been
excluded in this version of the thesis.

Paper III

EJN European Journal of Neuroscience

FENS Federation of European Neuroscience Societies

European Journal of Neuroscience, pp. 1–15, 2018 doi:10.1111/ejn.13805

Changes in neuronal activity of cortico-basal ganglia–thalamic networks induced by acute dopaminergic manipulations in rats

Nedjeljka Ivica, Ulrike Richter, Joel Sjöbom, Ivani Brys, Martin Tamtè and Per Petersson
Department of Experimental Medical Sciences, Integrative Neurophysiology and Neurotechnology, Neuronano Research Center, Lund University, BMC, S-221 84, Lund, Sweden

Keywords: akinesia, motor behavior, Parkinson's disease, systems neurophysiology

Abstract

The basal ganglia are thought to be particularly sensitive to changes in dopaminergic tone, and the realization that reduced dopaminergic signaling causes pronounced motor dysfunction is the rationale behind dopamine replacement therapy in Parkinson' disease. It has, however, proven difficult to identify which neurophysiological changes that ultimately lead to motor dysfunctions. To clarify this, we have here recorded neuronal activity throughout the cortico-basal ganglia–thalamic circuits in freely behaving rats during periods of immobility following acute dopaminergic manipulations, involving both vesicular dopamine depletion and antagonism of D1 and D2 type dopamine receptors. Synchronized and rhythmic activities were detected in the form of betaband oscillations in local field potentials and as cortical entrainment of action potentials in several basal ganglia structures. Analyses of the temporal development of synchronized oscillations revealed a spread from cortex to gradually also include deeper structures. In addition, firing rate changes involving neurons in all parts of the network were observed. These changes were typically relatively balanced within each structure, resulting in negligible net rate changes. Animals treated with D1 receptor antagonist showed a rapid onset of hypokinesia that preceded most of the neurophysiological changes, with the exception of these balanced rate changes. Parallel rate changes in functionally coupled ensembles of neurons in different structures may therefore be the first step in a cascade of neurophysiological changes underlying motor symptoms in the parkinsonian state. We suggest that balanced rate changes in distributed networks are possible mechanism of disease that should be further investigated in conditions involving dopaminergic dysfunction.

Introduction

Dopamine has been recognized as a key neuromodulator of the basal ganglia for almost half a century (Carlsson *et al.*, 1958; Hornykiewicz, 2002, 2006). The crucial importance of dopamine is particularly evident in Parkinson's disease (PD), where degeneration of midbrain dopaminergic neurons is the most characteristic neuropathological feature, and symptomatic therapy is primarily based on dopamine replacement. However, even though a large body of evidence shows that dopaminergic signaling is essential for normal motor function, we still neither fully understand the normal physiological effects of this transmitter substance on cortico-basal ganglia networks (Seamans & Yang, 2004; Costa *et al.*, 2006), nor the consequences of long-term depletion (Albin *et al.*, 1989; DeLong, 1990; Brown *et al.*, 2001). While striatum is considered to be the main neuronal target of dopamine, the dopaminergic innervation of other parts of the cortico-basal ganglia–thalamic loop is most probably also of key importance for circuit function. This includes, for example, thalamus (Freeman *et al.*, 2001; Sánchez-González *et al.*, 2005), pallidium (Lindvall & Björklund, 1979), the subthalamic nucleus (STN; Meibach & Katzman, 1979; Prensa & Parent, 2001), substantia nigra (Cheramy *et al.*, 1981; Smith & Kieval, 2000) and the cerebral cortex (Brown *et al.*, 1979; Berger *et al.*, 1986; Gaspar *et al.*, 1989) (see also Smith & Villalba, 2008; Richter *et al.*, 2013). The effects of dopamine release will depend on the type of receptors present in the postsynaptic plasma membrane, and striatal projection neurons show somewhat different expression patterns for neurons projecting either directly to the output nuclei of the basal ganglia [where dopamine receptor type 1 (D1R) is more common] or indirectly via external globus pallidus (GP) [where dopamine receptor type 2 (D2R) instead dominates (Gerfen & Surmeier, 2011)]. Because of this, it has been suggested that dopamine has a direct role in regulating the striatal output and the balance between these

Correspondence: Per Petersson, as above.
E-mail: Per.Petersson@med.lu.se

Received 26 September 2017, revised 11 December 2017, accepted 12 December 2017

Edited by Yoland Smith

Reviewed by: Aryn Gittis, Carnegie Mellon University, USA; Dieter Jaeger, Emory University, USA

The associated peer review process communications can be found in the online version of this article.

two parallel basal ganglia pathways (Albin *et al.*, 1989; DeLong, 1990).

In practical terms, the role of dopamine in motor control circuits has proven very challenging to investigate. This is perhaps not surprising given that in-depth circuit level analyses basically require parallel recordings in all parts of these highly interconnected circuits in freely behaving animals, in combination with pharmacological manipulations aimed at targeting different parts of the dopaminergic signaling. During recent years, we have developed recording methods that open up for this type of analyses (Ivica *et al.*, 2014; Tamtè *et al.*, 2016). Using this technology, we have here obtained parallel neuronal recordings throughout the cortico-basal ganglia–thalamic loop in rats during periods of exposure to transient pharmacological manipulations. These manipulations either targeted dopamine receptors (D1Rs and/or D2Rs) or the vesicular pool of dopamine, the latter by blocking the endogenous dopamine synthesis using the tyrosine hydroxylase (TH) inhibitor *alpha-methyl-p-tyrosine* (AMPT, a manipulation that can also to some extent affect noradrenaline levels due to shared transmitter synthesis pathways). In the analyses of local field potentials (LFPs), we furthermore compared these manipulations to chronic lesions, which were inflicted by injection of the neurotoxin *6-hydroxydopamine* (6-OHDA) into the medial forebrain bundle of one hemisphere in another group of rats.

By recording the neurophysiological changes induced by these pharmacological interventions, the hypothesized role of dopamine in different conceptual models of basal ganglia function could be put to test. Specifically, following acute pharmacological manipulations, we evaluated to what extent firing rate changes or excessive synchronization could be established, similar to observations in the parkinsonian condition (Bergman *et al.*, 1994; Wichmann & DeLong, 1996; Brown *et al.*, 2001; Levy *et al.*, 2002; Gatev *et al.*, 2006). By comparing neuronal population activity, reflected in the LFPs, between the acute manipulations and the chronic depletion in the 6-OHDA model, we could also search for potential differences in network synchronization resulting from long-term dopamine depletion and cell death (Mallet *et al.*, 2008; Degos *et al.*, 2009). Taken together, the current investigations were primarily aimed at clarifying which type of abnormal neurophysiological features that are most likely to cause the characteristic motor signs of parkinsonism.

Materials and methods

Animals

Eighteen adult female Sprague Dawley rats (250–290 g; Taconic Inc.) were used in the study. The animals were kept on a 12-h light cycle and received food and water *ad libitum*. All experiments were approved in advance by the Malmö/Lund ethical committee of animal experiments (M119-09, M23-14).

6-Hydroxydopamine lesions

Rats (n = 8) were anesthetized with fentanyl/medetomidine (0.3/0.3 mg/kg, i.p.) and fixed in a stereotaxic device (David Kopf instruments) with a horizontal cranium position. Two volumes of 6-OHDA hydrochloride (6.0 μg/μL free base dissolved in 0.02% ascorbate saline; Sigma-Aldrich) were injected into the medial forebrain bundle of the right hemisphere at the following coordinates from bregma and cortical surface: injection site 1 (2 μL): anteroposterior (AP): −3.6; mediolateral (ML): 1.8; and dorsoventral (DV): −8; injection site 2 (2.5 μL): AP: −4.5; ML: 1; DV: −8.0, tooth bar (TB) was at −4.5 for both injections. One week after lesioning, we could observe moderate motor impairment including asymmetric posture and gait and reduced forelimb dexterity. Animals with nearly complete (> 90%) loss of TH immunoreactivity in the striatum were included in the study.

Implantation of electrodes

The rats (n = 18) were implanted in both hemispheres with the microwire electrodes under fentanyl/medetomidine anesthesia (0.3/0.3 mg/kg, i.p.). Recording electrodes were implanted in eight areas in each hemisphere targeting different structures [distances are given in relation to bregma (AP/ML) and the cortical surface DV]. The targets were as follows: rostral forelimb area (RFA—a rodent supplementary motor area) with center the coordinates: AP: +3.75, ML: ±2.0, DV: −1.0 (Neafsey & Sievert, 1982), the forelimb area of the primary motor cortex (MI) with center coordinates: AP: +1.5, ML: ±2.8, DV: −1.0 (Gioanni & Lamarche, 1985), dorsolateral striatum (DLS) with center coordinates: AP: +0.25, ML: ±3.8, DV: −4.0 and dorsomedial striatum (DMS) with center coordinates: AP: +0.25, ML: ±2.8, DV: −4.0 (West *et al.*, 1990), GP with center coordinates: AP: −1.0, ML: ±2.875, DV: −6.5 (Chen *et al.*, 2011), ventrolateral/ventroanterior nuclei of the thalamus (VL/VA; projecting to MI) with center coordinates: AP: −2.5 ML: ±1.75; DV: −6.5 (Paxinos & Watson, 2007), the STN with center coordinates: AP: −3.5, ML: ±2.5, DV: −7.75 (Tai *et al.*, 2003) and substantia nigra pars reticulata (SNr) with center coordinates: AP: −5.125, ML: ±2.5, DV: −7.8 (Wang *et al.*, 2010). The electrode was implanted by micromanipulator (Kopf) and was fixated with dental acrylic to screws inserted in the skull. After surgery, the anesthesia was reversed by atipamezole hydrochloride (0.5 mg/kg), and buprenorphine (0.05 mg/kg) was administered as postoperative analgesic. Animals were allowed to recover for 10 days after which experiments were initiated and continued during a couple of months.

Recording electrodes

For details on electrode design, see Ivica *et al.* (2014). In brief, formvar-insulated tungsten wires (33 μm) were arranged into eight groups per hemisphere with 250 μm spacing between wires in each horizontal dimension and arranged according to the appropriate implantation depth for each group. Each of these 16 groups of wires consisted of a minimum of five recording channels and one reference channel (summing up to 128 recording channels and 16 reference channels, i.e., in total 144 wires). All wires were connected to a custom-made printed circuit board and linked through connectors/adaptors to the pre-amplifiers of the acquisition system. A silver wire of 120 μm thickness was attached to the skull screws and used as a ground connection from the animal to the recording system.

Experimental procedure

Each animal was placed in an open field (a circular space, 68 cm in diameter) where it was allowed to behave freely during the whole experiment, except for the times of drug injections or when motor tests for catalepsy were performed (chronically lesioned animals were not tested for catalepsy). All motility displayed during the experimental sessions were tracked using automated image analyses, and all movement episodes were subsequently also manually confirmed to make sure that comparisons of neurophysiological features were made across similar behavioral states.

For the catalepsy test, the animal was placed with both forepaws on a 9-cm high horizontal bar, and the duration of akinesia was

noted. The cataleptic behavior was considered to be present when the animal stayed in an immobile position with the forelimbs placed on the bar for at least 30 s. In each recording session, baseline conditions were first recorded for animals with acute dopaminergic manipulations for approximately 40–50 min. In AMPT experiments, AMPT was injected twice according to previously described procedures and catalepsy tests started approximately 250/140 min after the first/second injection. For D1R and/or D2R antagonist experiments, tests commenced around 30 min postinjection, in accordance with the pharmacodynamics of the agents used. The tests were performed in approximate intervals of 30 min (AMPT) and 10 min (haloperidol, SCH23390), respectively, until catalepsy was established, thereafter testing intervals were extended to 30 min. These tests were performed to monitor the persistence of motor signs over time under the effect of the injected drugs.

Behavioral assessments

In parallel with the electrophysiological recordings, the behavior was recorded via digital video (synchronized via an external pulse generator; Master-8, AMPI). The recorded videos were then analyzed offline for locomotion or grooming. All active periods occurring during baseline recording were excluded from further analyses to ensure a comparable behavioral state to the drug-treated conditions.

Pharmacology

The animals were intraperitoneally injected with either AMPT (*L-methyl-DL-tyrosine methyl ester hydrochloride*: Sigma-Aldrich, lot number 039K1642, CAS 7361-31-1), D1R antagonist (*R+ SCH23390 hydrochloride*: Sigma-Aldrich, lot number 100M4618, CAS 125941-87-9; 0.5 mg/kg diluted in saline), D2R antagonist (*haloperidol*: Jansen-Cilag AB, lot number 4011; CAS 52-86-8; 0.5 mg/kg diluted in saline) or a combination of D1R and D2R antagonists (0.5 mg/kg each). In AMPT experiments, two AMPT injections were given with an interval of 90 min [first injection: 250 mg/kg and second injection: 150 mg/kg; both diluted in saline; (Fuentes *et al.*, 2009; Santana *et al.*, 2014)]. The total length of the recording was adjusted according to the duration of the respective drug effects.

Data acquisition

For recordings, the implant was connected to headstages (unity-gain pre-amplifier with buffering capacity) and cables to a 128-channel recording system (Neuralynx Inc.) via custom-built adaptors. LFPs and single- and multi-unit activity were recorded in parallel. LFPs were filtered at 0.1–300 Hz and digitized at 1017 Hz, whereas action potentials were filtered at 600–9000 Hz and digitized at 32 kHz. Reference channels were selected in the software. Recording channels that were deemed to be out of place based on the histological examinations or that displayed too low signal to noise (typically due to excessive line noise) were excluded from further analyses.

Frequency analysis of LFPs

Local bipolar LFP time series were computed offline from all unique pairs of electrodes from the same structure. In order to obtain an overview of changes in the LFP frequency content during the experiment, time-frequency spectrograms were first calculated with a multitaper method (50%-overlapping 8-s windows, seven tapers) implemented in Chronux 2.0 for each LFP signal. Each spectrum was normalized to the pink noise background according to Halje *et al.*, 2012, which allowed us to describe deviations from the pink noise floor in terms of the unit dBpink. For each recording, all spectrograms within the same structure were then averaged to generate one spectrogram for each structure.

A computationally intensive but somewhat more specialized method for analyzing the frequency content was furthermore applied (Wen & Liu, 2016). The method allows to separate fractal and oscillatory components from the power spectrum, with the fractal component typically appearing as a descending straight line on the log–log plot suggesting a power-law relationship, and the oscillatory components as narrow-band peaks in specific frequency bands. The method was applied to 50%-overlapping 8-s windows of the LFP signals during certain windows of interest, and the oscillatory component was normalized to the fractal component, resulting in the unit $dB_{fractal}$. For each recording, all spectra within the same structure were averaged to generate one representative spectrum.

Identically generated spectra from structures in the lesioned hemisphere of animals with 6-OHDA lesions were compared to the average of baselines from experiments with acute dopaminergic manipulation.

Spike sorting and cell classification

Waveforms were clustered automatically with slightly modified algorithms from the Chronux toolbox (Fee *et al.*, 1996). All automatically generated clusters were reviewed to determine whether the resulting clusters, waveforms and inter-spike interval (ISI) distributions corresponded to the results typically obtained using manual sorting criteria (see, e.g., Halje *et al.*, 2012; Tamtè *et al.*, 2016). Clusters were solely modified by merging and splitting according to the cluster hierarchy imposed by the algorithm.

For the classification of putative principal cells (PCs) and interneurons (INs) in cortex and striatum (cf. Fig. 3A), the features valley width, peak width and peak-to-valley time were calculated for the average waveform of each cluster and reviewed for cluster separation. Cells with peak-to-valley time below 250 μs were considered INs (Barthó *et al.*, 2004; Sparta *et al.*, 2014).

In addition, units showing more than 3% ISI violations (spikes occurring within 1 ms) were deemed to be multi-units and were excluded in the further analyzes (the specific choice of ISI violation threshold did, however, not affect the separation of cell types).

Entrainment analyses

The phase synchronization between spike times and cortical LFPs was assessed by the spike-triggered average (STA) and the spike-field coherence (SFC, which can be interpreted as the normalized power spectrum of the STA; Fries *et al.*, 2001; Halje *et al.*, 2012). The SFC is frequency-dependent and ranges between 0 and 1, where 0 corresponds to the total absence of a phase relation between the spikes and the LFP component at frequency f, while 1 corresponds to the presence of a perfect phase relation, that is, all spikes occur at the exact same phase of the LFP. To assess the statistical significance of the SFC, 200 surrogate spike trains were generated by independently dithering all original spikes with a uniform probability in the range ± 5 s (Grun, 2009). The SFC corresponding to the original spike train was then considered significant for a certain frequency bin when it exceeded the 99th percentile of the surrogate SFCs for that bin.

Autocorrelograms and identification of cells with rhythmic firing

Autocorrelograms were computed using 1-ms bins and 500 lags. To make a first selection of oscillating cells based on the autocorrelograms, 200 surrogate cells with shuffled ISIs were generated for each unit (Grun, 2009). A periodogram was calculated, and cells with a power above the 99th percentile at any frequency below 50 Hz were selected. These cells were then manually validated with the additional criterion of having at least three peaks with the expected separation in the autocorrelogram (cf. Bergman *et al.*, 1994).

Tracking firing rates and LFP beta power over time

Firing rates were summed in 8-s bins for all units, aligned to the time of injection and cropped to the same length as the shortest experiment of its type (depending on drug used). Active periods during baseline as well as the time periods of each catalepsy test were excluded from the analyses.

The time-stretched firing rates presented in Fig. 6D were calculated by interpolating the *Z*-score of each unit (as seen in Fig. 6B) at 1000 points evenly distributed between −1 and 2, where 0 is the injection of the drug and 1 is the onset of catalepsy. These firing rates were then averaged across all units for each drug and normalized so that 0 is the mean during baseline and 1 is the mean during catalepsy (i.e., the average absolute firing rate from onset of catalepsy to, either 2 in scaled time, the end of catalepsy or the end of the experiment, whichever occurred first). The normalized data were then smoothed with a 21 sample moving average.

The beta band-power from each recording was first averaged over structures and then interpolated in time the same way as the firing rates, after which it was averaged across recordings and shifted so that the average beta power during baseline is 0.

Tissue preparation

Animals were anesthetized with a lethal dose of sodium pentobarbital (100 mg/kg) and transcardially perfused with 300 mL of 0.9 % saline, followed by 300 mL of ice-cold 4 % buffered paraformaldehyde. Heads were then fixated in 100 mL of 4 % paraformaldehyde until brains were removed. For cryoprotection, the tissue was then stored in 20 % sucrose solution in double distilled water (ddH_2O) at 4 °C for 3 days. Next, the brains were fast-frozen with dry ice and saved overnight in −20 °C. The brains were sectioned horizontally into 50-μm-thick slices using a freezing microtome. Slides were stored in −8 °C before staining.

Tyrosine hydroxylase staining and quantification

The size of the lesions was confirmed by TH immunohistochemistry as described in previous studies (Francardo *et al.*, 2011).

Sections were washed in phosphate buffer (PB) 0.01 M (5 min), hydrogen peroxide 0.3% diluted in methanol (20 min) and phosphate-buffered saline (PBS)/Tween 0.05% (5 min) and then incubated in 10% normal goat serum for 30 min, followed by incubation with primary antibody rabbit anti-TH (1:500; Chemicon) overnight at room temperature. On the following day, sections were rinsed in PBS/Tween 0.05% (5 min) and incubated with biotinylated goat anti-rabbit (1:200; Vector) for 2 h. After that, all sections were rinsed in PBS/Tween 0.05%, incubated in avidin–biotin complex (ABC Kit; Vector) for 1 h and stained with 3,3-diaminobenzidine and H_2O_2. TH striatal optical density was assessed using the ImageJ software (NIH) as described previously (Brys *et al.*, 2017) in areas adjacent to the striatal recording sites. The optical density of the ipsilateral corpus callosum was used as staining background and was subtracted from striatal values prior to comparison. Measurements indicated an almost complete (~100%) loss of dopaminergic terminals in the striatal region closest to the recording electrodes.

Nissl staining and verification of implantation coordinates

Sections were firstly rinsed in 10 mM PBS for 10 min. Next, they were rinsed in ddH_2O for 1 min and immediately thereafter stained for 15 min. The Nissl stain contained 0.1 g cresyl violet acetate, 100 mL ddH_2O and 250 μL glacial acetic acid. Sections were again rinsed with ddH_2O twice for 5 min and then left to dry for 1 h. After drying, sections were dehydrated with first 90 %, then 95 %, then 99.5 % ethanol for 3 min in each concentration. Sections were then dipped twice for 3 min in 100 % xylene 323 before mounting with DPX mounting media. The placement of the electrodes was histologically verified in cresyl violet-stained sections against anatomical landmarks and in animals where some recording channels were deemed to be out of place based on the histological examinations those channels were excluded from the dataset.

Statistical methods

Statistical tests for significant group difference that are not presented in this section are instead specified in Results and in the respective figure legends. Exact *P*-values for all tests are presented in Tables S1–S5.

In Fig. 2, group differences were tested using multi-way analysis of variance (*n*-way ANOVA) of the beta band-power with grouping variables indicating baseline/drug, animal and recording ID, the latter being treated as 'nested' in animal (Aarts *et al.*, 2014).

In Fig. 6B, a two-sample *t*-test was used. This paired test was based on the average absolute *z*-score of each cell for the specified intervals.

In Fig. 6D, significance was tested using a generalized mixed-effects model (GLME; fitglme in MATLAB). The formula (in Wilkinson notation) used for testing firing rate was:

$$MeanFR \sim Interval + (1|Structure) + (1|Animal) + (1|\ Animal : Recording) + (1|Animal : Recording : NeuronID)$$

where *MeanFR* is the average absolute firing rate of a unit during an interval, *Interval* is the measured interval (i.e., baseline, postinjection and postcatalepsy onset), *Structure* is the structure where the unit is located (RFA, M1, DMS, etc.), *Animal* is the ID of the animal, *Recording* is the ID of the recording, and *NeuronID* is a unique identifier for each unit so that its *MeanFR* can be followed across intervals. The basic expression M*eanFR ~ Interval* uses the interval as a fixed-effects predictor for *MeanFR*. The grouping term *(1|Structure)* accounts for random effect for the intercept of each structure (i.e., systematic differences in firing rate between structures). The grouping terms *(1|Animal) + (1|Animal:Recording) + (1|Animal: Recording:NeuronID)* do the same for animal, recording and neuron and also state that neurons are nested in recording, and recordings are nested in animal. The last grouping by neuron also ensures that it is a paired test (as we can follow one neuron over time). Similarly, the formula for testing the beta band-power was:

$$MeanBP \sim Interval + (1|Srucure) + (1|Animal) + (1|Animal : Recording) + (1|Animal : Recording : ChGroupID)$$

where *MeanBP* is the average band-power across all pairs of channels in a structure in a recording, and *ChGroupID* is a unique

identifier for each group in *MeanBP*, allowing for matching across intervals. The test was repeated 12 times [two interval comparisons and three drugs for the two measures (*MeanFR* and *MeanBP*)], hence, to correct for multiple comparisons, the *P*-values were multiplied by 12.

In Fig. S2, significance was tested using a generalized mixed-effects model (fitglme in MATLAB), using the formula (Wilkinson notation):

$$MeanFR \sim Interval + (1|Animal) + (1|Animal : Recording) + (1|Animal : Recording : NeuronID)$$

with the same variable meaning and term rationale as in 6*D*, but without the structure term, as the test was done separately for each structure. The test was repeated 128 times [two interval comparisons and four drugs, for two measures (up- and down-modulated units), and in all 8 structures], in order to correct for multiple comparisons the *P*-values were therefore multiplied by 128.

Results

Acute dopaminergic manipulations induce signs of parkinsonism with different delays

In total, 38 recordings with acute dopaminergic manipulations were performed in 10 adult female Sprague Dawley rats. All animals were recorded multiple times during a period of several weeks with at least 2 days rest between consecutive recordings to allow for drug washout (Morelli & Di Chiara, 1985; Kobayashi *et al.*, 1997; Sotnikova *et al.*, 2005). During experiments, the animals were placed in a circular open field where they could move around freely. In experiments involving acute pharmacological manipulations, rats were first recorded for at least 40 min during control conditions and then administered an intraperitoneal injection of AMPT, D1R antagonist, D2R antagonist or a combination of D1/D2R antagonists. Following injection, catalepsy tests were performed repeatedly throughout the experiment to test for the presence of drug-induced akinesia (Fuentes *et al.*, 2009). It became evident that all acute manipulations induced hypokinesia which was much more severe than what is normally observed in unilaterally chronically lesioned animals. In fact, all animals became virtually immobile following drug injection. Animals treated with D1R antagonist showed the fastest response to the drug (catalepsy after 20–30 min), followed by D2R antagonist and AMPT (90–120 min and 200–300 min, respectively). Similarly, the duration of pronounced akinesia differed between the drugs. The lengths of the recordings sessions were adapted accordingly, resulting in average recording lengths (mean ± SD) of 214 ± 93 min and 384 ± 77 min for the D1R and D2R antagonist, respectively; 383 ± 24 min for the D1/D2R antagonist and 362 ± 128 min for AMPT.

Dopaminergic manipulations induced distinct changes in neuronal activity

Local field potentials and unit activity were obtained in eight different brain structures in each hemisphere [rostral forelimb area (RFA—a rodent supplementary motor area), the forelimb area of the primary MI, dorsolateral/dorsomedial striatum (DLS/DMS), GP, ventrolateral/ventroanterior nuclei of the thalamus (VL/VA), STN and SNr], using 128 microwire electrodes centered on forelimb representation sub-regions. In order to probe for state-dependent changes in the synchronization of population activity, the spectral content of the LFPs was first analyzed throughout all experiments. To be exact, for the time-varying potential difference between all pairs of electrodes within one structure, a spectrogram was calculated, and their grand average was taken to define the overall spectrogram for that structure in each condition. In parallel with LFPs, unit activity was recorded in all channels where spiking neurons could be reliably detected and isolated. In Fig. 1, a representative experiment is shown (in this case a D1/D2R antagonist experiment) exemplifying the typical dataset collected during a single recording session. The top panel shows a spectrogram (from DLS) illustrating the temporal changes observed in LFP power in different parts of the frequency spectrum throughout the recording. In this example, a relative increase in low-frequency power (12–20 Hz) becomes visible from ~80 min after injection and becomes even more pronounced at ~170 min. An exaggerated synchronization of low-frequency basal ganglia activity of this type is in line with several previous studies reporting increased LFP power in the lower part of the beta band (typically 10–25 Hz) following dopamine depletion (Sebban *et al.*, 1999; Brown *et al.*, 2001; Cassidy *et al.*, 2002; Priori *et al.*, 2004; Costa *et al.*, 2006; Mallet *et al.*, 2008; Dejean *et al.*, 2009, 2011). Examining the beta power increase in the temporal domain revealed that this activity was typically not characterized by a stable oscillatory state, but instead stemmed from transient spindle-like activity which is also characterized by a difference in peak sharpness between peaks and troughs (Fig. 1B; see also Cole *et al.*, 2017; Dejean *et al.*, 2007; Halje *et al.*, 2012; Yael *et al.*, 2013; Yang *et al.*, 2013). It should, however, be pointed out that the observed increase in low-frequency LFP power in this brain structure, in this experiment, did not temporally match the onset of catalepsy (which started already ~20 min after injection of D1/D2R antagonists and remained throughout the recording session).

In the example recording shown, a relatively large fraction of all recorded cells displayed modulations in standardized firing rate after drug application, but with somewhat differing delay in relation to the time of drug injection (Fig. 1C).

Spectral content of LFPs is altered throughout cortico-basal ganglia–thalamic circuits

Interestingly, the neurophysiological changes induced in different parts of the cortico-basal ganglia–thalamic circuit showed certain differences between the different types of dopaminergic manipulations. In Fig. 2, time-averaged power density spectra have been constructed based on the recorded LFP spectrograms and are presented as mean ± SD of all animals. For comparison, a group of chronically 6-OHDA lesioned animals was also included (35 recordings in eight animals, with control condition represented by baseline data from intact animals). To ensure the comparison of similar behavioral states, only time periods when animals were relatively immobile were included in the analyses (the average of five 10-min periods on drug and one 10-min period during baseline).

When comparing the pharmacological manipulations, it became clear that dopamine antagonists resulted in certain spectral changes that resembled the blocking of dopamine synthesis with AMPT. In particular, an increase in LFP power in the low-beta band (12–20 Hz) was observed which was most pronounced in cortico-striatal circuits, where the difference to baseline reached significance for some parts of the cortico-striatal system in the AMPT, D2 and D1 + D2 groups (marked by asterisks in Fig. 2, $P < 0.05$ with Bonferroni correction for in total 40 comparisons, for details, see Table S1). Interestingly, this change in the synchronization of neuronal populations seemed to depend primarily on reduced D2R

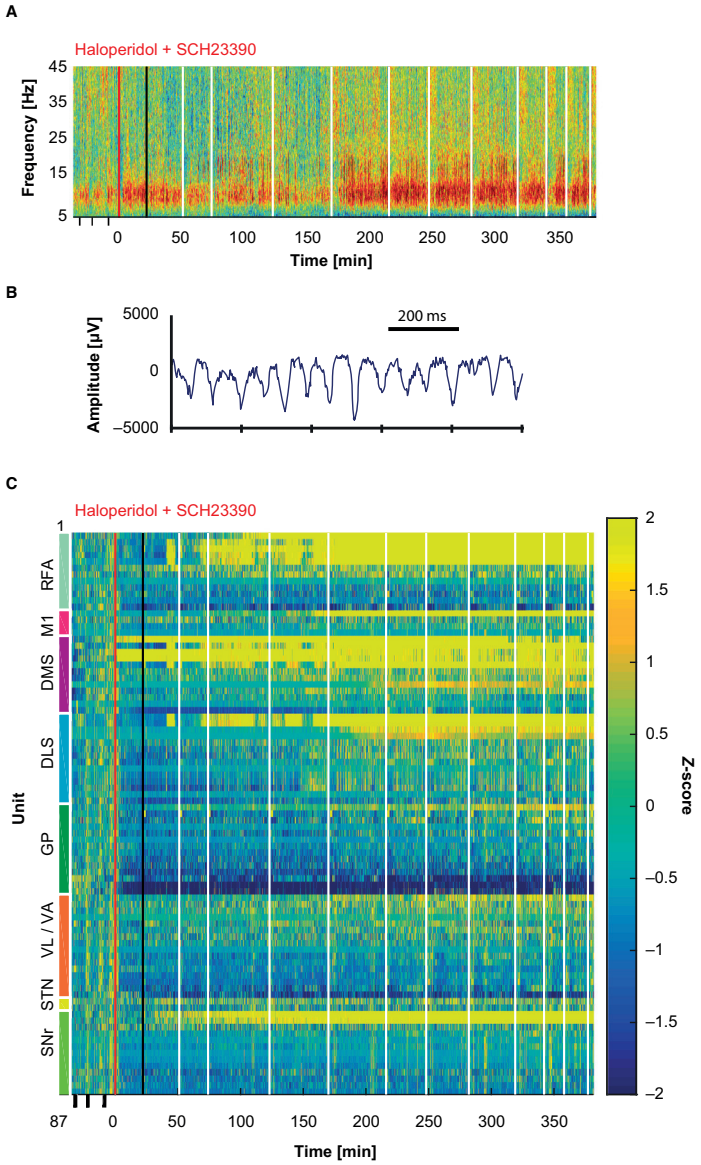

FIG. 1. Illustration of changes in local field potentials and firing rates during an example experiment with combined D1/D2R antagonist treatment [D1R antagonist SCH23390 (0.5 mg/kg) and D2R antagonist haloperidol (0.5 mg/kg)]. (A) Spectrogram representing the relative changes in frequency content of LFPs recorded from the DLS. The time of injection (t = 0 min) is denoted by the vertical red line. Black marks prior to the injection denote episodes of locomotor activity during baseline. Tests for catalepsy were performed at each of the black/white lines. Catalepsy had here started already at the first test performed (marked by black line) and remained throughout the experiment. Note that the relative increase in LFP power of low beta frequencies (12–20 Hz) appears much later than the onset of catalepsy. (B) Raw LFP trace recorded from a single electrode pair in DLS (about 185 min after injection), illustrating the typical temporal pattern of voltage fluctuations underlying an episode of increased low beta LFP power. (C) Alterations in standardized unit firing rates reveal drug-induced changes in several brain structures (structures are indicated by the colored bars to the left). Within each structure, the neurons are normalized to z-scores during baseline and sorted according to mean standardized rate change. Note the highly variable delay in rate dynamics across cells in relation to the time of injection. D1R, dopamine receptor type 1; D2R, dopamine receptor type 2; DLS, dorsolateral striatum; LFP, local field potentials. [Colour figure can be viewed at wileyonlinelibrary.com]

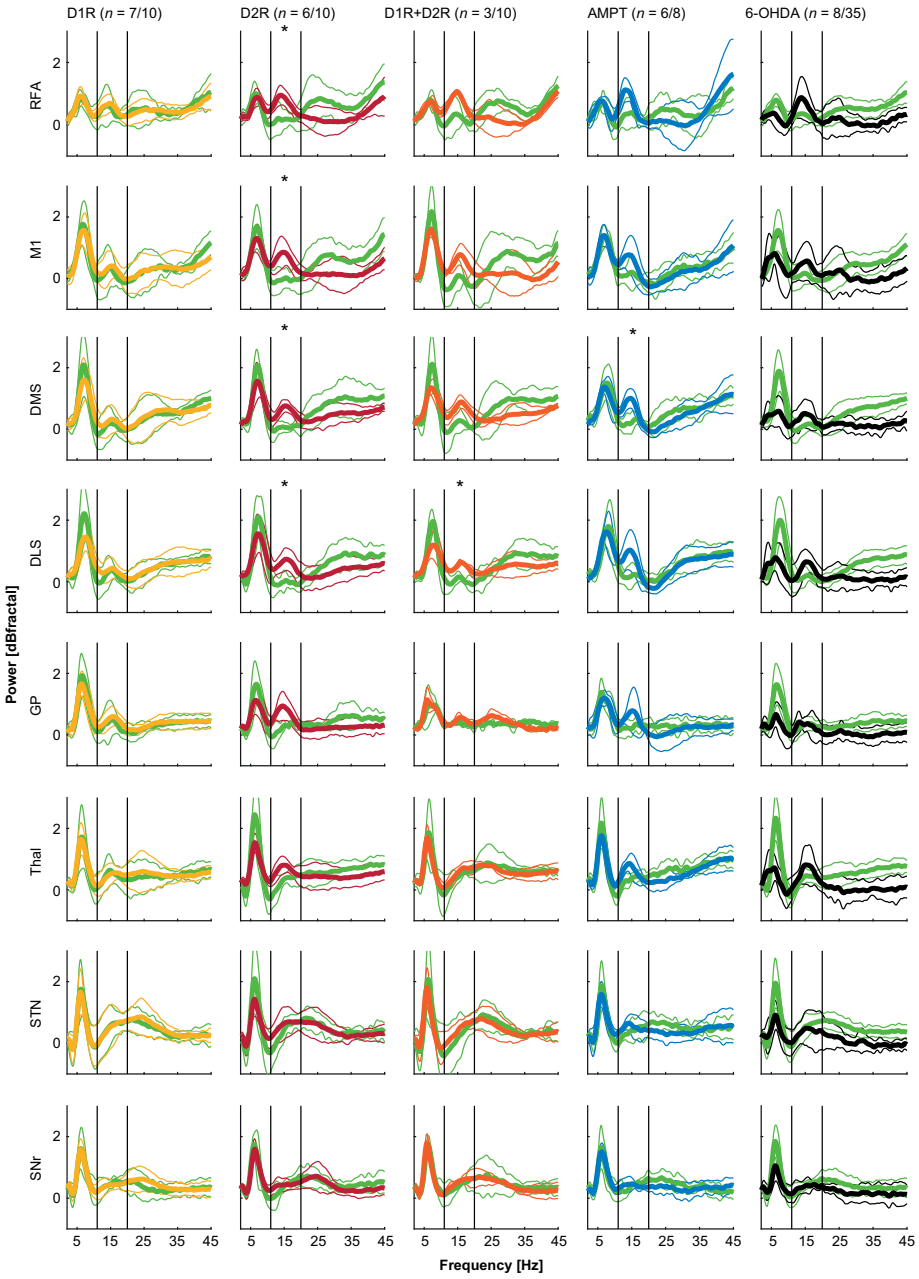

FIG. 2. Changes in LFP spectral content following dopaminergic manipulations. Mean power spectral density across animals during baseline (green traces) and drug-treated periods [colored traces: D1R antagonist (yellow), D2R antagonist (maroon), D1R + D2R antagonist (orange), AMPT (blue) and chronic 6-OHDA lesion (black)]. Asterisks in the marked 12–20 Hz band denote significant differences ($P < 0.05$ after Bonferroni correction ($n = 40$); control conditions in 6-OHDA animals were constructed from the average of all baseline recordings in the acute experiments, see Table S1 for details on *P*-values). D1R, dopamine receptor type 1; D2R, dopamine receptor type 2; LFP, local field potentials; 6-OHDA, 6-hydroxydopamine. [Colour figure can be viewed at wileyonlinelibrary.com]

signaling, because D1R antagonism alone resulted in more moderate spectral changes (albeit from baseline conditions with somewhat higher beta band-power). This was somewhat unexpected, given that motor manifestations in the form of hypokinesia/catalepsy were very similar across the different dopamine antagonists.

The low beta peak was also clearly visible in the chronically lesioned animals, and as a whole, the spectral profile of LFPs recorded in the chronic animals appeared strikingly similar to the acutely dopamine-depleted animals. However, the increase in low beta power in 6-OHDA lesioned animals was not statistically different to a reference control condition which was constructed from baseline recordings in the intact animals (two-sample *t*-test of the beta band-power; $P < 0.05$ with Bonferroni correction for in total 40 comparisons; however, it should be cautioned that the unpaired design in this case might result in lower statistical power). All analyses were here performed in the immobile state, but it may nevertheless be worth mentioning that during more active periods a distinct high beta peak (20–35 Hz) was frequently observed in the lesioned hemispheres in accordance with previous reports in moving animals (a weak trace of this high beta peak is visible in cortex also in the current data; Sharott *et al.*, 2005; Avila *et al.*, 2010; Brazhnik *et al.*, 2012).

Taken together, all the experimentally induced reductions in dopaminergic signaling were found to be associated with a tendency for increased beta LFP oscillations—resembling oscillations reported in PD patients (Kühn *et al.*, 2009).

Acute dopaminergic manipulations induce rate changes in the cortico-basal ganglia–thalamic circuits

We next analyzed firing rate changes of neurons recorded within each of the different structures. Because cells cannot be reliably matched over separate recordings several weeks apart, units recorded in the same channel during two different recording sessions were treated as different cells even when spike shapes were similar. Cells in cortex and striatum were divided into putative PCs and INs based on spike shape features, according to previously described and validated methods (Barthó *et al.*, 2004; Gage *et al.*, 2010; Roux *et al.*, 2014; Sparta *et al.*, 2014), whereas cells in the other structures were not further sub-divided (Fig. 3A). All structures turned out to have sub-populations of cells that significantly changed their firing rate in the drug-treated state compared to baseline (same periods as for LFPs, $P < 0.05$; Mann–Whitney *U*-test was used for comparison of firing rate distributions of each unit on/off drug, followed by a binomial test for significant number of up/downregulated cells, assuming the same probability of increasing/decreasing firing rate). For the dopamine antagonists, the proportions of cells showing positive vs. negative modulation following drug injection were, however, mixed, and for most structures, neither of the fractions was significantly larger than the other [$P < 0.05$, binomial test with Bonferroni correction ($n = 96$); cf. Burkhardt *et al.*, 2009]. More specifically, for the D1R antagonist, none of the analyzed structures had a significantly larger fraction of either type (Fig. 3B). Following systemic treatment with the D2R antagonist changes were also largely balanced, but cells in M1 tended to increase their firing rate. For the subgroup of putative PCs in M1, this fraction was significantly larger than the fraction of cells showing decreased firing rate ($P = 0.026$; Fig. 3C). The most noticeable effects on firing rates were observed following pharmacological reduction in the endogenous levels of dopamine by treatment with AMPT. In these experiments, a clear tendency for cells to decrease their firing rate was observed in several structures, reaching significance in relation to the proportion of cells increasing their rate only in cortical PCs (RFA: $P = 0.0053$, M1: $P = 0.0074$; Fig. 3D). Notably, antagonizing both receptor subtypes concomitantly did not induce a comparable reduction in rate; in these experiments, only the thalamic motor nucleus was found to have a significantly larger fraction of cells decreasing their firing rate ($P = 0.0037$; Fig. 3E; further details on statistics are presented in Table S2).

Thus, rate changes were observed in a majority of the recorded cells, but involved in most cases relatively equal fractions of cells showing increased/decreased firing rate within the same structure. Moreover, in situations where net changes were indeed observed in some structures, this pattern could not be simply explained by the predominant type of excitatory/inhibitory anatomical connectivity between structures as has been proposed in classical models (Albin *et al.*, 1989; DeLong, 1990). Yet, this complex pattern of rate changes is perhaps not so surprising, considering that network level interactions between structures in essence are overlaid on the individual direct effects of an altered dopaminergic tone on most cell groups (Smith & Villalba, 2008; Rommelfanger & Wichmann, 2010).

Acute dopaminergic manipulations induce entrainment to cortical LFP

It is possible that changes in average firing rates are not the only feature of the unit activity that is affected by dopaminergic manipulations. It has, for example, been suggested that, at least after chronic dopamine depletion, an increased synchronization of single unit activity may be more central than changes in overall rate (Nini *et al.*, 1995; Raz *et al.*, 2000; Fuentes *et al.*, 2010; Santana *et al.*, 2014). In particular, it is thought that widespread synchronization of beta oscillatory activity in basal ganglia circuits can arise as a consequence of cortical patterning of basal ganglia activity. Evidence supporting this view comes, for example, from studies showing that both striatal, GPe and STN neurons tend to fire action potentials in phase with cortical slow oscillations (Magill *et al.*, 2000, 2001; Tseng *et al.*, 2001), see also (Fuentes *et al.*, 2010; Richter *et al.*, 2013). We therefore next searched for evidence of cortical entrainment of unit activity. In particular, we wanted to investigate whether synchronized activity in the form of low-frequency LFP oscillations in primary MI affects spike timing in various structures of the cortico-basal ganglia–thalamic loop. For this purpose, STAs and SFCs related to an LFP reference signal recorded in M1 were created for each recorded unit for the selected time periods of interest (five 10-min periods on drug and one 10-min period during baseline). Figure 4A and B shows the STA and the SFC for an example cell (in RFA), for which it is evident that the exposure to the drug (D2R antagonist) induced pronounced entrainment to M1 LFP activity in the beta-range.

Entrainment to cortical LFPs should, however, not be considered a purely pathophysiological phenomenon. Indeed, we found clear indications of cell spiking entrainment to M1 LFP oscillations in the theta band (6–12 Hz) in several parts of the circuit, both during control conditions and after drug exposure. We therefore decided to investigate to what extent cells were entrained to the theta or beta band during baseline and after drug exposure. Overall, a substantial increase in the fractions of cells entrained to either theta- or beta range cortical oscillations was observed after drug application compared to baseline conditions (Fig. 4C; *P*-values for the respective drugs are presented in Table S3). Although relatively fewer cells were entrained during baseline, there was a tendency for these theta-entrained cells to remain entrained to the same LFP frequency range after drug (Fig. 4D).

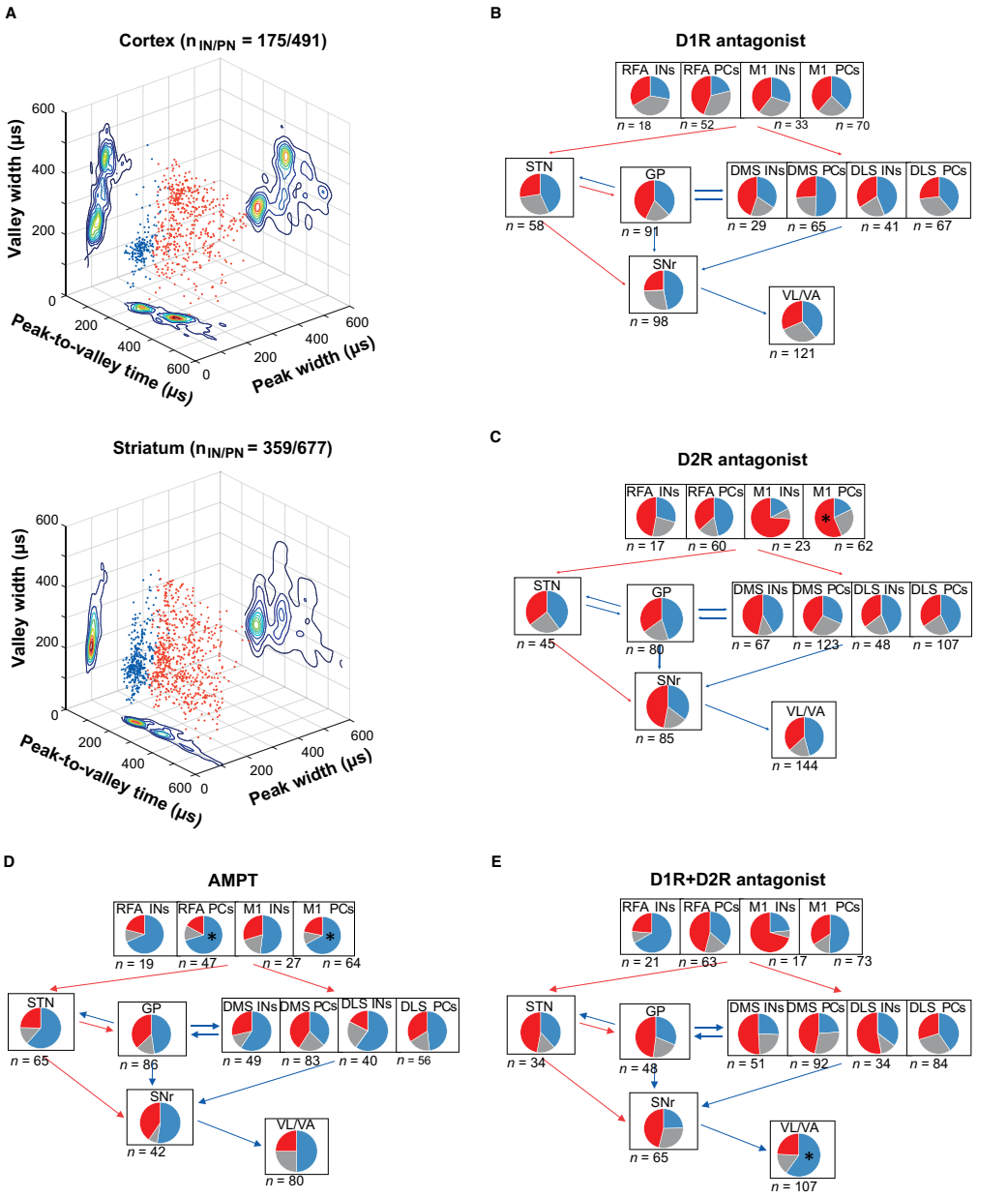

FIG. 3. Firing rate changes following pharmacological dopaminergic manipulations. (A) Summary of spike shape features represented in a 3D feature space for all neurons recorded from cortex (rostral forelimb area, M1) and striatum (dorsomedial striatum, dorsolateral striatum). Cluster densities for the respective 2D projection are shown for each pair of features by heat colored iso-density curves. Putative interneurons (peak-to-valley times ≤ 265 µs) are represented by dots colored in blue and principal cells (peak-to-valley times > 265 µs) in red. (B–E) Drug-induced firing rate changes divided by structure and cell-type. Fraction of cells showing a significant increase/decrease in firing rate (drug vs. baseline) is represented by red/blue slices, and the gray area represents non-modulated cells. Asterisks mark cell groups with a significant net change in rate ($P < 0.05$, binomial test with Bonferroni correction ($n = 96$); numbers below each box indicate total number of cells recorded for each drug condition. Red and blue arrows between boxes denote the principal glutamatergic and GABAergic anatomical connections. [Colour figure can be viewed at wileyonlinelibrary.com]

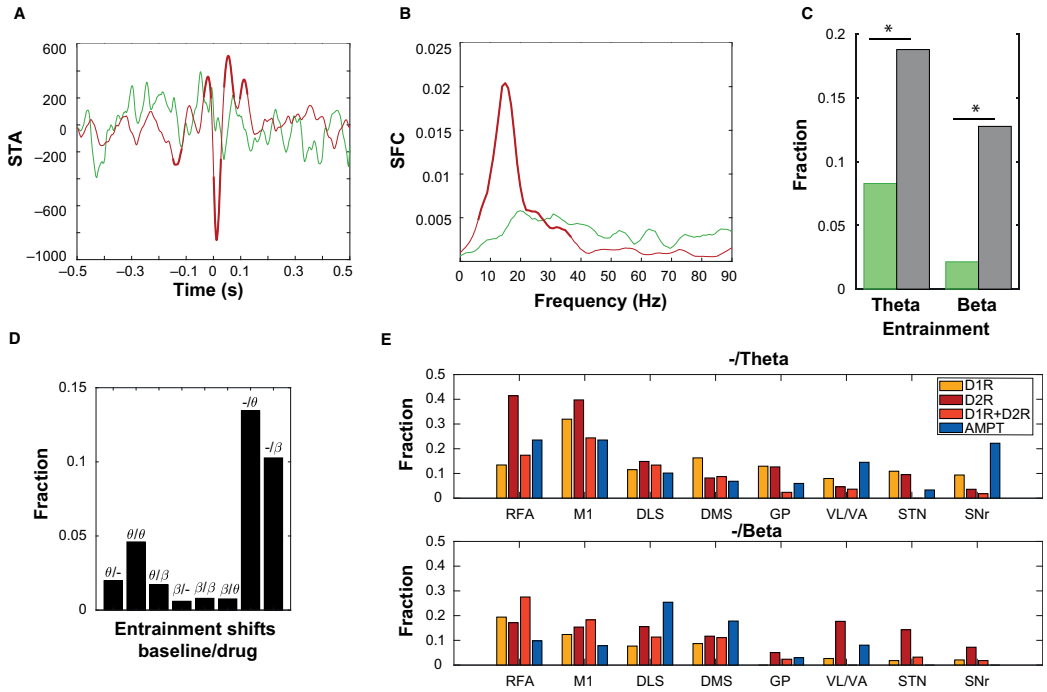

FIG. 4. Entrainment of neuronal spiking to M1 LFP oscillations. (A) STA of the M1 LFP shown for an example cell in RFA before (green) and after (maroon) treatment with D2R antagonist (parts of the STA where values exceed the 99% confidence interval are indicated with bold maroon lines). (B) The corresponding spike-field coherence plotted for the same unit. Coherence values exceeding the 99% confidence interval are marked in bold in the spectrum (6–37 Hz). (C) Fraction of the entrained cells (gray) in the theta and low beta band following drug treatment compared to baseline (green; cells are pooled over all structures and drugs; asterisks mark an upper binomial cumulative density probability < 0.05). (D) Fraction of cells shifting from/to being entrained to either theta or low beta, or both, before and after drug treatment displayed as (baseline/drug), the non-entrained state is marked with [-]. (E) Fraction of cells becoming entrained to either theta or low beta after drug treatment separated by type of drug and structure. D2R, dopamine receptor type 2; LFP, local field potentials; RFA, rostral forelimb area; STA, spike-triggered average. [Colour figure can be viewed at wileyonlinelibrary.com]

To further characterize the drug-induced entrainment of spiking activity to low-frequency oscillations in M1, we also analyzed the ability of each of the drugs to induce spike entrainment in the different structures (Fig. 4E). While there were no statistical differences between the four drugs with respect to fraction of cells entrained, we found a main effect of structure ($P = 0.0003$ for theta and $P = 0.0023$ for beta, two-way ANOVA, see also Table S4). In general, cortico-striatal circuits tended to have higher fraction of cells showing entrainment to M1 LFP than deeper structures.

Acute dopaminergic manipulations induce oscillatory spiking in single cells

As many cells showed entrainment of spiking to M1 low-frequency LFP oscillations, we also investigated whether synchronized activity feeding into the cortico-basal ganglia–thalamic loop is further propagated, or perhaps even arises, as a consequence of rhythmic firing in single cells with pacemaker-like properties. To this aim, autocorrelograms were constructed for all cells before and after drug administration, revealing several examples of cells with highly rhythmic firing patterns. An example cell (in VL/VA) displaying periodic firing corresponding to beta frequency following drug administration is shown in Fig. 5A.

For the population of cells showing rhythmic firing, theta and beta frequency range oscillations dominated (peak frequencies are plotted in Fig. 5B; with a hump around 15 Hz corresponding to the LFP low beta peak oscillation frequency). Also, in agreement with the entrainment analysis, theta oscillating cells were found to be present both before and after drug treatment, whereas strong beta rhythmicity in single cell firing principally showed up only after drug treatment. We furthermore noted that, in contrast to spike-LFP entrainment, the groups of cells showing distinct rhythmic spiking before and after drug, respectively, were found to be largely mutually exclusive (fractions separated by treatment are shown in Fig. S1). It should, however, be cautioned that the total number of cells observed with strong rhythmic firing properties was very low (only 121 out of 3048 cells).

The link between neurophysiological features and motor symptoms

The most consistent finding across all types of dopaminergic manipulations was the induction of synchronized oscillatory activity

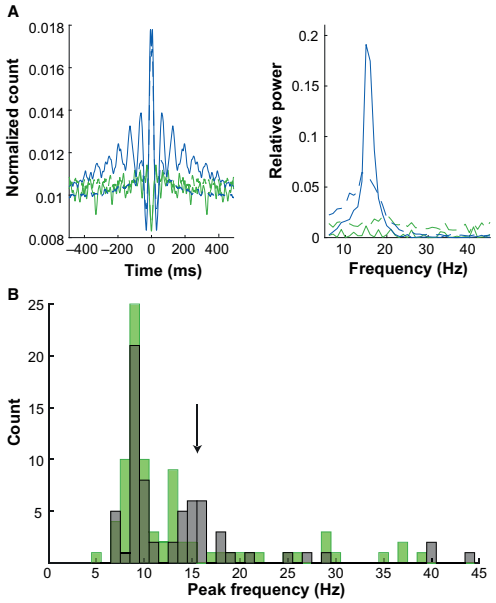

FIG. 5. Rhythmic neuronal spiking before and after pharmacological dopamine manipulations. (A) Left: Autocorrelogram of spiking activity in an example ventrolateral/ventroanterior neuron showing enhanced rhythmic firing following AMPT treatment (blue) compared to baseline (green). Right: Power spectral density of the autocorrelation shown to the left revealing a distinct frequency peak in the low beta band. Dashed lines denote confidence intervals (99%). (B) Histogram displaying the distributions of peak frequencies of all cells with strong rhythmic firing before (green) or after (gray) drug administration (recording periods as in Fig. 2). [Colour figure can be viewed at wileyonlinelibrary.com]

patterns, which involved cells in all parts of the cortico-basal ganglia circuit. Yet, as pointed out in relation to the example experiment illustrated in Fig. 1, clear signs of exaggerated synchronization of neuronal activity sometimes arose only after motor symptoms were already manifest, making this neurophysiological feature less plausible as a causal mechanism behind motor dysfunction. To investigate the link to motor dysfunction in further detail, we therefore studied the temporal development of the different neurophysiological features in relation to the time point of drug injection and onset of catalepsy, respectively.

For LFPs, the relative increase in beta band-power (12–20 Hz) was analyzed following pharmacological manipulations. Neuronal data obtained while the catalepsy tests were performed were excluded from the analyses (in total 4 min/test) because the handling of the animals inevitably caused a certain amount of stress resulting in a suppression of low-frequency oscillations. Overall, the temporal development of beta band-power showed that both the D1R and the D2R antagonist induced a gradual increase that relatively poorly matched the onset of motor symptoms (pooled data from all D1 or D2R experiments are shown in Fig. 6A, onset of catalepsy and significant beta increase are marked with vertical lines and bars, respectively). For the D2R antagonist, it was noted that beta oscillations emerged relatively shortly after D2R antagonist treatment in corticostriatal structures and thalamus. These cortical oscillations then progressively expanded to also include other parts of the cortico-basal ganglia–thalamic loop at a later time point. For the D1 antagonist, catalepsy was present before the detection of increased beta in any of the recorded structures.

As expected, the temporal development of action potential entrainment to M1 LFP beta oscillations for units recorded throughout the loop showed a similar relatively slow onset and gradual increase. Based on previously reported data, we also searched for a more general transition from regular to more burst firing patterns in the recorded units but could not establish any consistent drug-associated effects in this respect (Bergman *et al.*, 1994; Kaneoke & Vitek, 1996). Hence, none of these investigated features appear sufficient to explain the rapid onset of akinesia following, in particular, D1R antagonist treatment [median latency to first positive catalepsy test (Fig. 6A and B) was ~20 min]. Interestingly, firing rate changes could potentially provide the missing mechanistic link. Plotting the deviation from the mean firing rate observed on the baseline for each 8-s time bin during the experiments revealed significant rate changes already 10 min after D1R antagonist treatment [$P = 1.4391 \times 10^{-08}$, two-sample *t*-test (−20 −10) vs. (10 20); Fig. 6B, left]. Antagonizing D2Rs also induced a relatively immediate response [$P = 1.1607 \times 10^{-26}$, two-sample *t*-test (−20 −10) vs. (10 20)], in particular in GP (Fig. S2). Yet, in the D2 experiments, the larger part of the observed rate changes occurred during later phases of the recording (Fig. 6B, right, bottom). Conversely, AMPT induced no significant rate changes immediately after the first injection [Fig. 6C; $P = 0.6356$, paired *t*-test for mean $|z|$ of each neuron during (−20, −5) minutes compared to (5, 20) minutes]. This is consistent with the much slower effect of this drug on dopamine signaling (due to a significant synaptic recycling of vesicular dopamine; Sotnikova *et al.*, 2005; Fuentes *et al.*, 2009) and, in effect, served as an important negative control showing that rate changes unrelated to pharmacological effects were minor. Hence, our data suggest that even when significant net changes in firing rate are not observed for the recorded anatomical structures, the relative increase and decrease within different sub-populations of cells may nevertheless be highly relevant and could potentially represent the first signs of pathogenic neuronal activity that eventually bring about the emergence of motor symptoms.

To analyze the temporal relationship between physiological changes and the onset of akinesia in further detail, we plotted changes in firing rates and LFP beta power as a function of time against each other for all three drugs (Fig. 6D). All time axes were scaled from 'time of injection' ($t = 0$) to 'time of first positive catalepsy test' [$t = 1$; on average corresponding to 239 min for AMPT (first injection), 20 for the D1 antagonist and 58 for the D2 antagonist]. To facilitate direct comparisons, the average absolute *Z*-score on the left *y*-axis is normalized from baseline ($y = 0$) to the early cataleptic period ($y = 1$), and the beta power on the right *y*-axis is shifted to average baseline power ($y = 0$). Significant changes are denoted by asterisks and hash-signs, see Table S5 for details (on average, the time intervals marked for the tests correspond to 72 min for AMPT, 6 for the D1 antagonist and 18 for the D2 antagonist). These plots clearly illustrate that when catalepsy had first been observed rate changes had already approached the values observed during the akinetic period for all three drugs. In contrast, the increase in beta power was more gradual, and for the D1 antagonist, it occurred with such a long delay after the onset of catalepsy that it could not be detected on the time scale plotted. Because our data point to rate changes in a diverse group of neurons located in different structures as a potential pathophysiological mechanism for the induction of akinesia, we decided to break down the dataset even further and analyze the rate changes of cell groups that either increase or decrease their firing rate separately for all the different structures

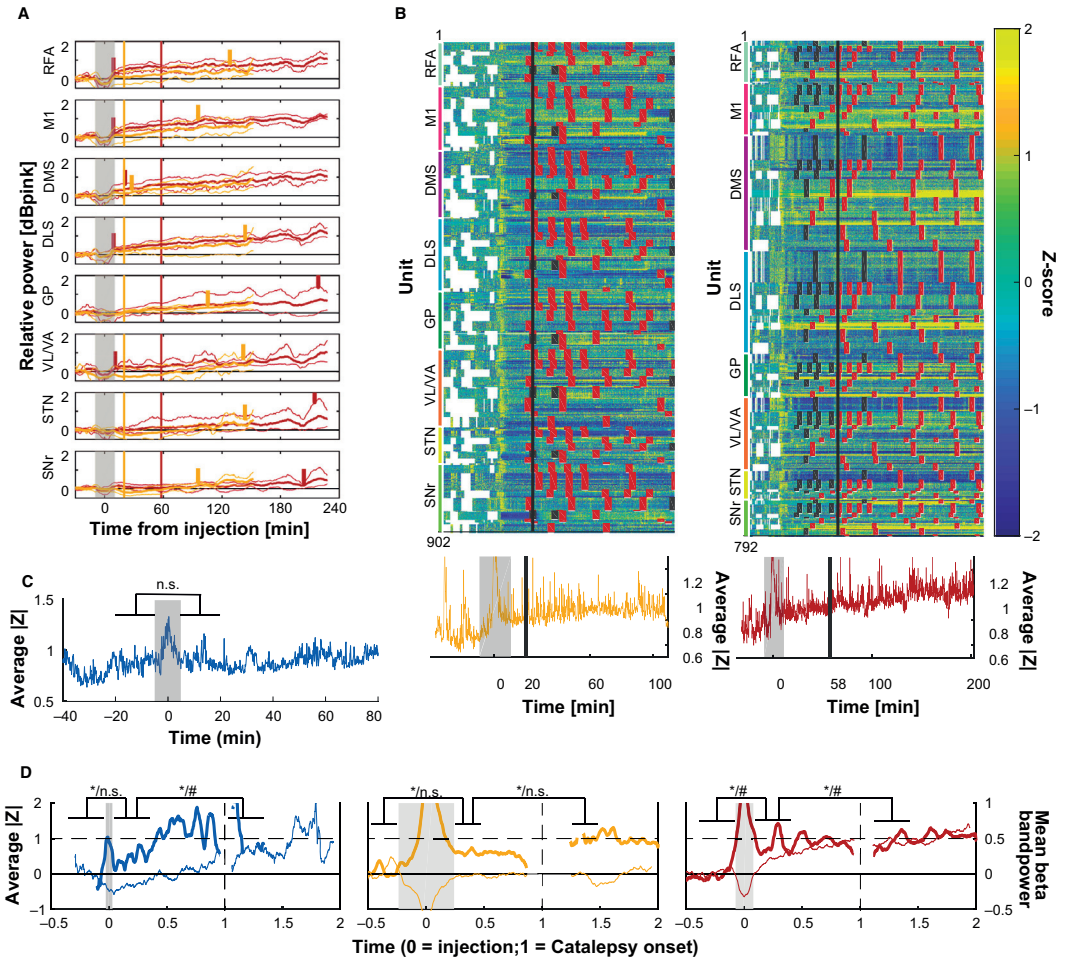

FIG. 6. Temporal development of electrophysiological features in relation to the onset of motor symptoms. (A) Changes in relative band-power in the low beta over time (mean ± 99% CI; drug injection at $t = 0$; vertical lines denote the median time point of first positive catalepsy test, and vertical bars mark the time point after which beta power is consistently higher than baseline CI; yellow = D1R and maroon = D2R antagonist). Note the relatively fast onset of cortico-striatal/thalamic beta oscillations after D2R antagonist followed by a much later increase in deeper structure and the comparatively slow band-power increases after D1R antagonist arising after onset of catalepsy. (B) Rate changes in individual cells. Top: Deviations from average baseline firing rates (drug injection at $t = 0$; gray vertical lines denote the median time point of first positive catalepsy test; white bins during baseline denote active periods that were excluded from analyses and gray/red bins negative/positive catalepsy tests). Bottom: Averaged absolute deviations from mean baseline firing rates. Significant rate changes are observed shortly after administration of D1R (left/yellow) and D2R (right/maroon) antagonists, preceding the first evidence of catalepsy. For the D2R antagonist, the immediate response to the drug is followed by further rate changes developing gradually over time. (C) Averaged absolute deviations from mean baseline firing rates following first AMPT injection. The observed absence of firing rate changes is in complete accordance with the lack of motor signs during the first hour. (D) Changes in beta power (thin line; right *y*-axis) and firing rates (thick line; left *y*-axis) plotted with an *x*-axis scaling adapted to latency of catalepsy [drug injection at $t = 0$ (first injection for AMPT) and catalepsy onset at $t = 1$]. The average absolute *Z*-score on the left *y*-axis is normalized from baseline ($y = 0$) to the early cataleptic period ($y = 1$). The beta power on the right *y*-axis is shifted to average baseline power ($y = 0$). Note that rate changes consistently precede the first detection of catalepsy. Gray shaded and white areas denote periods excluded from further analyses because of manual handling of the animals or locomotion (nine D1R, eight D2R and four AMPT experiments were included). Statistical differences mark changes between the indicated time periods (late baseline, early postinjection and early catalepsy). '*' = significant rate change, '#' = significant beta power change, 'n.s.' = non-significant. D1R, dopamine receptor type 1; D2R, dopamine receptor type 2. [Colour figure can be viewed at wileyonlinelibrary.com]

and for all drugs. This analysis showed that the subgroup of neurons in the different structures that decrease their firing rate in response to the drug often had the fastest response. However, signs of akinesia generally arose later on in the experiments when the subgroup of cells that increase their firing rate started displaying significant rate changes. This division was most noticeable for AMPT and the D1

antagonist, whereas the D2 antagonist induced a more diverse response in the two subgroups across structures (Fig. S2).

Discussion

Beta frequency oscillations in basal ganglia structures is a frequent finding in PD patients (Brown *et al.*, 2001; Kühn *et al.*, 2009). However, motor activity and even resting tremor are known to strongly suppress these oscillations (Brittain & Brown, 2014; Qasim *et al.*, 2016). The association between oscillations and motor symptoms has therefore been a matter of some debate. In a number of studies a disconnect has been shown between the emergence of motor signs and the development of increased power in the beta-band. For example, in rodent chronic models of PD, robust akinesia was established already the first day after 6-OHDA lesions, whereas beta oscillations in sensorimotor cortex were reliably detected only several days later (Mallet *et al.*, 2008; Degos *et al.*, 2009). Similarly, recordings in basal ganglia structures and MI following acute treatment with D1R/D2R antagonists in urethane-anesthetized animals (Mallet *et al.*, 2008), or in awake behaving rats (Degos *et al.*, 2009), showed no evidence of enhanced beta, even though akinesia developed rapidly in the same animals in the awake state. On the other hand, beta oscillations following D1R/D2R antagonist treatment have been reported in several other studies (Sebban *et al.*, 1999; Dejean *et al.*, 2009, 2011), demonstrating that acute dopamine manipulations under certain conditions can induce beta oscillations resembling those observed following chronic lesions. Our results show that, in particular, acute D2R antagonism leads to pronounced beta oscillations that gradually spread from thalamus and cortico-striatal circuits to also include deeper structures of the basal ganglia over time. Yet, the display of akinesia/catalepsy in our experiments after D1R antagonist treatment clearly preceded the development of beta oscillations, which would seem to rule out a causal role.

In our experiments, we found no strong evidence for net changes in firing rate following dopaminergic manipulations that could be matched to the classical models of basal ganglia pathophysiology in PD (Albin *et al.*, 1989; DeLong, 1990). Clearly, however, acute dopaminergic manipulations in rodents differ in several ways from chronic lesions in primates, which is the model system from which several of the first observations of rate changes in animal models of PD originate (Miller & DeLong, 1987; Filion & Tremblay, 1991; Bergman *et al.*, 1994). The chronic condition involves neuronal cell death and almost certainly a range of plastic changes that have no counterpart in acute experiments making chronic lesions in animals a more valid model for PD (Ingham *et al.*, 1997; Chu *et al.*, 2015). On the other hand, for the direct investigation of the role of dopamine in motor circuits, acute dopaminergic manipulations have an advantage over chronic models in that firing rates of individual neurons can be tracked during the course of an experiment comprising both control conditions and drug-treated states. In addition to the selective dopaminergic manipulations we here also included a broader manipulation (AMPT) affecting both dopamine and noradrenaline, thus closer approaching the clinical situation (Zarow *et al.*, 2003), which, however, in several respects resulted in neurophysiological changes resembling those induced by the receptor antagonists. In previous studies applying an acute pharmacological design, mixed results have been reported with respect to changes in firing rates following dopaminergic manipulations (Filion, 1979; Costa *et al.*, 2006; Burkhardt *et al.*, 2009). This relatively diverse pattern of rate changes has been hard to interpret from a functional perspective. Interestingly, our results suggest that these changes—although complex and diverse—may in fact be a significant neurophysiological mechanism underlying motor dysfunctions which deserves to be investigated in further detail in future studies.

Moreover, a strict division between the analyses of rate and rhythmicity in cell firing may in itself be misleading. In simulations of activity patterns arising in cortex as a consequence of modifications of input from external sources, it has been shown that cortical beta oscillations could in fact be induced by transient rate changes in thalamocortical projections [Sherman *et al.*, 2016; also discussed in a recent study on beta oscillations in PD patients (Cole *et al.*, 2017)]. Intriguingly, the transient bouts of synchronized activity observed in our experiments (see Fig. 1B) display the same non-sinusoidal shape in the temporal domain, with a clear difference in sharpness between peaks and troughs that are described in these studies (cf. Cole *et al.*, 2017).

In conclusion, by performing the first measurements of neuronal activity in all the main structures of the cortico-basal ganglia–thalamic loop in parallel in freely behaving animals, we have here, on a circuit level, characterized the neurophysiological changes in both rate and rhythm induced by various experimental interventions targeting dopaminergic signaling. The observed changes differ between drugs and structures, but based on the temporal development of the different features following drug injections, we propose that a complex set of rate changes, involving several brain structures in parallel, initiates the neurophysiological state change, which then gradually develops to include all the other neurophysiological features associated with the acute and chronic hypodopaminergic state.

Supporting Information

Additional supporting information can be found in the online version of this article:

Table S1. Baseline/drug low beta band (12–20 Hz) compared by multi-way nested ANOVA.
Table S2. Significant cell fractions increasing/decreasing their firing rate during drug/baseline.
Table S3. Significant entrainment baseline/drug to theta or beta band.
Table S4. Entrainment to theta or beta band separated by drug and structure.
Table S5. Test for significant changes in beta power and firing rate [applying a generalized mixed effects model (GLME), see Methods for details].
Table S6. Summary of the number of cells showing changes in average standardized firing rate as a result of drug treatment.
Fig. S1. Fraction of cells exhibiting rhythmic neuronal spiking.
Fig. S2. Changes in firing rates, split into averages from up- and down-modulated units plotted for all drugs and structures.

Acknowledgements

The study was supported by grants from the Bergvall, Crafoord, MJ Fox, Kocks, Olle Engkvist, Parkinson, Parkinson Research, the Swedish Brain, Åhlen and Åke Wiberg Foundation, Goljes minne, Sven-Olof Jansons livsverk, Fysiografiska Sällskapet and from the VR grant #MH-2011-24 and the Erasmus Mundus Action 2 program. The current affiliation of Ivani Brys is Universidade Federal do Vale do São Francisco. José de Maniçoba, s/n — Centro—Petrolina, PE, Brazil, 56304205.

Conflict of Interest

The authors declare no competing financial interests.

Author contributions

NI performed the naive drug-treated animal experiments and sorted the unit data; UR and JS developed analytical approaches and analyzed the data; IB and MT performed experiments in 6-OHDA lesioned animals; PP and NI designed the experiments, contributed in analyses and wrote the manuscript.

Data accessibility

The data that support the findings of this study are available from the corresponding author upon reasonable request.

Abbreviations

6-OHDA, 6-hydroxydopamine; AMPT, alpha-methyl-*p*-tyrosine; AP, anteroposterior; D1R/2R, dopamine 1/2 receptor type; ddH_2O, double distilled water; DLS, dorsolateral striatum; DMS, dorsomedial striatum; DV, dorsoventral; GLME, generalized mixed-effects model; GPe, globus pallidus pars externa; GP, globus pallidus; INs, interneurons; ISI, inter-spike interval; LFP, local field potential; M1, primary motor cortex; ML, mediolateral; PB, phosphate buffer; PBS, phosphate-buffered saline; PCs, principal cells; PD, Parkinson's disease; RFA, rostral forelimb area; SFC, spike-field coherence; SNr, substantia nigra pars reticulata; STA, spike-triggered average; STN, subthalamic nucleus; TB, tooth bar; TH, tyrosine hydroxylase; VL/VA, ventrolateral/ventroanterior nuclei.

References

Aarts, E., Verhage, M., Veenvliet, J.V., Dolan, C.V. & van der Sluis, S. (2014) A solution to dependency: using multilevel analysis to accommodate nested data. *Nat. Neurosci.*, **17**, 491–496.

Albin, R.L., Young, A.B. & Penney, J.B. (1989) The functional anatomy of basal ganglia disorders. *Trends Neurosci.*, **12**, 366–375.

Avila, I., Parr-Brownlie, L.C., Brazhnik, E., Castañeda, E., Bergstrom, D.A. & Walters, J.R. (2010) Beta frequency synchronization in basal ganglia output during rest and walk in a hemiparkinsonian rat. *Exp. Neurol.*, **221**, 307–319.

Barthó, P., Hirase, H., Monconduit, L., Zugaro, M., Harris, K.D. & Buzsáki, G. (2004) Characterization of neocortical principal cells and interneurons by network interactions and extracellular features. *J. Neurophysiol.*, **92**, 600–608.

Berger, B., Trottier, S., Gaspar, P., Verney, C. & Alvarez, C. (1986) Major dopamine innervation of the cortical motor areas in the Cynomolgus monkey. A radioautographic study with comparative assessment of serotonergic afferents. *Neurosci. Lett.*, **72**, 121–127.

Bergman, H., Wichmann, T., Karmon, B. & DeLong, M.R. (1994) The primate subthalamic nucleus. II. Neuronal activity in the MPTP model of Parkinsonism. *J. Neurophysiol.*, **72**, 507–520.

Brazhnik, E., Cruz, A.V., Avila, I., Wahba, M.I., Novikov, N., Ilieva, N.M., McCoy, A.J., Gerber, C. *et al.* (2012) State-dependent spike and local field synchronization between motor cortex and substantia Nigra in Hemiparkinsonian rats. *J. Neurosci.*, **32**, 7869–7880.

Brittain, J.-S. & Brown, P. (2014) Oscillations and the basal ganglia: motor control and beyond. *Neuroimage*, **85**, 637–647.

Brown, R.M., Crane, A.M. & Goldman, P.S. (1979) Regional distribution of monoamines in the cerebral cortex and subcortical structures of the rhesus monkey: concentrations and in vivo synthesis rates. *Brain Res.*, **168**, 133–150.

Brown, P., Oliviero, A., Mazzone, P., Insola, A., Tonali, P. & Di Lazzaro, V. (2001) Dopamine dependency of oscillations between subthalamic nucleus and pallidum in Parkinson's disease. *J. Neurosci.*, **21**, 1033–1038.

Brys, I., Bobela, W., Schneider, B.L., Aebischer, P. & Fuentes, R. (2017) Spinal cord stimulation improves forelimb use in an alpha-synuclein animal model of Parkinson's disease. *Int. J. Neurosci.*, **127**, 28–36.

Burkhardt, J.M., Jin, X. & Costa, R.M. (2009) Dissociable effects of dopamine on neuronal firing rate and synchrony in the dorsal striatum. *Front. Integr. Neurosci.*, **3**, 28.

Carlsson, A., Lindqvist, M., Magnusson, T. & Waldeck, B. (1958) On the presence of 3-hydroxytyramine in brain. *Science*, **127**, 471.

Cassidy, M., Mazzone, P., Oliviero, A., Insola, A., Tonali, P., Di Lazzaro, V. & Brown, P. (2002) Movement-related changes in synchronization in the human basal ganglia. *Brain*, **125**, 1235–1246.

Chen, L., Qi, R., Chen, X.Y., Xue, Y., Xu, R. & Wei, H.J. (2011) Modulation of the activity of globus pallidus by dopamine D1-like receptors in Parkinsonian rats. *Neuroscience*, **194**, 181–188.

Cheramy, A., Leviel, V. & Glowinski, J. (1981) Dendritic release of dopamine in the substantia nigra. *Nature*, **289**, 537–542.

Chu, H.-Y., Atherton, J.F., Wokosin, D., Surmeier, D.J. & Bevan, M.D. (2015) Heterosynaptic regulation of external globus pallidus inputs to the subthalamic nucleus by the motor cortex. *Neuron*, **85**, 364–376.

Cole, S.R., van der Meij, R., Peterson, E.J., de Hemptinne, C., Starr, P.A. & Voytek, B. (2017) Nonsinusoidal beta oscillations reflect cortical pathophysiology in Parkinson's disease. *J. Neurosci.*, **37**, 4830–4840.

Costa, R.M., Lin, S.-C., Sotnikova, T.D., Cyr, M., Gainetdinov, R.R., Caron, M.G. & Nicolelis, M.A.L. (2006) Rapid alterations in corticostriatal ensemble coordination during acute dopamine-dependent motor dysfunction. *Neuron*, **52**, 359–369.

Degos, B., Deniau, J.-M., Chavez, M. & Maurice, N. (2009) Chronic but not acute dopaminergic transmission interruption promotes a progressive increase in cortical beta frequency synchronization: relationships to vigilance state and akinesia. *Cereb. Cortex*, **19**, 1616–1630.

Dejean, C., Gross, C.E., Bioulac, B. & Boraud, T. (2007) Synchronous high-voltage spindles in the cortex-basal ganglia network of awake and unrestrained rats. *Eur. J. Neurosci.*, **25**, 772–784.

Dejean, C., Hyland, B. & Arbuthnott, G. (2009) Cortical effects of subthalamic stimulation correlate with behavioral recovery from dopamine antagonist induced akinesia. *Cereb. Cortex*, **19**, 1055–1063.

Dejean, C., Arbuthnott, G., Wickens, J.R., Le Moine, C., Boraud, T. & Hyland, B.I. (2011) Power fluctuations in beta and gamma frequencies in rat globus pallidus: association with specific phases of slow oscillations and differential modulation by dopamine D1 and D2 receptors. *J. Neurosci.*, **31**, 6098–6107.

DeLong, M.R. (1990) Primate models of movement disorders of basal ganglia origin. *Trends Neurosci.*, **13**, 281–285.

Fee, M.S., Mitra, P.P. & Kleinfeld, D. (1996) Automatic sorting of multiple unit neuronal signals in the presence of anisotropic and non-Gaussian variability. *J. Neurosci. Meth.*, **69**, 175–188.

Filion, M. (1979) Effects of interruption of the nigrostriatal pathway and of dopaminergic agents on the spontaneous activity of globus pallidus neurons in the awake monkey. *Brain Res.*, **178**, 425–441.

Filion, M. & Tremblay, L. (1991) Abnormal spontaneous activity of globus pallidus neurons in monkeys with MPTP-induced Parkinsonism. *Brain Res.*, **547**, 142–151.

Francardo, V., Recchia, A., Popovic, N., Andersson, D., Nissbrandt, H. & Cenci, M.A. (2011) Impact of the lesion procedure on the profiles of motor impairment and molecular responsiveness to L-DOPA in the 6-hydroxydopamine mouse model of Parkinson's disease. *Neurobiol. Dis.*, **42**, 327–340.

Freeman, A., Ciliax, B., Bakay, R., Daley, J., Miller, R.D., Keating, G., Levey, A. & Rye, D. (2001) Nigrostriatal collaterals to thalamus degenerate in Parkinsonian animal models. *Ann. Neurol.*, **50**, 321–329.

Fries, P., Reynolds, J.H., Rorie, A.E. & Desimone, R. (2001) Modulation of oscillatory neuronal synchronization by selective visual attention. *Science*, **291**, 1560–1563.

Fuentes, R., Petersson, P., Siesser, W.B., Caron, M.G. & Nicolelis, M.A. (2009) Spinal cord stimulation restores locomotion in animal models of Parkinson's disease. *Science*, **323**, 1578–1582.

Fuentes, R., Petersson, P. & Nicolelis, M.A.L. (2010) Restoration of locomotive function in Parkinson's disease by spinal cord stimulation: mechanistic approach. *Eur. J. Neurosci.*, **32**, 1100–1108.

Gage, G.J., Stoetzner, C.R., Wiltschko, A.B. & Berke, J.D. (2010) Selective activation of striatal fast-spiking interneurons during choice execution. *Neuron*, **67**, 466–479.

Gaspar, P., Berger, B., Febvret, A., Vigny, A. & Henry, J.P. (1989) Catecholamine innervation of the human cerebral cortex as revealed by comparative immunohistochemistry of tyrosine hydroxylase and dopamine-beta-hydroxylase. *J. Comp. Neurol.*, **279**, 249–271.

Gatev, P., Darbin, O. & Wichmann, T. (2006) Oscillations in the basal ganglia under normal conditions and in movement disorders. *Movement Disord.*, **21**, 1566–1577.

Gerfen, C.R. & Surmeier, D.J. (2011) Modulation of striatal projection systems by dopamine. *Annu. Rev. Neurosci.*, **34**, 441–466.

Gioanni, Y. & Lamarche, M. (1985) A reappraisal of rat motor cortex organization by intracortical microstimulation. *Brain Res.*, **344**, 49–61.

Grun, S. (2009) Data-driven significance estimation for precise spike correlation. *J. Neurophysiol.*, **101**, 1126–1140.

Halje, P., Tamtè, M., Richter, U., Mohammed, M., Cenci, M.A. & Petersson, P. (2012) Levodopa-induced dyskinesia is strongly associated with resonant cortical oscillations. *J. Neurosci.*, **32**, 16541–16551.
Hornykiewicz, O. (2002) Dopamine miracle: from brain homogenate to dopamine replacement. *Movement Disord.*, **17**, 501–508.
Hornykiewicz, O. (2006) The discovery of dopamine deficiency in the parkinsonian brain. *J. Neural Tr. S.*, **70**, 9–15.
Ingham, C.A., Hood, S.H., Mijnster, M.J., Baldock, R.A. & Arbuthnott, G.W. (1997) Plasticity of striatopallidal terminals following unilateral lesion of the dopaminergic nigrostriatal pathway: a morphological study. *Exp. Brain Res.*, **116**, 39–49.
Ivica, N., Tamtè, M., Ahmed, M., Richter, U. & Petersson, P. (2014) Design of a high-density multi-channel electrode for multi-structure parallel recordings in rodents. 36th Annual International IEEE EMBS Conference of the IEEE Engineering in Medicine and Biology Society. pp. 393–396.
Kaneoke, Y. & Vitek, J.L. (1996) Burst and oscillation as disparate neuronal properties. *J. Neurosci. Meth.*, **68**, 211–223.
Kobayashi, T., Araki, T., Itoyama, Y., Takeshita, M., Ohta, T. & Oshima, Y. (1997) Effects of L-dopa and bromocriptine on haloperidol-induced motor deficits in mice. *Life Sci.*, **61**, 2529–2538.
Kühn, A.A., Tsui, A., Aziz, T., Ray, N., Brücke, C., Kupsch, A., Schneider, G.-H. & Brown, P. (2009) Pathological synchronisation in the subthalamic nucleus of patients with Parkinson's disease relates to both bradykinesia and rigidity. *Exp. Neurol.*, **215**, 380–387.
Levy, R., Ashby, P., Hutchison, W.D., Lang, A.E., Lozano, A.M. & Dostrovsky, J.O. (2002) Dependence of subthalamic nucleus oscillations on movement and dopamine in Parkinson's disease. *Brain*, **125**, 1196–1209.
Lindvall, O. & Björklund, A. (1979) Dopaminergic innervation of the globus pallidus by collaterals from the nigrostriatal pathway. *Brain Res.*, **172**, 169–173.
Magill, P.J., Bolam, J.P. & Bevan, M.D. (2000) Relationship of activity in the subthalamic nucleus-globus pallidus network to cortical electroencephalogram. *J. Neurosci.*, **20**, 820–833.
Magill, P.J., Bolam, J.P. & Bevan, M.D. (2001) Dopamine regulates the impact of the cerebral cortex on the subthalamic nucleus-globus pallidus network. *Neuroscience*, **106**, 313–330.
Mallet, N., Pogosyan, A., Sharott, A., Csicsvari, J., Bolam, J.P., Brown, P. & Magill, P.J. (2008) Disrupted dopamine transmission and the emergence of exaggerated beta oscillations in subthalamic nucleus and cerebral cortex. *J. Neurosci.*, **28**, 4795–4806.
Meibach, R.C. & Katzman, R. (1979) Catecholaminergic innervation of the subthalamic nucleus: evidence for a rostral continuation of the A9 (substantia nigra) dopaminergic cell group. *Brain Res.*, **173**, 364–368.
Miller, W.C. & DeLong, M.R. (1987). *Altered Tonic Activity of Neurons in the Globus Pallidus and Subthalamic Nucleus in the Primate MPTP Model of Parkinsonism*. Springer, Boston, MA, pp. 415–427.
Morelli, M. & Di Chiara, G. (1985) Catalepsy induced by SCH 23390 in rats. *Eur. J. Pharmacol.*, **117**, 179–185.
Neafsey, E.J. & Sievert, C. (1982) A second forelimb motor area exists in rat frontal cortex. *Brain Res.*, **232**, 151–156.
Nini, A., Feingold, A., Slovin, H. & Bergman, H. (1995) Neurons in the globus pallidus do not show correlated activity in the normal monkey, but phase-locked oscillations appear in the MPTP model of Parkinsonism. *J. Neurophysiol.*, **74**, 1800–1805.
Paxinos, G. & Watson, C. (2007) *The Rat Brain in Stereotaxic Coordinates*. Academic Press, New York, NY.
Prensa, L. & Parent, A. (2001) The nigrostriatal pathway in the rat: a single-axon study of the relationship between dorsal and ventral tier nigral neurons and the striosome/matrix striatal compartments. *J. Neurosci.*, **21**, 7247–7260.
Priori, A., Foffani, G., Pesenti, A., Tamma, F., Bianchi, A.M., Pellegrini, M., Locatelli, M., Moxon, K.A. *et al.* (2004) Rhythm-specific pharmacological modulation of subthalamic activity in Parkinson's disease. *Exp. Neurol.*, **189**, 369–379.
Qasim, S.E., de Hemptinne, C., Swann, N.C., Miocinovic, S., Ostrem, J.L. & Starr, P.A. (2016) Electrocorticography reveals beta desynchronization in the basal ganglia-cortical loop during rest tremor in Parkinson's disease. *Neurobiol. Dis.*, **86**, 177–186.
Raz, A., Vaadia, E. & Bergman, H. (2000) Firing patterns and correlations of spontaneous discharge of pallidal neurons in the normal and the tremulous 1-methyl-4-phenyl-1,2,3,6-tetrahydropyridine vervet model of parkinsonism. *J. Neurosci.*, **20**, 8559–8571.
Richter, U., Halje, P. & Petersson, P. (2013) Mechanisms underlying cortical resonant states: implications for levodopa-induced dyskinesia. *Rev. Neurosci.*, **24**, 415–429.
Rommelfanger, K.S. & Wichmann, T. (2010) Extrastriatal dopaminergic circuits of the Basal Ganglia. *Front. Neuroanat.*, **4**, 139.
Roux, L., Stark, E., Sjulson, L. & Buzsáki, G. (2014) In vivo optogenetic identification and manipulation of GABAergic interneuron subtypes. *Curr. Opin. Neurobiol.*, **26**, 88–95.
Sánchez-González, M.A., García-Cabezas, M.A., Rico, B. & Cavada, C. (2005) The primate thalamus is a key target for brain dopamine. *J. Neurosci.*, **25**, 6076–6083.
Santana, M.B., Halje, P., Simplício, H., Richter, U., Freire, M.A.M., Petersson, P., Fuentes, R. & Nicolelis, M.A.L. (2014) Spinal cord stimulation alleviates motor deficits in a primate model of Parkinson disease. *Neuron*, **84**, 716–722.
Seamans, J.K. & Yang, C.R. (2004) The principal features and mechanisms of dopamine modulation in the prefrontal cortex. *Prog. Neurobiol.*, **74**, 1–58.
Sebban, C., Zhang, X.Q., Tesolin-Decros, B., Millan, M.J. & Spedding, M. (1999) Changes in EEG spectral power in the prefrontal cortex of conscious rats elicited by drugs interacting with dopaminergic and noradrenergic transmission. *Br. J. Pharmacol.*, **128**, 1045–1054.
Sharott, A., Magill, P.J., Harnack, D., Kupsch, A., Meissner, W. & Brown, P. (2005) Dopamine depletion increases the power and coherence of beta-oscillations in the cerebral cortex and subthalamic nucleus of the awake rat. *Eur. J. Neurosci.*, **21**, 1413–1422.
Sherman, M.A., Lee, S., Law, R., Haegens, S., Thorn, C.A., Hämäläinen, M.S., Moore, C.I. & Jones, S.R. (2016) Neural mechanisms of transient neocortical beta rhythms: converging evidence from humans, computational modeling, monkeys, and mice. *Proc. Natl. Acad. Sci. USA*, **113**, E4885–E4894.
Smith, Y. & Kieval, J.Z. (2000) Anatomy of the dopamine system in the basal ganglia. *Trends Neurosci.*, **23**, S28–S33.
Smith, Y. & Villalba, R. (2008) Striatal and extrastriatal dopamine in the basal ganglia: an overview of its anatomical organization in normal and Parkinsonian brains. *Movement Disord.*, **23**(Suppl 3), S534–S547.
Sotnikova, T.D., Beaulieu, J.-M., Barak, L.S., Wetsel, W.C., Caron, M.G. & Gainetdinov, R.R. (2005) Dopamine-independent locomotor actions of amphetamines in a novel acute mouse model of Parkinson disease. *PLoS Biol.*, **3**, e271.
Sparta, D.R., Hovelso, N., Mason, A.O., Kantak, P.A., Ung, R.L., Decot, H.K. & Stuber, G.D. (2014) Activation of prefrontal cortical parvalbumin interneurons facilitates extinction of reward-seeking behavior. *J. Neurosci.*, **34**, 3699–3705.
Tai, C.-H., Boraud, T., Bezard, E., Bioulac, B., Gross, C. & Benazzouz, A. (2003) Electrophysiological and metabolic evidence that high-frequency stimulation of the subthalamic nucleus bridles neuronal activity in the subthalamic nucleus and the substantia nigra reticulata. *FASEB J.*, **17**, 1820–1830.
Tamtè, M., Brys, I., Richter, U., Ivica, N., Halje, P. & Petersson, P. (2016) Systems-level neurophysiological state characteristics for drug evaluation in an animal model of levodopa-induced dyskinesia. *J. Neurophysiol.*, **115**, 1713–1729.
Tseng, K.Y., Kasanetz, F., Kargieman, L., Riquelme, L.A. & Murer, M.G. (2001) Cortical slow oscillatory activity is reflected in the membrane potential and spike trains of striatal neurons in rats with chronic nigrostriatal lesions. *J. Neurosci.*, **21**, 6430–6439.
Wang, Y., Zhang, Q.J., Liu, J., Ali, U., Gui, Z.H., Hui, Y.P., Chen, L., Wu, Z.H. *et al.* (2010) Noradrenergic lesion of the locus coeruleus increases apomorphine-induced circling behavior and the firing activity of substantia nigra pars reticulata neurons in a rat model of Parkinson's disease. *Brain Res.*, **1310**, 189–199.
Wen, H. & Liu, Z. (2016) Separating fractal and oscillatory components in the power spectrum of neurophysiological signal. *Brain Topogr.*, **29**, 13–26.
West, M.O., Carelli, R.M., Pomerantz, M., Cohen, S.M., Gardner, J.P., Chapin, J.K. & Woodward, D.J. (1990) A region in the dorsolateral striatum of the rat exhibiting single-unit correlations with specific locomotor limb movements. *J. Neurophysiol.*, **64**, 1233–1246.
Wichmann, T. & DeLong, M.R. (1996) Functional and pathophysiological models of the basal ganglia. *Curr. Opin. Neurobiol.*, **6**, 751–758.
Yael, D., Zeef, D.H., Sand, D., Moran, A., Katz, D.B., Cohen, D., Temel, Y. & Bar-Gad, I. (2013) Haloperidol-induced changes in neuronal activity in the striatum of the freely moving rat. *Front. Syst. Neurosci.*, **7**, 110.
Yang, C., Ge, S.-N., Zhang, J.-R., Chen, L., Yan, Z.-Q., Heng, L.-J., Zhao, T.-Z., Li, W.-X. *et al.* (2013) Systemic blockade of dopamine D2-like receptors increases high-voltage spindles in the globus pallidus and motor cortex of freely moving rats. *PLoS One*, **8**, e64637.
Zarow, C., Lyness, S.A., Mortimer, J.A. & Chui, H.C. (2003) Neuronal loss is greater in the locus coeruleus than nucleus basalis and substantia nigra in Alzheimer and Parkinson diseases. *Arch. Neurol.*, **60**, 337–341.

Paper IV

This unpublished manuscript has been
excluded in this version of the thesis.

Thank you for reading!

Printed by Tryckeriet i E-huset, Lund 2021

LUND UNIVERSITY
Faculty of Medicine

Doctoral Dissertation Series 2021:9
ISBN 978-91-8021-015-7
ISSN 1652-8220